POLARISATION EFFECTS IN SEMICONDUCTOR OPTICAL AMPLIFIERS

by

Séverine Philippe

A thesis submitted for a degree of

Doctor of Philosophy

in the University of Dublin

Under the supervision of

Dr Louise Bradley

School of Physics

Trinity College Dublin

October 2006

This thesis has not been sumitted as an exercise for a degree at any other university. The work described herein is entirely my own, with the exception of the assistance mentioned in the acknowledgements and the collaborative work noted in the publications.

I hereby agree that the library may lend or copy the thesis upon request.

Séverine Philippe

ABSTRACT

Optical switches based on SOAs are critical elements for the implementation of all-optical gating. The various wavelength conversion schemes are limited by their polarisation sensitivity. The polarisation sensitivity of SOAs, due to different gain and refractive indices in the TE and TM modes is well known and the resulting non-linear polarisation rotation can also be used for optical switching. Manufacturers characterize their devices in the continuous wave (CW) regime. However low gain anisotropy does not mean preservation of the input signal state of polarisation and for switching applications both CW and pulsed sources are used. The object of this thesis is to experimentally investigate the origins of the polarisation effects and how they affect the performance of SOAs, both in the continuous wave and dynamic regimes.

Firstly, without optical injection, analysis of the amplified spontaneous emission spectra shows that, as quoted by the manufacturer, the single-pass gains of the TE and TM modes are almost equal. A small birefringence is also observed. Then measurement and modelling of the change in polarisation undergone by a single CW beam are undertaken. TE and TM gains are found to be close under low optical injection but their difference increases with increasing injected power, the TE gain becoming increasingly larger than the TM gain. The phase difference between TE and TM modes is found to get closer to zero as the injected power is increased. Finally a small rotation of the principal axis, to a maximum of 5° is observed. Pump probe studies in the CW regime show that polarisation effects can potentially increase the extinction ratio by a maximum of 2dB or decrease it by 1.5dB, compared to cross gain modulation only. The polarisation dependent dynamics are found to vary widely. Both interband and intraband contribution are studied. The fast recovering (~5ps) gain compression observed in the co-polarised configuration is prevalent for the TETE case, which shows the highest potential for ultrafast all-optical gain switching. When injecting light polarised along the eigen modes of the device, the polarisation rotation measured is low, less than 10°. Finally polarisation dependent detection is used to study the dynamics of the change in polarisation. Linearly polarised light at 45° is injected. The change in polarisation is found to be mainly a change in the ellipticity. Although its recovery is dominated by the slow interband effects, an improved performance (faster response and higher extinction ratio), compared to gain switching only, can be obtained by carefully choosing the orientation of the output polarizer.

ACKNOWLEDGEMENTS

Firstly I would like to thank my supervisor Dr Louise Bradley for giving me the opportunity to perform this work in the Semiconductor Photonics Group, for her expertise and guidance as well as her general enthusiasm towards research.

This research would not have been possible without the financial support of Enterprise Ireland and the Irish Research Council for Science, Engineering and Technology.

Special thanks to our collaborators also working on SOAs. In Dublin City University, Dr Pascal Landais, Dr Brendan Kennedy who provided the CW model and Dr Frederic Surre. In Ensenada, Mexico, Dr Miguel Martinez-Rosas for his infinite patience when faced with temperamental laser systems, his sense of humour and the much missed endless conversations about everything, and Dr Horacio Soto and his group for the warm welcome during my visit there.

I would also like to thank all the members of the Semiconductor Photonics Group in Trinity College over the last four years as well as the members of the Radio & Optical Communications Group in Dublin City University.

Finally and most importantly I thank all my friends and family. Special thoughts go to the people who passed away over the last few years, in particular Mireille and Jacques Batut and my grand parents Jean-Marie and Jeanne Lacroix.
To Aoife, Niamh and Frances, thanks for all the good times. To my mum Thérèse and my brother Damien, thank you for all the support, trust and friendship.

PUBLICATIONS AND PRESENTATIONS

Publications

"Experimental investigation of polarisation rotation in semiconductor optical amplifiers", Kennedy, B.F., Philippe, S., Landais, P., Bradley, A.L., Soto, H., IEE Proceedings: Optoelectronics, vol.151, n 2, April, 2004, pp 114-118

"Dynamic Pump-Probe Studies of TE and TM Modes in Semiconductor Optical Amplifiers", S. Philippe, F. Surre, A.L. Bradley, P. Landais, M. Martinez-Rosas, Proceedings of SPIE - The International Society for Optical Engineering, vol.5825, Opto-Ireland 2005: Optoelectronics, Photonic Devices, and Optical Networks, 2005, pp 267-274.

"Polarisation Dependent Dynamics in Bulk Semiconductor Optical Amplifiers", S. Philippe, A.L. Bradley, F. Surre, P. Landais, B. Kennedy, M. Martinez-Rosas, IEEE ICTON 2006 proceedings, April 2006, vol.2, pp 157-160

"Polarization Resolved Four-Wave-Mixing-Based Measurement in Bulk Material Semiconductor Optical Amplifier", F. Surre, B. Kennedy, P. Landais, S. Philippe, A.L. Bradley, IEEE ICTON 2006 proceedings, April 2006, vol.2, pp 169-172

"Investigation of Optimum Wavelength Converter Based on Nonlinear Polarization Rotation in a Bulk SOA", B.F. Kennedy, S. Philippe, F. Surre, A.L. Bradley and P. Landais, IEE Poceedings, 2006, accepted for publication.

"Investigation of Polarization Dependent Gain Dynamics in a Bulk SOA", B.F. Kennedy, S. Philippe, F. Surre, A.L. Bradley, D. Reid and P. Landais, Optics Communications, 2006, accepted for publication.

Conferences

"Change of the polarisation state in a semiconductor optical amplifier", B. Kennedy, S. Philippe, P. Landais, A. L. Bradley, H. Soto, presented at the SIOE conference 2003 in Cardiff (UK).

"Study of polarization dependence of signal injected into a semiconductor optical amplifier using frequency resolved optical gating", B. Kennedy, P. Landais, S. Philippe, M. Martinez-Rosas, A. L. Bradley, presented at the SIOE conference 2004 in Cardiff (UK).

"Temporal and spectral dependence on polarization of the input signal in a semiconductor optical amplifier", B.F. Kennedy, S. Philippe, P. Landais, A.L. Bradley and H. Soto, OSA-Optical amplifiers and their applications, San Francisco, June 2004 (US).

"Measurement of the chirp introduced to a picosecond pulse injected into an SOA as a function of input polarization", B.F. Kennedy, S. Philippe, P. Landais, A.L. Bradley and H. Soto, ETOS, Cork, July 2004 (IRL).

"Pump-probe studies of non-linear polarization rotation in semiconductor optical amplifiers", S. Philippe, B. Kennedy, M. Martinez-Rosas, A. L. Bradley, P. Landais, presented at the ETOS conference 2004 in Cork (IRL).

"Influence of pulse power in dynamic measurements of semiconductor optical amplifiers", S. Philippe, F. Surre, P. Landais, A.L. Bradley, presented at the SIOE conference 2005 in Cardiff (UK).

"Change of the polarisation state in a semiconductor optical amplifier", S. Philippe, B. Kennedy, M. Martinez-Rosas, A. L. Bradley, P. Landais, presented at the SPIE conference 2005 in Dublin (IRL).

"Pump-probe studies of polarisation effects in semiconductor optical amplifiers using a counter-propagation configuration", S. Philippe, A.L. Bradley, P. Landais, F. Surre, M. Martinez-Rosas, presented at the IPRA 2005 conference in San Diego (US).

"Polarisation resolved dynamic measurements of semiconductor optical amplifiers", S. Philippe, F. Surre, P. Landais, A.L. Bradley, presented at the SPIE conference 2005 in Warsaw (POL).

"Polarisation Dependent Dynamics in Bulk Semiconductor Optical Amplifiers" (invited), S. Philippe, A.L. Bradley, F. Surre, P. Landais, B. Kennedy, M. Martinez-Rosas, presented at the ICTON 2006 conference in Nottingham (UK).

"Polarization Resolved Four-Wave-Mixing-Based Measurement in Bulk Material Semiconductor Optical Amplifier" (invited), F. Surre, B. Kennedy, P. Landais, S. Philippe, A.L. Bradley, presented at the ICTON 2006 conference in Nottingham (UK).

CONTENTS

CHAPTER 3: CHARACTERIZATION OF POLARISATION EFFECTS IN THE CONTINUOUS WAVE REGIME

CHAPTER 4: CONTINUOUS WAVE PUMP-PROBE MEASUREMENTS

CHAPTER 5: POLARISATION DEPENDENT DYNAMICS

CHAPTER 6: DYNAMICS OF NONLINEAR POLARISATION ROTATION

CHAPTER 7: CONCLUSIONS AND FUTURE WORK

CHAPTER 1 :
INTRODUCTION AND THESIS OVERVIEW

1. Introduction

The ever increasing volume of data being transferred across the world has been driving the demand for capacity and speed in communication systems. In modern digital communication systems especially, the speed and capacity can be enhanced by increasing the frequency of the carrier used in the system [1]. Compared to conventional cable and wireless systems, optical communications offer the possibility to carry many more channels because of the high carrier frequency of light and the large bandwidth of the optical fibres. Therefore, once a suitable matching transmission medium was found, optical waveguides, optical communications developed rapidly. Optical amplification is needed in optical communication networks because of attenuation and dispersion in optical fibres. Attenuation causes power loss thereby limiting the transmission distance, while dispersion leads to pulse broadening and limits the fibre bandwidth. Therefore in long-haul optical fibre communication systems, the signal needs to be regenerated. The need for linear amplification led to the development of the semiconductor optical amplifiers (SOA) in the 1980s. However with the arrival of the erbium doped fibre amplifier (EDFA) in the 1990s, the SOAs were almost out-competed as linear amplifiers [2], and up to now EDFAs have been the amplifier of choice, more so than SOAs. In order to avoid distortion of the input signal, amplifiers must provide the same gain for all the data bits. With typical recovery times in the millisecond region, much longer than the bit period, EDFAs average the power over very long bit sequences, thus avoiding distortion of the signal. On the other hand SOAs have recovery times in the hundreds of picoseconds, which leads to patterning effects in the Gigabit per second regime [3]. Other advantages of fibre amplifiers are high gain, low insertion loss, low noise figures and negligible non-linearities [4]. However, unlike SOAs, they require an external pump laser and are not suitable for integration. On the other hand, because of their small size, simple electronic pumping, high non-linearities and potential for integration, SOAs offer a wider range of applications. All-optical data processing is probably the most interesting and promising aspect of the SOA as they are key elements

in the development of all-optical switches and all-optical logical gates. Thus the information can be processed while remaining in its optical format, thereby avoiding the introduction of electronics elements in the system.

At present the speed and capacity of optical communications is limited by the optical/electronic conversion devices used for switching functions. The limit for these electronic elements is 40Gbit/s, the so-called electronic bottleneck [5]. Currently 40Gbit/s systems have just reached the stage where they are commercially available, while the next generation of 160Gbit/s systems is under active study in several research laboratories [6]. At these data rates all-optical processing becomes a necessity. While SOAs have lower gain and higher noise figures than EDFAs, they can be used in integrated optical systems. Moreover due to their gain saturation effect, fast response and strong non-linearities, they are not only suitable for amplification, but also and perhaps even more so for signal processing applications. Indeed the nonlinear behavior that is a drawback for the SOA as a linear amplifier makes it a good choice for an optically controlled optical gate. The first demonstrations of optically controlled SOA gates, using cross-gain modulation (XGM), were reported in 1992 [2]. In this simple configuration, one input signal is used to saturate the gain and thereby modulate a second signal. Because of the significant role of gain saturation [7] the modulation bandwidth is not directly limited by the 100ps carrier dynamics and bit rate capabilities of 100Gbit/s have been reported using the XGM technique [8]. Recent work suggests that even higher bit rate capabilities could be achieved with the use of quantum dot (QD) material in the SOA active region [9], while larger gain bandwidth can be obtained using quantum dash (QH) structures [10]. Cross phase modulation (XPM) takes advantage of the relation between the carrier density and the refractive index of the SOA. In this case, high performance gates are achieved by placing SOAs in interferometric configurations, where the optical input signal controls the phase difference between the interferometer arms. The carrier density change required for a phase shift of π rad, and hence the input signal level needed, is small [11] so that efficient conversion is obtained for a large range of wavelength [2]. Wavelength conversion at 100Gbit/s has been demonstrated using a Mach-Zender interferometer switch [12]. As well as XGM and XPM, it is also possible to use four-wave mixing (FWM). In this case the efficiency of the conversion is strongly dependent on the detuning between the pump and probe signals, and wavelength conversion at 100Gb/s

has been achieved for conversion over 3.2nm wavelength [13]. All the techniques described above are limited by their sensitivity to the polarisation of the optical input signals, therefore polarisation effects in SOAs must be thoroughly characterized in order to implement and optimize the various switching schemes.

The polarisation sensitivity of SOAs, due to different gain and refractive indices in the TE and TM modes, is well known. Although considerable efforts have been made to reduce this sensitivity, using strain and different waveguide structures, and gain anisotropy of less than 2dB has been achieved, this does not imply preservation of the state of polarisation of the input beam. Moreover manufacturers characterize their devices in the continuous wave (CW) regime, with the polarization sensitivity in particular usually given for single beam injection of a low power CW signal. Therefore any modification of the SOA structure, introduced in order to achieve polarisation insensitivity in this regime, is not taking account of the consequences in the dynamic regime. Indeed not only does low polarisation sensitivity in the CW regime not necessarily imply low polarisation sensitivity in the dynamic regime but the implementation of these techniques can potentially introduce even greater differences in the polarisation dependence of the SOA dynamics. As far as switching applications are concerned, both CW and pulsed sources are used. Therefore knowledge of the polarisation dependence of the SOA behaviour in all the different operation regimes is critical.

The change of polarisation and the gain experienced by a laser beam as it travels through the SOA are both altered when a second laser beam is injected into the device. This phenomenon, non-linear polarisation rotation, can potentially be used for high speed all-optical switching applications [14-17]. While a large amount of work focussing on its applications has been performed, the underlying physical mechanisms are not thoroughly understood. In order to optimise non-linear polarisation switching and determine its limitations, the mechanisms governing the dynamics of the change in polarisation and its recovery must be determined.

2. Thesis overview

To this day no extensive study of the SOA polarisation sensitivity in the different operation regimes and its application to all-optical switching has been presented. The object of this thesis is to experimentally investigate the origins of the polarisation effects and how they affect the performance of SOAs, both in the continuous wave and dynamic regimes. As polarisation sensitivity in SOAs cannot be totally suppressed, its understanding is necessary in order to determine how to optimize the different all-optical switching techniques. In the first experiments the CW behaviour of the device is studied. The gain and birefringence effects are first measured without optical injection, thus characterizing the inherent properties of the SOA. Then the change in polarisation undergone by a single CW beam is investigated, allowing us to study the input power dependence of the gain anisotropy and birefringence of the device and compare these experimental results to the data provided by the manufacturer. Finally the change in the output probe polarisation caused by injection of a pump signal is measured as a function of bias current and pumping parameters, providing an assessment of the expected extinction ratio due to carrier density pulsation. The second set of experiments focuses on the dynamic behaviour of the device. The polarisation dependent dynamics are first presented, injecting light polarised along the eigen modes and at 45°, in order to determine the best configuration for cross-gain modulation. This is followed by a characterization of the dynamics of non-linear polarisation rotation, where the optimization and limitations of this technique are presented. The work carried out and presented in the subsequent chapters is summarized below.

Chapter 2 introduces the basic principles behind optical amplification in SOAs, radiative processes and p-n junctions. The technology used to manufacture travelling wave SOAs and reduce their polarisation sensitivity is then presented, emphasizing the importance of facet reflectivity, material gain, confinement factor and birefringence. The different mechanisms of carrier recombination are described, as well as the carrier dynamics following optical injection into the device. In this chapter the experimental investigation of the main characteristics of the device under test is also presented. Finally a model based on the traveling wave description of the E-field in the amplifier cavity is described and used to illustrate some of the device characteristics as well as the inhomogeneous distributions of carriers and photons in SOAs.

Chapter 3 presents an experimental study of polarisation rotation in the continuous wave (CW) regime. Firstly the principles of polarisation of light and means by which it can be described, measured and controlled are reviewed. Two techniques are then used to investigate the gain and birefringence along the two eigen modes of the component waveguide, with and without optical injection. First the Hakki-Paoli method [18] is used to extract the gain and refractive indices of the TE and TM modes from the polarisation resolved amplified spontaneous emission spectra, measured without injection. The single-pass gain of the TE and TM modes are found to be almost equal without optical injection and experimental evidence of the inherent birefringence of the device is presented. The second investigation takes into account the variation of the eigen modes gain and refractive indices as a function of the input power of a single injected CW beam. At low input power the gains of the TE and TM modes are close, as quoted by the manufacturer, but their difference was found to increase with injected power. On the other hand the phase difference between TE and TM gets closer to zero as the injected power is increased. Finally a rotation of the eigen axis under CW injection, to a maximum of 5°, is observed.

In Chapter 4 pump-probe studies in the continuous wave (CW) regime are undertaken in order to assess the potential of non-linear polarisation rotation for optical switching applications and to determine which parameters characterizing the non-linear polarisation rotation are most sensitive, namely the orientation or the ellipticity of the state of polarisation. The experimental set-up uses free space optics only, so as not to disturb the polarisation state of the input and output beams. While pulsed sources are needed for ultrafast switching applications, using CW sources allows us to accurately measure the states of polarisation with a polarimeter. The output polarisation of the probe beam is monitored as a function of pumping parameters and of the SOA bias current. It is found to be strongly dependent on bias current and pump power but less susceptible to pump polarisation. The change in polarisation is shown to potentially increase the extinction ratio by a maximum of 2dB or decreases it by 1.5dB, compared to cross gain modulation only. Unlike what is observed in the single beam experiment, under pump-probe conditions the gain and birefringence effects are found to be dependent on probe input polarisation with the ellipticity parameters being the most sensitive to the presence of the pump signal.

The next two chapters present an investigation of the polarization dependence of the SOA dynamics in the picosecond regime by pump-probe experiments, using a free space contra-propagation set up.

In Chapter 5, the polarisation dependent dynamics are studied. The output probe intensity is monitored for different pump and probe input states of polarisation, allowing the polarisation dependence of the device response to be studied. The input states of polarisation considered are linear, oriented along TE, TM and 45° for both the co and cross polarised cases. The results are then discussed in terms of the induced gain compression and the associated timescales. When injecting along the eigen modes of the device, the cross-polarised data are dominated by the slower interband effects and show a low cross gain compression. The maximum gain compression is found to be higher for the TMTM case, 13dB, against 10dB for the TETE case. However the contribution of the slow gain compression is also larger for TMTM, over 7dB, while it remains under 3dB for TETE. The fast recovery times are similar in both cases, between 4.5 and 7ps, showing potential for ultrafast gating. It follows that the prevalence of the fast intraband effects in the TETE case shows the highest potential for ultrafast all-optical gain switching.

Chapter 6 focuses on the change in the probe state of polarisation due to the injection of the pump as well as the dynamics of this change. To this end polarisation dependent detection is used, where a polarizer is placed in front of the detector. Firstly the cross-polarised cases of light polarised along the eigen modes of the device are studied as these are most commonly used by other authors [19-21] and rotation of the eigen axes is investigated. We then focus on the 45° injection, where a change in the state of polarisation is expected. The rotation of the eigen modes was found to be small, less than 10°, therefore the influence of polarisation rotation is expected to be small as long as light is injected along these eigen modes. Under given experimental conditions, for the 45° injection the change in polarisation is mainly a change in the ellipticity, the output probe polarisation becoming more linear under the influence of the pump signal. Although in that case the dynamics of the polarisation modification is found to be dominated by the interband effects, a fast recovery can still be achieved by the right

choice of polarizer orientation and the extinction ratio is improved compared to gain switching.

In chapter 7 the work performed in this thesis and the main conclusions arising from it are summarized. Based on these conclusions, a guideline for potential future work is suggested.

REFERENCES

[1] H. Ghafouri-Shiraz, *The Principles of Semiconductor Laser Diodes and Amplifiers, Analysis and Transmission Line Laser Modeling*: Imperial College Press, 2004.

[2] K. E. Stubkjaer, "Semiconductor optical amplifier-based all-optical gates for high-speed optical processing," *IEEE Journal on Selected Topics in Quantum Electronics*, vol. 6, pp. 1428-1435, 2000.

[3] J. Mork, M. L. Nielsen, and T. W. Berg, "The Dynamics of Semiconductor Optical Amplifiers, Modeling and Applications," in *Optics & Photonics News*, July 2003.

[4] M. J. Connelly, *Semiconductor Optical Amplifiers*: Kluwer Academic Publishers, 2002.

[5] R. T. R. Almeida, K. Potratz, L. C. Bueno, M. E. V. Segatto, E. Oliveira, and L. C. Calmon, "Addressing the electronic bottleneck to virtual topology design of optical networks," *Microwave and Optoelectronics Conference, 2003. IMOC 2003. Proceedings of the 2003 SBMO/IEEE MTT-S International*, vol. 2, pp. 925-930 vol.2.

[6] H. G. Weber, R. Ludwig, U. Feiste, C. Schmidt, C. Schubert, J. Berger, E. Hilliger, M. Kroh, and T. Yamamoto, "High-speed all-optical signal processing in optical communication systems," *Pacific Rim Conference on Lasers and Electro-Optics, CLEO - Technical Digest*, pp. 610, 2002.

[7] T. Durhuus, B. Mikkelsen, C. Joergensen, S. L. Danielsen, and K. E. Stubkjaer, "All-optical wavelength conversion by semiconductor optical amplifiers," *Journal of Lightwave Technology*, vol. 14, pp. 942-954, 1996.

[8] A. D. Ellis, A. E. Kelly, D. Nesset, D. Pitcher, D. G. Moodie, and R. Kashyap, "Error free 100Gbit/s wavelength conversion using grating assisted cross-gain

modulation in 2mm long semiconductor amplifier," *Electronics Letters*, vol. 34, pp. 1958-1959, 1998.

[9] M. van der Poel, E. Gehrig, O. Hess, D. Birkedal, and J. M. Hvam, "Ultrafast gain dynamics in quantum-dot amplifiers: Theoretical analysis and experimental investigations," *IEEE Journal of Quantum Electronics*, vol. 41, pp. 1115-1123, 2005.

[10] A. Somers, W. Kaiser, J. P. Reithmaier, A. Forchel, M. Gioaninni, and I. Montrosset, "Optical gain properties of InAs/InAlGaAs/InP quantum dash structures with a spectral gain bandwidth of more than 300 nm," *Applied Physics Letters*, vol. 89, pp. 061107, 2006.

[11] D. Cotter, R. J. Manning, K. J. Blow, A. D. Ellis, A. E. Kelly, D. Nesset, I. D. Phillips, A. J. Poustie, and D. C. Rogers, "Nonlinear Optics for High-Speed Digital Information Processing," *Science*, pp. 1523-1528, 19 November 1999.

[12] R. P. Schreieck, M. H. Kwakernaak, H. Jackel, and H. Melchior, "All-optical switching at multi-100-Gb/s data rates with Mach-Zehnder interferometer switches," *Quantum Electronics, IEEE Journal of*, vol. 38, pp. 1053-1061, 2002.

[13] A. E. Kelly, A. D. Ellis, D. Nesset, R. Kashyap, and D. G. Moodie, "100Gbit/s wavelength conversion using FWM in an MQW semiconductor optical amplifier," *Electronics Letters*, vol. 34, pp. 1955-1956, 1998.

[14] D. Lenstra, Y. Liu, M. T. Hill, G.-D. Khoe, and H. J. S. Dorren, "Nonlinear polarization rotation in semiconductor optical amplifiers: Theory and application to all-optical flip-flop memories," *IEEE Journal of Quantum Electronics*, vol. 39, pp. 141-148, 2003.

[15] H. Soto, J. C. Dominguez, Erasme D., and G. Guekos, "Demonstration of an all-optical switch using cross-polarization modulation in semiconductor optical amplifiers," *Microwave and Optics Technology Letters*, vol. 29, (3), pp. 205-209, 2001.

[16] H. Soto, J. D. Topomondzo, D. Erasme, and M. Castro, "All-optical NOR gates with two and three input logic signals based on cross-polarization modulation in a semiconductor optical amplifier," *Optics Communications*, vol. 218, pp. 243-247, 2003.

[17] M. F. C. Stephens, M. Asghari, R. V. Penty, and I. H. White, "Demonstration of ultrafast all-optical wavelength conversion utilizing birefringence in semiconductor optical amplifiers," *IEEE Photonics Technology Letters*, vol. 9, pp. 449-451, 1997.

[18] B. Hakki and T. Paoli, "Gain spectra in GaAs double-heterostructure injection lasers," *Journal of Applied Physics*, vol. 46 (6), pp. 1299-1306, 1975.

[19] K. L. Hall, J. Mark, E. P. Ippen, and G. Eisenstein, "Femtosecond Gain Dynamics in Ingaasp Optical Amplifiers," *Applied Physics Letters*, vol. 56, pp. 1740-1742, 1990.

[20] C. T. Hultgren and E. P. Ippen, "Ultrafast Refractive-Index Dynamics in Algaas Diode-Laser Amplifiers," *Applied Physics Letters*, vol. 59, pp. 635-637, 1991.

[21] J. Mark and J. Mork, "Subpicosecond Gain Dynamics in Ingaasp Optical Amplifiers - Experiment and Theory," *Applied Physics Letters*, vol. 61, pp. 2281-2283, 1992.

CHAPTER 2 :
THE SEMICONDUCTOR OPTICAL AMPLIFIER

1. Introduction

A semiconductor optical amplifier (SOA) can be described as a diode laser operating below threshold that amplifies an injected light signal by means of stimulated emission. A schematic diagram of the SOA under test is shown on Figure 1. A bias current is applied to the active region, providing the energy needed for optical gain. The optical confinement is provided by an embedded waveguide. In SOAs, the transverse magnetic (TM) mode is the vertical mode and the transverse electric (TE) mode is the horizontal mode. By extension the vertical and horizontal directions are referred to as the TM and TE directions. In the most basic SOA structure, the TM confinement of the carriers is due to the different refractive indices of the semiconductor layers, while the TE confinement factor comes from the carrier distribution due to the applied bias current.

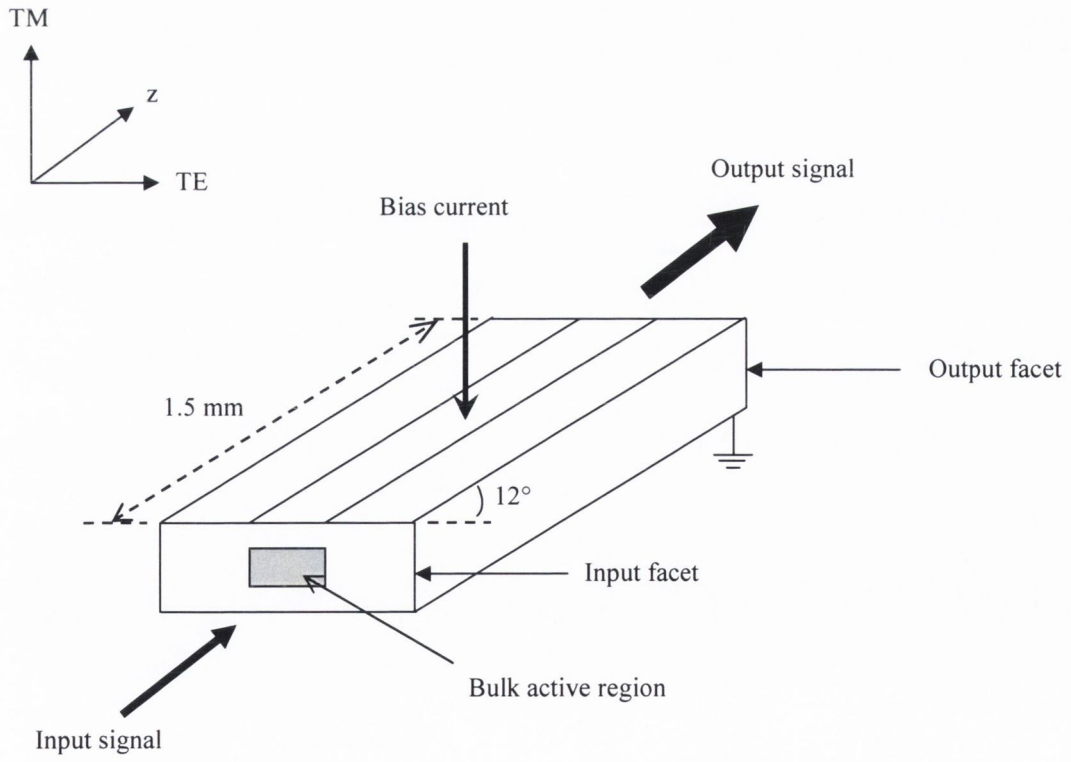

Figure 1. Schematic diagram of the SOA under test

The travelling wave SOA under test is a commercial component, obtained from Optospeed. It is a 1.5mm long bulk InGaAsP active region surrounded by InP. This structure was grown by MOCVD and it is quoted as having low polarisation dependent gain. Both facets are anti-reflection (AR) coated, with a tilted output of 12^{0} to reduce the Fabry-Perot resonance due to the residual reflectivity of the facets.

In this chapter the basic principles behind optical amplification in SOAs are introduced, followed by a review of device technology. Then the different mechanisms of carrier recombination and gain dynamics are given. Finally the main characteristics of the device under test are presented, as well as a model based on the traveling wave description of the E-field in the amplifier waveguide.

2. Basic principles

2.1 Radiative processes

In an SOA, the carriers (electrons) are provided by the applied bias current. They occupy energy states in the conduction band (CB) of the active region, leaving holes in the valence band (VB). The three radiative processes taking place between two energy levels, spontaneous emission, stimulated emission and stimulated absorption are shown on Figure 2.

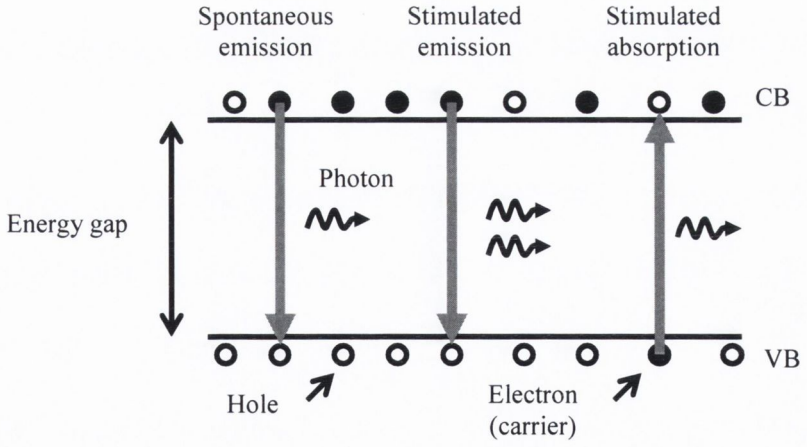

Figure 2. Spontaneous and stimulated radiative processes in a two level system.

A CB carrier can spontaneously recombine with a VB hole and thereby emit a photon with random phase and direction (spontaneous emission). When a photon of suitable energy is incident on the material it can cause stimulated emission, also called

stimulated recombination. The CB carrier recombines with a VB hole, losing its energy in the form of a photon. The photon generated by stimulated recombination has the same frequency, direction of propagation and phase as the stimulating photon. An incident photon of sufficient energy can also stimulate a carrier from the VB to the CB. In this case the incident photon is lost by stimulated absorption. When the system is not at equilibrium, the density of electrons in the upper state and of holes in the lower state having been increased, the recombination rate increases [1], contributing additional photons to the field of stimulating photons already present. Hence the rate of stimulation grows with the photon density. However the stimulated absorption increases also, thus reducing the photon density.

In a SOA, a bias current is injected, creating a population inversion. In this case there are more carriers in the CB than in the VB, therefore the stimulated emission process is dominant compared to the stimulated absorption and the SOA exhibits optical gain. Therefore population inversion is the vital condition for optical amplification. Even without any optical input, part of the spontaneous emission is amplified, thereby creating noise and reducing the carrier population available for optical gain. This is called amplified spontaneous emission (ASE).

2.2 The p-n junction

In semiconductors, population inversion is formed by forward biasing a heavily doped p-n junction [2], as shown on Figure 3. For such heavily doped degenerate semiconductors, the Fermi energy level lies above the conduction band edge in an n-type material, and below the valence band edge in a p-type material. When these two types of material are joined to form a p-n junction, diffusion of majority carriers occurs. Electrons diffuse toward the p-side and holes toward the n-side. For every electron that leaves the n region, because of diffusion across the surface, an uncompensated positively ionized donor is left behind, and for every hole that leaves the p region, an uncompensated negatively ionized acceptor is created. These carriers leave from points near the surface of contact. As a result, the p and n regions are separated by what is known as a depletion region, a region that is depleted of holes and electrons but contains positively ionized donor atoms on one side and negatively ionized acceptors atoms on the other side [3]. Because of the high electrostatic field produced in the depletion region, the concentration of mobile carriers, holes and electrons, are very

small compared to the impurity concentration over most of the depletion region. The presence of charges on either side of the junction creates an electric field, E, directed from n to p. Holes from p to n and electrons from n to p continue to diffuse because of the gradients of carrier densities resulting in a total diffusion current from p to n. Simultaneously the electric field forces the holes to drift from n to p and the electrons to drift from p to n, resulting in a total drift current from n to p. When a forward bias is applied, the electric field at the junction is reduced and so is the voltage across the junction.

Because of the position of the Fermi energy levels, these carrier movements create a very narrow region in which there are both electrons in the conduction band and holes in the valence band. Therefore population inversion is achieved in this region, called the depletion region, where carrier recombination is possible. The refractive index of the depletion region is higher than that of the surrounding layers so the light is confined by total internal reflection, because of the lower carrier density, as predicted by the Kramer-Kronig relation [4]. Hence a refractive index step exists between the active region and the surroundings, which effectively forms a dielectric waveguide to confine light propagating along the structure thus creating an optical waveguide [5, 6].

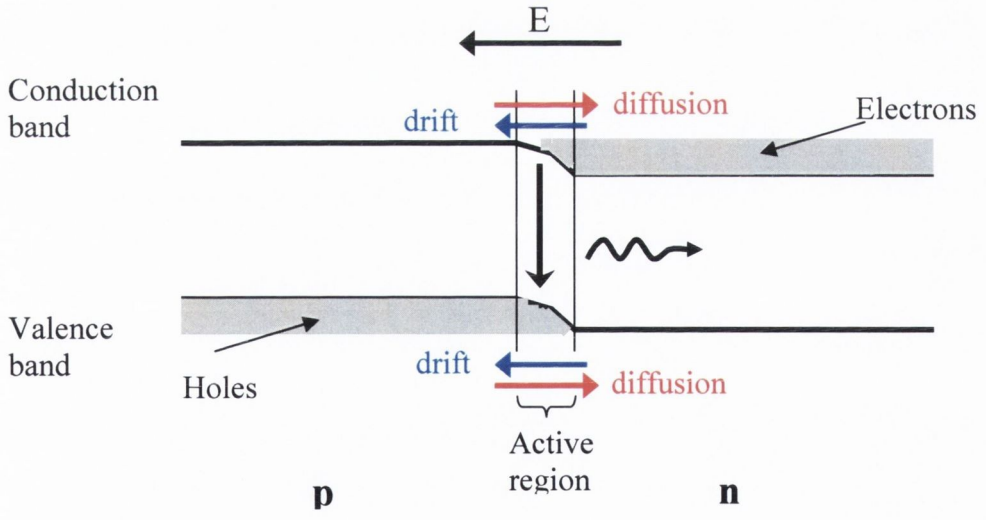

Figure 3. Forward biased p.n. junction showing the formation of a depletion region.

2.3 Double heterojunction

All the SOAs available today exploit the double heterojunction structures in order to provide efficient confinement of electrons and holes, by embedding the active region between p- and n-type cladding layers of a higher bandgap, as shown on Figure 4.

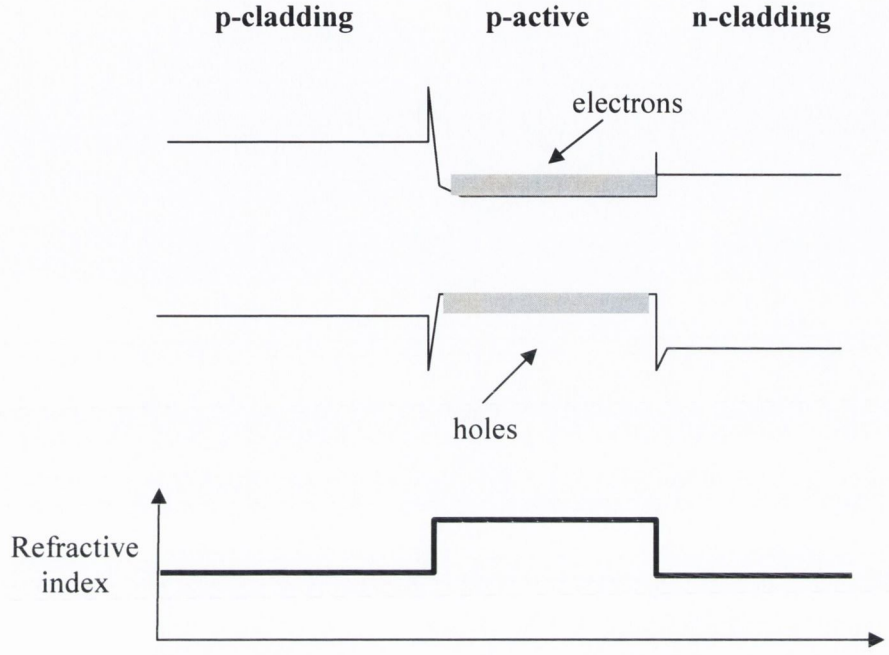

Figure 4. Band structure of a forward biased double heterojunction and associated variation in refractive index.

Electrons and holes can now move freely to the active region under forward bias. However the potential barrier, which results from the band gap difference between the active region and the cladding layers, confines the carriers to the active region. This dramatically reduces diffusion of carriers from the active region. The second main advantage of the double heterojunction is that the cladding layers have a lower refractive index than the active region. This means that the optical beams injected into the material will be confined close to the active layer, which is desirable because this is the section of the material where the optical gain takes place. This index guiding reduces the internal loss in the material.

2.4 Optical amplification

The overall gain in the active region can be quantified by two material parameters [2]: the material gain coefficient, g_m, and the loss coefficients of the active region, α_a, and the cladding region ,α_c. The imperfection of the waveguiding action is taken into account by a weighing factor Γ. Γ is the optical confinement factor, defined as the ratio between the optical field confined in the active region to the total optical field flowing across the structure. The overall gain, G_s, is given by:

$$G_s = \exp[\Gamma(g_m - \alpha_a) - (1-\Gamma)\alpha_c]L \qquad (1)$$

Where the gain and loss coefficient are measured in cm^{-1} and L is the length of the waveguide in cm.

Different gain parameters are used to describe SOA properties and the nomenclature varies. It is therefore useful to define here the most common parameters. The *material gain coefficient*, mentioned above, depends on the band structure of the material and the nature of the transitions [6, 7]. The gain undergone by a beam travelling along the length of the SOA is referred to as the *single pass gain*, the *chip gain*, the *facet-to-facet gain* or the *intrinsic gain*. In a travelling wave SOA the single pass gain equals the overall gain but in a Fabry-Perot SOA it is not the case and the positive feedback [2] has to be taken into account. The *modal gain*, also called the *effective gain*, is the single pass gain calculated for a single mode of the device. Finally the *signal gain*, sometimes called the *fibre-to-fibre gain* in fiberised SOAs is measured experimentally as the ratio of the output power to the input power, it has a smaller value than the facet-to-facet gain because it includes the coupling losses.

3. Travelling wave SOAs

SOAs can be classified in two ways, depending on their mode of operation or their structures [2]. The operational classification is briefly discussed here while different structures are described later in more details. In a Fabry-Perot (FP) SOA the signal is reflected at the facets and passes many times through the waveguide, while in a travelling wave (TW) SOA, the reflections are negligible. This study is based on the latter, which is less sensitive to fluctuation in bias current, temperature and signal

polarisation. In a FP SOA the resonating characteristics of the cavity modulate the material gain spectrum, introducing ripples along the amplifier gain spectrum and thereby decreasing the bandwidth of the amplifier. Typically the bandwidth of a FP SOA lies between 8-43GHz, while the bandwidth of a TW SOA reaches 20THz [2]. As the photon travel back and forth continuously across a FP SOA due to reflections at the end facets, it saturates faster than the TW SOA. Saturation output power up to 10Bm can be achieved for TW SOAs, against -7dBm for FP SOAs.

A number of methods are used in order to minimise reflections in TW SOAs. While in the device used in this work antireflection (AR) coatings and angled facet are used, other structures are available, such as flared facet and window facet waveguides.
The power reflectivity, R, for normal incidence at the interface of two dielectrics of refractive indices n_1 and n_2 is given by:

$$R = \left(\frac{n_2 - n_1}{n_2 + n_1} \right)^2 \qquad (2)$$

Because of the high refractive index of InGaAsP (typically $3<n<4$) the reflectivity at the semiconductor-air interface results in a significant amount of feedback at the facets of the SOA. In order to achieve wideband low facet reflectivity, multilayer dielectric antireflection coatings are necessary [8]. The analysis of reflection coatings used in SOA design is complex because of the SOA waveguide mode being distributed in the active and cladding regions, which have different refractive indices. Although effective facet reflectivity lower than 10^{-4} has been achieved by carefully selecting the refractive index and thickness of a single layer AR coating [8], the reflectivity in that case is polarisation and wavelength dependent. The use of multilayer coatings can reduce the polarisation dependence of the reflectivity and broaden the low reflectivity wavelength range.

The modification of the SOA structure is usually used in conjunction with the AR coatings to minimize reflections. Figure 5 shows diagrams of the three main reflectivity reducing structures. In an angled facet SOA, Figure 5 (a), the active region is slanted away from the facet cleavage plane, thereby reducing the effective facet reflectivity. It can be shown [8] that the effective reflectivity decreases as the facet angle increases. However increasing the facet angle also decreases the coupling efficiency and increases

the polarisation sensitivity of the AR coating. Therefore a trade off must be found in order to determine the optimal facet angle, which usually lies between 5° and 15°. In the device used in this work a facet reflectivity of the order of 10^{-5} [9, 10] is achieved with a combination of AR coating and 12° angle facets.

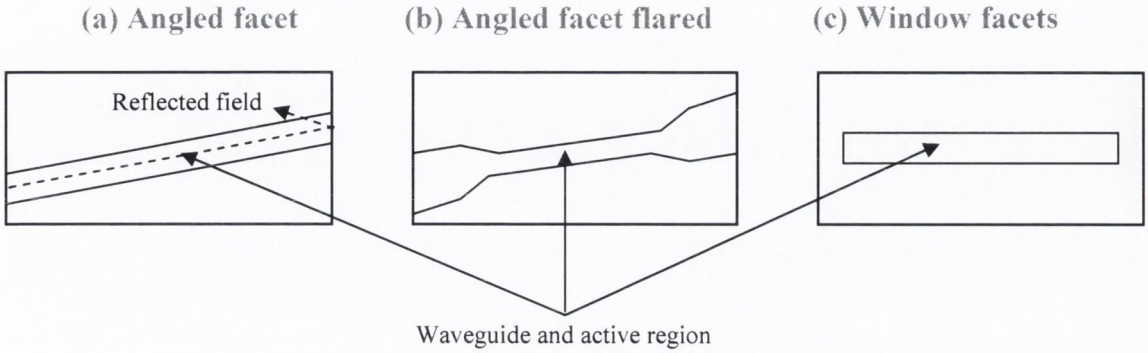

Figure 5. Top view of SOA structures used to reduce reflectivity at the facets.

The facet reflectivity also decreases as the width of the waveguide increases. However if the waveguide is too wide higher order transverse modes can appear. For this reason flare waveguides can be used, where the waveguide is broadened near the facet of the SOA only, as shown on Figure 5 (b), thus preserving the single mode operation condition [8].

In order to further reduce the polarisation dependence of the facet reflectivity, window facets are sometimes used [8], where a transparent region is present between the active region and the end facets, as shown on Figure 5 (c). This transparent region has an energy bandgap greater than the signal photon energy so that stimulated absorption is not possible. The guided field from the waveguide propagates in the widow region at some angle due to diffraction and is partially reflected at the end facet. The reflected field continues to broaden in space so only a small fraction is coupled back into the active region. The effective reflectivity decreases with increasing window region length but the coupling efficiency is degraded for long window regions.

4. Polarisation sensitivity

In addition to the polarisation sensitivity of the reflectivity of the output facets, a number of properties of SOA are polarisation dependent. The modal gain and refractive index discrepancies between the TE and TM modes of an SOA are well known. In fact

the TE and TM modes of a planar waveguide satisfy different wave equations [11]. Although the main cause of the polarisation sensitivity in SOAs is often attributed to the difference between the confinement factor, Γ, in TE and TM modes [8], other groups have shown that it is not the only contributing factor [12, 13]. In fact modelling and calculations of confinement factor and gain for each mode are often based on approximations applied to the TE wave equation only and have therefore limitations. The approximation (3) is especially widely used [5, 8] even though it was derived with a weak guiding assumption and can lead to an overestimation of the TM gain [12, 14].

$$g_{\text{mod}} \approx \sum_i \Gamma_i^{S_z} g_i \qquad (3)$$

Where g_{mod} is the modal gain and g_i is the plane wave bulk material gain or absorption in the i^{th} layer of confinement factor Γ_i, and S_z is the z component of the Poynting vector. Recent work [13] suggests that the difference in material gain between the TE and TM modes, caused by strain, is also a major contributor to the polarisation sensitivity of SOAs. The effect of strain is discussed in more details in section 6.

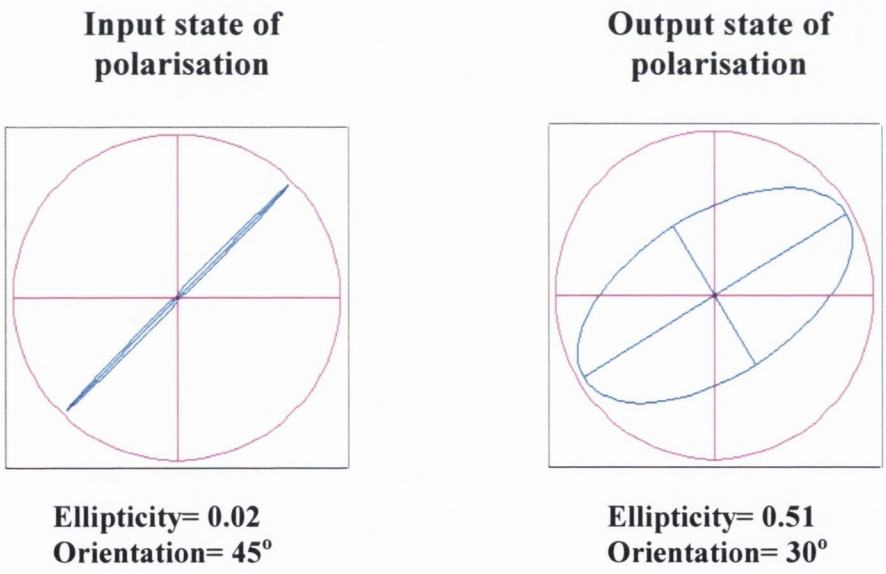

Figure 6. Direct polarisation measurements of the input and output signals state of polarisation demonstrating the polarisation sensitivity of the device in the continuous wave regime. I_{bias}=300mA, λ_{in}=1574nm, Pin=-3.7dBm.

Even though low polarisation sensitivity is quoted by the manufacturer for the device under test in this work, polarisation effects can be easily observed in our device, as

shown on Figure 6. Here the state of polarisation of the input and output beams are measured with a polarimeter. The input is set at an almost linear state with an orientation of 45°. It is clearly altered as it passes through the SOA and exits the SOA with an ellipticity increased to 0.51 and rotated by 5°. Low polarisation sensitivity refers to a difference in signal gain of less than 2dB between the TE and TM modes. However even a small difference in gain causes a rotation of the signal polarisation if it is not injected along one of the eigen modes. The fact that elliptical polarisations can be observed when injecting an input signal linearly polarised shows the birefringence of the device. In this case a phase shift is introduced between the TE and TM components of the electric field due to the different refractive indices of the TE and TM modes.

5. SOA structures

The polarization sensitivity of SOAs can be reduced via the structural design [8] and/or the introduction of strain. SOAs can be based on bulk materials, quantum wells or quantum dots. The exact structure of the bulk SOA under test has not been disclosed, however based on the work of different groups using similar devices [9, 10], the device is most probably a ridge waveguide SOA.

5.1 Bulk devices

The thickness of the individual active layers defines whether a device is a bulk or a quantum-well device: in bulk materials the dimensions of the layer are larger than the de Broglie wavelength of the carriers. Bulk devices are commercially available from a variety of manufacturers.

5.1.1 Square cross-section

Square shaped sub-micron bulk active regions in regrown buried structures achieve polarisation insensitivity through choice of nearly square cross section of the active layer [8, 9]. The rotational symmetry of the structure provides the polarisation insensitivity. The main disadvantage of this structure is its far-field divergence, which causes coupling problems, as a largely divergent beam is harder to collect. To improve coupling losses and facet reflectivity taper and window structures are required. The

small square active layer and the need of taper and window structures result in a complicated multi-step growth procedure.

5.1.2 Low tensile-strained bulk active region

As discussed below in more detail, the material gain of the TE and TM modes is dependent on the strain present in the structure. In the case of low tensile-strained bulk SOAs, the polarisation sensitivity of the structure is counterbalanced by the polarisation dependent gain of the material imposed by the strain. These structures are simple compared to quantum well structures. Additionally, compared to square cross section bulk structures, they have more design flexibility and their fabrication is simple.

5.1.3 Ridge waveguide

In a ridge waveguide, as shown on Figure 7, transversally the light is guided by the active layer and the cladding, while laterally the guiding effect is generated by the index contrast introduced through the ridge.

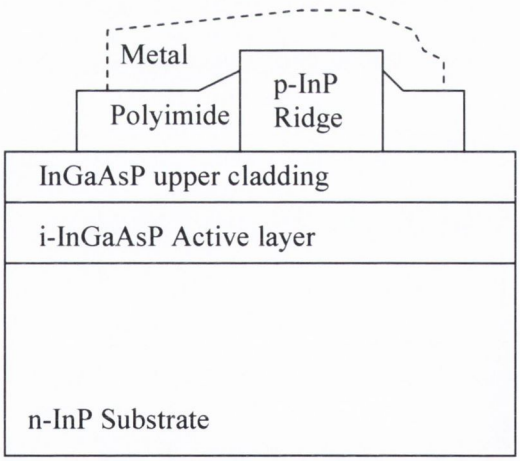

Figure 7. Ridge waveguide SOA structure.

Ridge waveguide SOAs offer the possibility to tune the gain ratio between TE and TM by simple geometrical means of changing the active region dimension, through alterations in ridge width, active layer or cladding thicknesses [9]. Reducing the ridge width, extending the cladding thickness or increasing the active layer thickness enhances the TM to TE chip gain ratio, while increasing the ridge width, reducing the

cladding thickness or reducing the active region thickness enhances the TE to TM chip gain ratio.

5.2 Quantum well devices

As discussed before, the active region of a conventional bulk SOA consists of a layer of semiconductor sandwiched between two layers of higher energy bandgap. If the layer thickness is less than approximately 20nm then the occupation states available for confined electron and holes is no longer continuous but discrete. Such a thin active layer sandwiched between two cladding layers of higher bandgap energy is termed a quantum well (QW). The active layer is usually referred to as the well layer while the adjacent cladding layer is usually referred to as the barrier layer. A multi quantum well (MQW) SOA can be fabricated by stacking well and barrier layers. Compared to bulk SOAs, QW SOA have a wider optical bandwidth, higher saturation output power and low noise figure [9]. The gain in a quantum well is inherently polarisation dependent, but this polarisation dependence is function of strain. Polarisation insensitive devices have been obtained by introducing tensile strain to the barriers, the wells or by alternating tensile and compressive strained quantum wells. However the realization of high gain polarisation independent MQW SOAs requires a complex technology.

5.3 Quantum dot devices

In principle the quantum dots (QD) devices are identical to bulk and QW SOAs except that the active region consists of a number of QD layers. A practical way of growing high density high quality QDs is by self assembly through the Stranski Krastanow growth technique. In this method a thin layer of dot material, the wetting layer, is formed beneath the QDs. Because it is mainly through this layer that carriers are fed into the active states in the dots, the properties of the wetting layer are important for the overall performance of the device [15]. When a bias current is applied, the wetting layer acts as a carrier reservoir for the excited state of the QDs, while optical gain is provided by transitions between the excited state and ground state of the QD. Therefore in some respect the QD SOA can be considered a three level system, unlike bulk devices which behave more like a two level system. Advantages of QD SOAs include large optical bandwidth, low threshold current densities, high saturation powers, low noise figure and

fast gain recovery. However their growth is complex and longer device are needed because of the small modal gain values of QDs.

5.4 Quantum dash devices

Very recently new devices based on quantum dashes (QH) have attracted attention. A quantum dash is an elongated nanostructure whose cross section is similar to that of a shallow quantum dot, 3–4nm x 310–20 nm, while its length is hundreds of nanometers [16]. While less work on their optical properties has been done in comparison to QD, they exhibit promising results. In particular a spectral gain bandwidth of over 300nm has been achieved [17]. The carrier and gain dynamics governing the response of QH structures are not known in details. The initial fast gain recovery of QH was found to be slower than that of QD and the associated phase change to be larger, two properties which could limit their use in high speed systems [18, 19]. However large variations in dynamic behaviour are expected with the energy level structure of both QD and QW devices, which have not been investigated yet.

6. Strain effects

Introducing strain by lattice mismatch between the layers of optoelectronic components, such as diode lasers, can lead to significant enhancement of their performances, including reduced threshold current density, improved efficiency and temperature sensitivity, and high-speed performance [20, 21]. In a waveguide the transitions associated with TE and TM modes are different [20], with TM transitions involving light holes while TE transitions involve a mixture of light (25%) and heavy (75%) holes [22]. Since compressive strain leads to enhanced TE gain while tensile strain leads to enhanced TM gain, strain can also be used to reduce the polarisation sensitivity of SOAs [23-26].

The active region of a bulk SOA is made of a direct band-gap semiconductor, InGaAsP in our case. A simplified representation of the band structure is shown on Figure 8 for an unstrained bulk semiconductor. The valence bands are threefold [27], with the heavy holes and light holes bands degenerate at the centre and a band split-off. Axial strain breaks the cubic symmetry of the semiconductor lattice causing a splitting of the degeneracy of the light and heavy hole states at the valence band maximum. In the case

of highly strained structures, the resulting band structure is highly anisotropic. For high compressive strains the light hole is shifted downward, which can lead to suppression of the TM mode of the waveguide. For high tensile strain however the light hole band shifts significantly above the heavy hole states, causing the TM mode to become dominant.

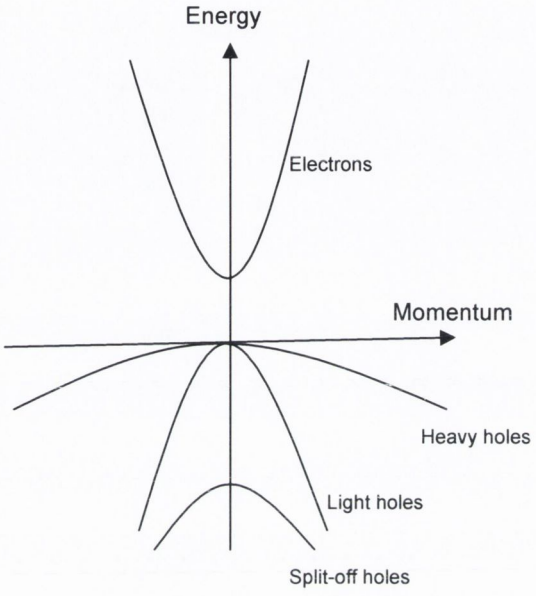

Figure 8. Simplified band-edge structure of a direct gap semiconductor.

In any heterostructure there usually is some residual strain in the active region, induced by the imperfection of the lattice matching between the active region and the cladding layer. While such a small strain probably does not alter significantly the shape of the band structure, it can cause a split of the degeneracy of the light and heavy holes valence bands. It has been shown that a typical lattice mismatch of 0.01%, realistic for quasi lattice-matched structures, can cause a split of 6-8meV [13]. This is too small to suppress any of the modes of the waveguide, both TE and TM are still amplified and similar gain spectra are measured for both modes in section 9.1. But since the TE and TM modes involve different transitions with non-degenerate hole states, they are not as strongly coupled as would be expected with degenerate VBs, i.e. the cross-saturation [28] is reduced. Therefore strain effects are clearly involved in the polarisation sensitivity of SOAs. In fact this removal of the valence bands degeneracy has been used to justify the assumption that TE and TM modes couple to different reservoirs of holes and only interact via gain saturation [29].

7. Carrier recombination in bulk semiconductors

There are two basic types of electron-hole recombination mechanisms in SOAs: radiative and non-radiative. Radiative recombination occurs when a conduction band electron recombines with a valence band hole leading to the emission of a photon. As discussed before there are three processes of radiative recombination: spontaneous emission, stimulated emission and stimulated absorption. The spontaneous radiative recombination rate R_{rad} is given by:

$$R_{rad}=B_{rad}N^2$$

Where B_{rad} is the bimolecular radiative recombination coefficient and N is the carrier density.

Electrons can also recombine with holes nonradiatively. Nonradiative recombination depletes the electron population without photon emission, leading to a decrease of the amount of light that can be generated by radiative recombination. Auger recombination is usually the most important nonradiative recombination mechanism in long wavelength devices [7]. There are many forms of Auger recombination, the most common in long-wavelength devices being CCCH, CHHS and CHHL [7] as shown on Figure 9. The Auger recombination rate R_{aug} is given by :

$$R_{aug}=C_{aug}N^3$$

Where C_{aug} is the Auger coefficient.

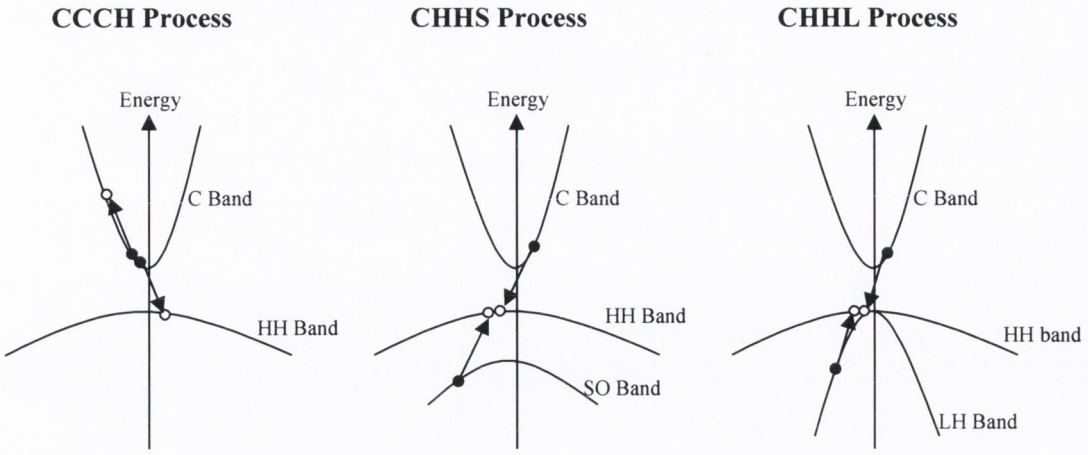

Figure 9. Relevant Auger processes: CCCH, CHHS, CHHL. C represents the conduction band and H,L and S represent the heavy hole (HH), light hole (LH) and split-off (SO) valence bands, respectively.

Material defects and surface defects can also cause significant nonradiative recombination. Defects can occur in the active region of a SOA during the fabrication process or as the device ages. The end facets can also absorb impurities from the air that can then form nonradiative recombination centres. The recombination rate R_{tr} due to defects is given by :

$$R_{tr}=A_{tr}N$$

Where A_{tr} is the trap and surface recombination coefficient.
The total recombination rate R is given by:

$$R(N)=A_{tr}N+B_{rad}N^2+C_{aug}N^3$$

8. Gain dynamics

For all optical signal processing applications, the dynamic behaviour of the amplifiers is of prime interest. In this section the evolution of the carrier density is described and the processes of spectral hole burning and carrier heating, which are commonly used in relation to non-linear gain in SOAs are defined. Then the different mechanisms for excitation and relaxation of carriers are discussed. These mechanisms do not occur in strict sequence, but rather may overlap in time [30].

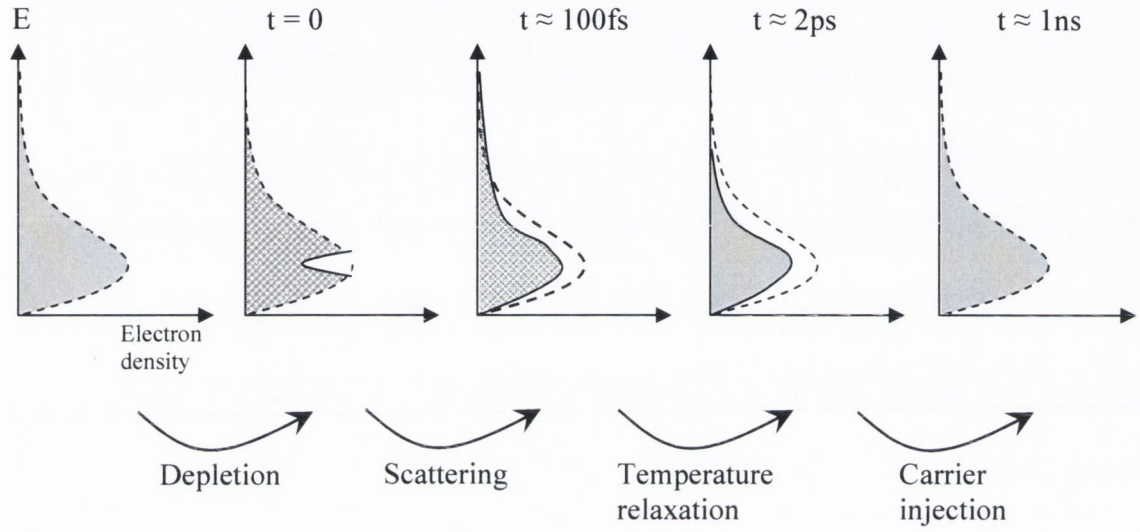

Figure 10. Qualitative illustration of the evolution of the carrier distribution in the active region of the SOA. Following stimulated emission induced by a short optical pulse, the distribution recovers to equilibrium by carrier-carrier scattering, carrier temperature relaxation and carrier injection.

When an optical beam is injected into a SOA, electrons in the conduction band are depleted because of the stimulated emission responsible for the input beam amplification. The reduction in the density of excited electrons causes a decrease in the gain as well as a change of the refractive index. Figure 10 illustrates the evolution of the carrier distribution in the SOA after injection of an optical pulse [15]. Recovery from carrier heating occurs via LO-phonon interactions and within a few picoseconds a quasi-equilibrium (Fermi-Dirac) distribution at the lattice temperature is established. From this point on the state of the amplifier (gain and refractive index) can be characterized by the total carrier density, which recovers to its initial state on a

timescale of hundreds of picoseconds by carrier injection via the applied bias current. Prior to the establishment of a Fermi-Dirac distribution, the distribution is a non-equilibrium state is governed mainly by spectral hole burning (SHB) and carrier heating (CH) [31-34].

SHB refers to a localized reduction in the number of carriers at the transition energies. It occurs due to the intense stimulated emission at the wavelength of the injected signal. Carrier heating effects can have different sources [2], injection heating is due to the injected carriers having a high energy in order to reach the active layer. Stimulated emission depletes lower energy carriers in both the conduction and valence bands and leaves those with higher than average energy. Free carrier absorption [31], and in particular free hole absorption in InGaAsP [35], has also been suggested as a main mechanism of CH. Auger recombination, where the energy released during an electron-hole recombination is absorbed by another carrier, which is excited to a higher energy level also contributes to CH [36]. Two photon absorption (TPA), where a carrier transits to a higher energy level by absorption of the energy of two photons also leads to carrier depletion and can be a significant source of carrier heating at high input intensities [37].

After SHB modification of the carrier density by a short optical pulse, the electrons and holes are redistributed throughout the conduction and valence band through carrier-carrier scattering and carrier-phonon scattering. The electrons and holes quickly approach quasi Fermi-Dirac distributions. The number of carriers does not change. However the energy of the carriers decreases, because of spontaneous phonon emission that transfers energy to the lattice. Therefore redistribution and thermalization of carrier populations happens in conjunction with the transfer of energy from the carriers to the lattice via electron-phonon interaction. In the conduction band, the timescales associated with the individual scattering events is less than 50fs and the time it takes to cool an optically-heated electron gas is approximately 165fs. The resulting hot LO phonon gas subsequently cools by acoustic phonon emission [31]. Carrier lattice thermalization brings the temperatures of the free carriers and the lattice to the same value in a timescale of 1.5ps to 4ps [30, 31]. The system then recovers to its initial state by interband transitions, i.e. carrier injection by the applied bias current.

Depending on the duration of the pulse injected into the SOA, the effect of the different mechanisms involved in the dynamic gain response may not all be observed [38]. For very short pulses, less then 100fs, SHB and CH dominate. On the other hand in the nanosecond regime only interband effects can be observed. However in the picosecond regime, for pulses shorter than about 12ps as is the case in the present experimental investigation, all the effects have to be taken into account. It is also important to note that although carrier dynamics in SOAs are usually discussed in terms of electrons in the conduction band, the same effects happen for holes in the valence band.

9. Characterization of SOAs

There are different methods, for characterizing SOAs and their response, both as a function of device parameters, the most common ones being bias current, temperature and output power, and injection signal parameters, for example wavelength, input power and state of polarisation. All the figures presented in this section represent curves that were determined experimentally with the device under test, except Figure 11 where one set of curves available from the manufacturer for a similar device is given. The SOA is temperature controlled at 20°C by means of a Peltier cooler. The signals are coupled in and out of the SOA using aspheric lenses mounted on three-axes micro-positioners.

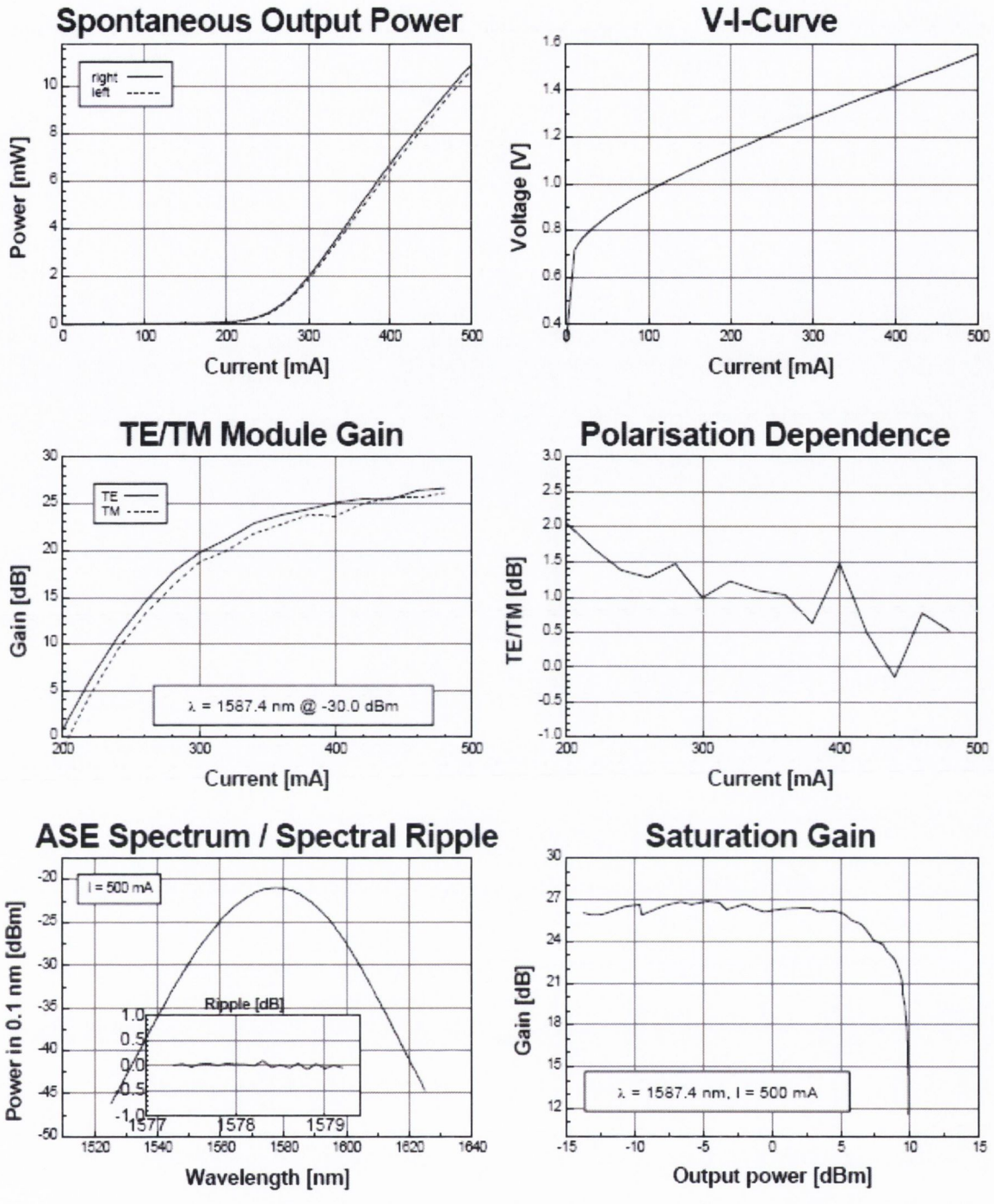

Spectral ASE data		Power data		Measurement	
λ_{peak}:	1578.3 nm	Opt. P_{left}:	10.7 mW	Date:	10.12.02
λ_{center}:	1577.5 nm	Opt. P_{right}:	10.94 mW	T_{sens}:	20 °C
Bandwidth:	30.2 nm	PDG:	1.5 dB	OP:	RBR
Ripple:	0.17 dB	$Gain_{max}$:	26.6 dB		
		3 dB P_{sat}:	8.2 dBm		

Figure 11. Certificate of conformance of a SOA similar to the device under test (provided by the same supplier).

9.1 Amplified spontaneous emission

The light-output characteristics are presented on Figure 12. The output power is measured using a germanium integrating sphere connected to Melles Griot power meter and placed directly after the coupling lens. Similar results are obtained on both sides of the SOA. As the bias current is increased, the number of injected carriers increases. Below 220mA, the rate of radiative and non-radiative carrier recombination is higher than the rate of generation of excited carriers and no light is emitted. Above 220mA, the amplified spontaneous emission (ASE) dominates.

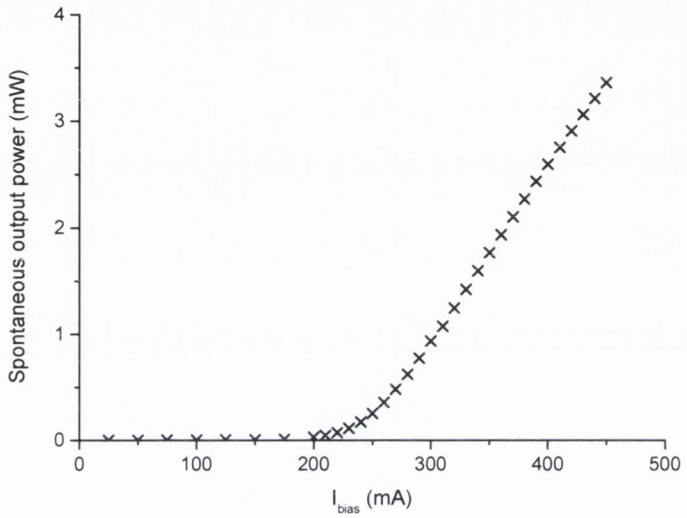

Figure 12. L-I curve of the device under test.

The spontaneous emission is only amplified over a finite range of wavelengths where optical gain occurs. Its spectrum is measured with a fiberised Agilent optical spectral analyser (OSA) with a resolution of 0.7nm. The emission spectrum of the ASE is shown at a bias current of 400mA on Figure 13. It features a peak at 1574nm and a 3dB linewidth of 27nm. The large difference between the output powers measured on Figure 12 and Figure 13 is due to the coupling of the output signal into a patch optical fibre connected to the OSA.

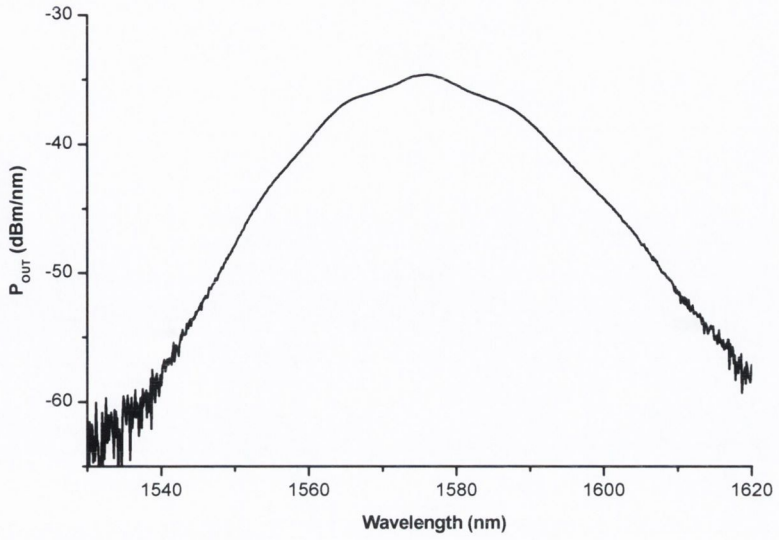

Figure 13. Spontaneous output emission spectrum for I_{bias}=400mA.

As will be discussed in the next chapter, the single pass gain can be calculated from the ASE spectrum over a range of wavelengths and bias currents. Figure 14 shows the single pass gain spectra of the TM mode at two bias currents. At 450mA, a peak gain of about 28dB is measured around 1577nm while at 300mA a peak gain of about 23dB is measured around 1582nm. The gain increases with bias current as more carriers are available for optical gain, while the peak wavelength decreases slightly. These values are consistent with the module gain given by the manufacturer.

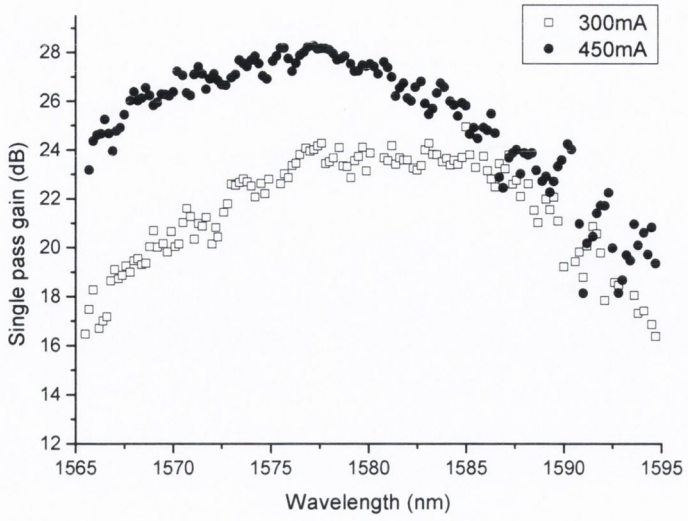

Figure 14. Single pass gain calculated from the ASE spectra of the TM mode at two different values of bias current.

9.2 Continuous wave injection

Because of the small dimensions of the waveguides, the optimisation of the input signal injection is of prime importance. In order to ensure correct optical injection, the output of the SOA is monitored by means of an OSA. As the input signal travels through the SOA, a peak appears on top of the ASE spectrum. Then as the injection is optimised, the power of the peak increases while the ASE level decreases due to the depletion of the carriers by stimulated emission. Figure 15 shows the spectra with and without injected signal. A decrease of the ASE level by 6dB when injecting a 2.3dBm signal is observed, demonstrating good optical injection.

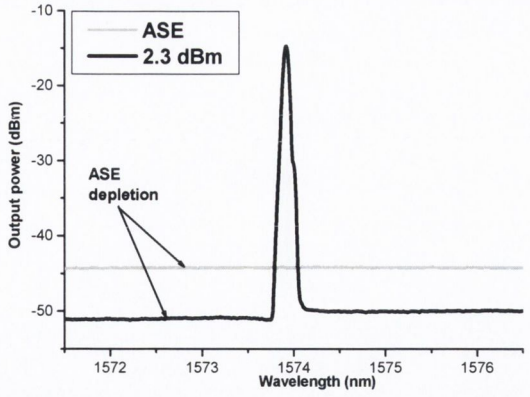

Figure 15. Spectrum of the SOA output with and without light injection, showing depletion of the ASE level as carriers are used for signal amplification.

The signal gain is measured using the OSA. The ASE noise is taken into account as well as the losses due to the coupling into the fibre. The ASE level is measured for each data point and subtracted from the output signal, while the OSA coupling loss is added to the measured output signal. However the coupling losses encountered at the input and output of the SOA are not added since it is the signal gain that is measured here, not the single-pass gain. It is interesting to note here that the gain values provided by the manufacturer seem to match the single pass gain (chip gain) rather than the signal gain. It is therefore very probable that in this case an estimate of the coupling losses have been added to the measured data [2].

The signal gain of the TE and TM modes are given on Figure 16 as a function of bias current and input signal wavelength. At lower bias currents, a negative gain is measured as losses (due to coupling and carrier recombination) dominate. From 250mA, the signal is amplified. As the bias current is increased, the population inversion increases causing the signal gain to increase as the availability of carriers increases. Above 325mA the signal gain stabilises as the availability of carriers is no longer a limiting factor.

Amplification in SOAs is restricted to a finite range of wavelength due to two major reasons. Firstly it is because of the waveguiding properties of the device, as optical waveguides possess a finite bandwidth. And secondly it is also due to the finite bandwidth of the optical gain. The measurement of the signal gain as a function of wavelength was limited by the wavelength range of the tuneable laser source. As was

the case for the ASE spectrum and single pass gain spectrum, a maximum is observed between 1575 and 1580nm. At lower wavelength absorption occurs, the gain then increases with wavelength and reaches its maximum and then decreases slightly towards higher wavelengths.

The only information regarding the polarisation dependence of the gain provided by the manufacturer is the difference between the TE and TM gains as a function of bias current. The measured data are shown in the inset of Figure 16(a). The polarisation dependence varies with bias current with no clear trend and reaches a maximum difference of 2dB at 150mA. As can be seen on Figure 16(b) the gain difference decreases with increasing wavelength, measured at a constant bias current of 350mA and an input power of -17.5dBm. The polarisation sensitivity was also found to be dependent on input power, as will be discussed in more details in chapter 3.

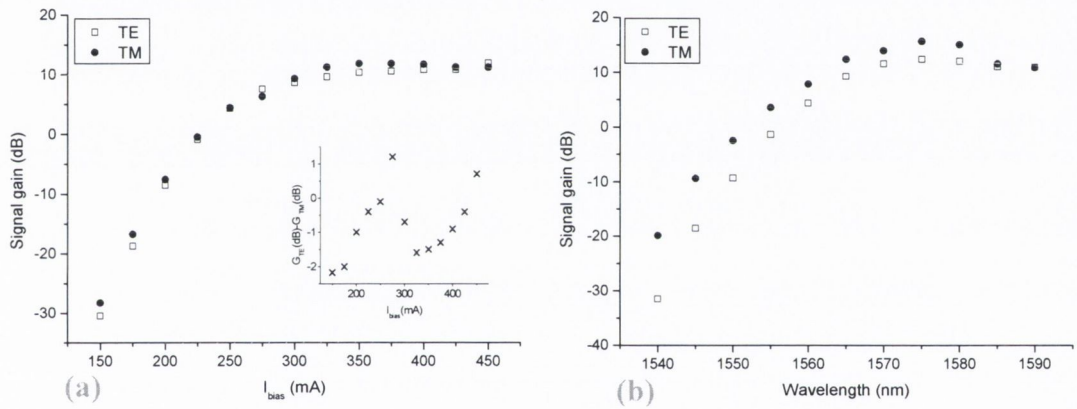

Figure 16. Signal gain of the TE and TM modes, (a) measured as a function of bias current λ=1580nm, P_{in}=-17.5dBm, polarisation dependence as defined by manufacturer given in the inset, (b) measured as function of wavelength, I_{bias}=350mA, Pin=-17.5dBm.

Amplification in SOAs is also limited to a finite range of input and hence output power [2]. The bias current creates a fixed amount of population inversion at a particular rate and on the other hand the amplification process is continuously draining the inverted population by stimulated emission. As the input power is increased, a point comes where the rate of draining due to amplification is greater than the rate of pumping, such that the population inversion level can no longer be maintained at a constant value and

starts to fall. This saturation is often characterized by the signal gain versus output power curve, as shown on Figure 17. The saturation output power is found at the -3dB point, for the device under test P_{sat}=-0.14dBm for the TE mode, which corresponds to an input power of -9.5dBm. Saturation occurs earlier for the TM mode where P_{sat}=-2.6dBm for $P_{in\,(SAT)}$ = -17.5dBm.

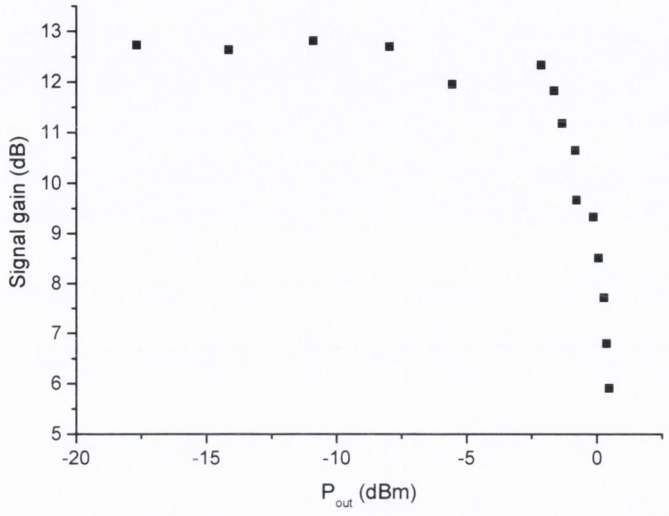

Figure 17. Signal gain versus output power measured for the TE mode, showing gain saturation, I_{bias}=350mA, λ=1580nm.

High saturation output power is a desirable characteristic for power booster applications, where gain saturation can lead to signal distortion, as well as multichannel systems where gain saturation limits the achievable gain. However gain saturation is useful for switching applications, where a high intensity beam is used to saturate the gain and therefore modulate the output of a probe beam. In that case the output signal of a low power (probe) beam is modulated by the gain saturation induced by a high power (pump) signal. This will be investigated both in the continuous wave regime, chapter 4 and the dynamic regime, chapter 5 and 6.

9.3 Dynamics

For switching applications the behaviour of the SOA in the dynamic regime must be investigated. To this end pump probe studies are usually performed, where two pulses are injected into the device and the output of the probe signal is monitored as a function of time delay between pump and probe pulses. Figure 18 shows a typical contra propagation pump probe curve obtained in the gain regime. Depending on the time delay, the probe either travels independently from the pump signal, or experiences gain compression due to pump amplification. The gain compression is either due to the pump and probe signal being both amplified and in the device at the same time or the probe experiencing the carrier depletion due to the pump once the pump pulse has left the SOA after being amplified. In the latter case, the gain recovery can be studied. The dynamic behaviour of the SOA under test is the subject of chapters 5 and 6.

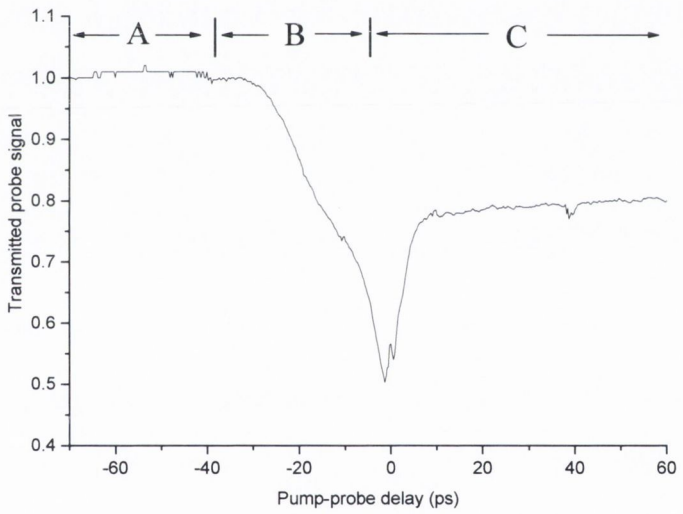

Figure 18. Typical contra-propagation pump-probe curve. Showing probe transmission (signal normalised by its value when not affected by the pump) as a function of pump probe delay. A: probe travels independently from pump pulse, B: probe gain decreases as pump pulse is amplified, C: probe gain compression recovers.

9.4 Aging of devices

The device under test was used intensively for almost four years. Over this amount of time degradation of the SOA properties can be expected. In particular a clear increase in the Fabry-Perot ripples due to residual reflections at the input facets was observed, especially in the TM mode. An increase in facet reflectivity causes an increase in optical feedback. Since part of the input signal is reflected and re-amplified, the gain of the amplifier may also increase. However because of the extra depletion of carriers by photons travelling back and forth in the cavity, the saturation power decreases. While the ripples measured earlier on had amplitudes lower than 0.3dB, they later increased to 2-3dB. This could explain the fact that the output saturation power measured from Figure 17 is significantly lower than that provided by the manufacturer.

10. Model

A model was developed [39], based on previous work performed by T.Durhuus et al [40]. It is briefly described here and used to illustrate some of the SOA gain properties as well as the relationship between the amplified spontaneous emission and the carrier density distribution in the device.

10.1 Principle

This model is based on a numerical solution of the travelling wave description of the E-field in the amplifier cavity [41-43]. The cavity is divided into sections with a constant carrier density and the program calculates the variation of the E-field and carrier density in each section along the SOA, as shown on Figure 19. The main advantage of this method is that the spatial dependence of the light and of the carrier density can be accessed. As well as the forward and backward propagating signal field in each section, $E_{(+/-)m}$, the intensity of spontaneously emitted photons, $I_{(+/-)sp}$, propagating in both forward and backward directions is also included. The reflectivity of each end facet is taken into account by r_1 and r_2 respectively. The positions at the beginning and end of each section are represented by the variables z_{-m} and z_{+m} respectively, where m is the section number.

The plane wave spectrum of the E-field traveling through section m is given by :

$$E_m(w,z) = \int_{-\infty}^{+\infty} \hat{E}_m(t,z)e^{iwt}\,dt$$

Where w is the optical frequency. It is then decomposed into forward (+) and backward (-) traveling fields as follows:

$$E_m(w,z) = E_m^+(w,z) + E_m^-(w,z)$$

The same method is used for the electric field due to the signal, E, and the spontaneous intensity, I_{sp}.

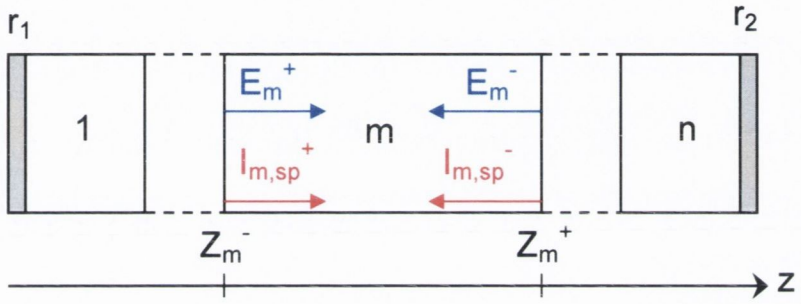

Figure 19. Model principle

For a consistent solution, boundary conditions apply. They are given for the electric field of the signal, E, but the same set of boundary conditions apply for the spontaneous intensity, I. For section m:

$$E_m^+(w,z_m^-) = E_{m-1}^+(w,z_{m-1}^+)$$
$$m = 2....n$$
$$E_m^-(w,z_m^+) = E_{m+1}^-(w,z_{m+1}^-)$$
$$m = 1....n-1$$

With special case where m =1 : $E_1^+(w,z_1^-) = r_1 E_1^-(w,z_1^-) + E^{in}(w)$

Where E^{in} is the electric field of the input signal.

And where m =n : $E_n^-(w,z_n^+) = r_2 E_n^+(w,z_n^+)$

The electric field in the time domain is described by the slowly varying envelope function, F (boundary conditions apply):

$$F_m^{\pm}(t, z_m^{\pm}) = \sqrt{G_{s,m}} e^{i\phi_m} \left[1 - i\frac{\Gamma}{2} \frac{\partial g(\omega, N)}{\partial \omega} L_m \frac{\partial}{\partial t} \right] . F_m^{\pm}(t - \tau_m, z_m^{\mp})$$

Where G_s is the single pass gain, ϕ_m is the phase shift induced by the propagation through section m, g_m is the material gain, Γ the confinement factor, L_m the length of the section and τ_m is the transit time through section m.

And the carrier density N_m in each section is calculated using the rate equation:

$$\frac{dN_m}{dt} = \frac{I_m}{eV_m} - R(N_m) - \left[g(\omega, N_m) S_{m,sig} + a_m (N_m - N_0) S_{m,spon} \right] \frac{c}{n_{g,0}}$$

Where I_m and V_m are the current and voltage applied to the section, e is the elementary charge, $R(N) = A_{tr}N + B_{rad}N^2 + C_{aug}N^3$ is the recombination rate as defined earlier, g is the material gain, $S_{m,sig}$ and $S_{m,spon}$ are the average photon densities for the signal and spontaneous emission, a_m is the gain coefficient, N_0 is the carrier density at transparency, c is the celerity of light and $n_{g,0}$ is the group index.

10.2 Material gain

The material gain function [43] used in this model is given by:

$$g(\omega, N_m) = a_m (N_m - N_0) - \gamma (\omega - \omega_p (N_m))^2$$

Where, a_m and γ are gain constants, N_0 is the carrier density at transparency and w_p is the peak wavelength.

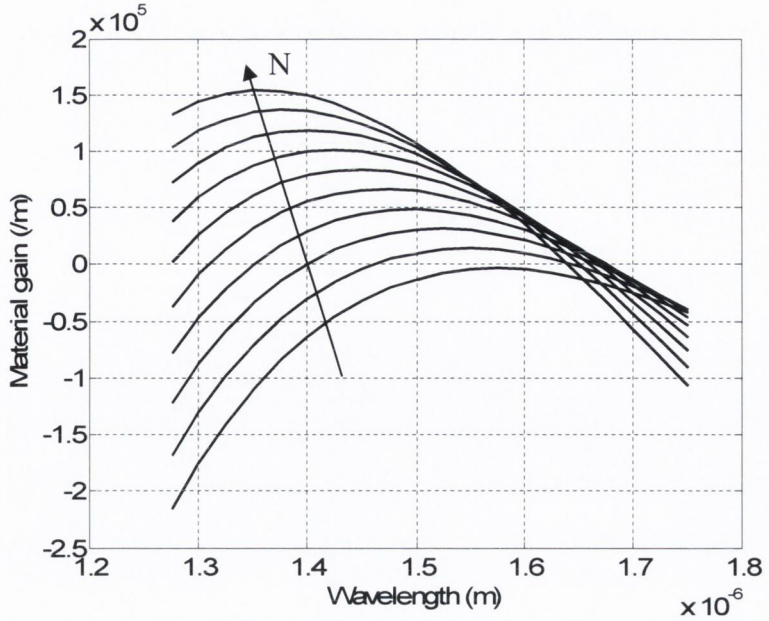

Figure 20. Material gain (m^{-1}) as a function of wavelength (m), calculated for a range of carrier densities, N ($10^{24}m^{-3}$ to $10^{23}m^{-3}$).

As can be seen on Figure 20, the range of wavelength over which amplification by the medium occurs is greater than what is measured experimentally for the device because in SOAs the gain bandwidth is not only limited by that of the material gain but also by the bandwidth of the embedded optical waveguide. As expected [10], the peak of the material gain increases linearly with carrier density, while the peak wavelength decreases linearly with carrier density. This is consistent with the single-pass gain measured experimentally in section 9.1, where the maximum gain was found to increase with bias current and a decrease in the peak wavelength with bias current was observed.

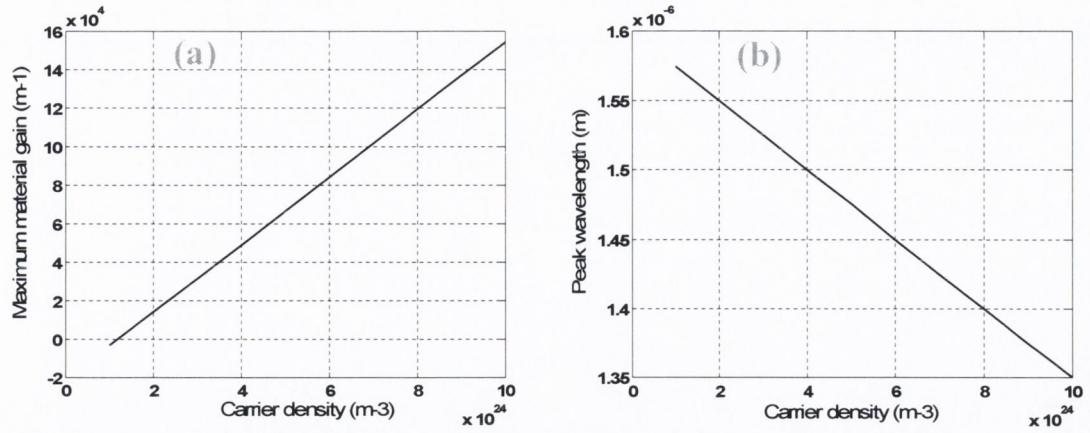

Figure 21. Coordinates of the peak material gain determined from the previous figure, (a) maximum material gain (m^{-1}) vs. carrier density (m^{-3}), (b) peak wavelength (m) vs. carrier density (m^{-3}).

10.3 Longitudinal carrier distribution

Looking first at the distribution without optical injection, carriers are provided by the bias current and depleted by the various recombination mechanisms, both radiative and non-radiative. The carrier density and spontaneous photon density in each section are given on Figure 22 (a) and (b) respectively, for different values of bias current.

When no optical signal is injected, the carrier distribution along the length of the device is symmetrical. ASE in the active region leads to a depletion of carriers, strongest at either end of device. Both the carrier density and spontaneous photon density increase with bias current. However as can be seen on Figure 22 (a), a slight decrease of carrier density with bias current can occur close to the facets. This is due to the higher depletion by the ASE.

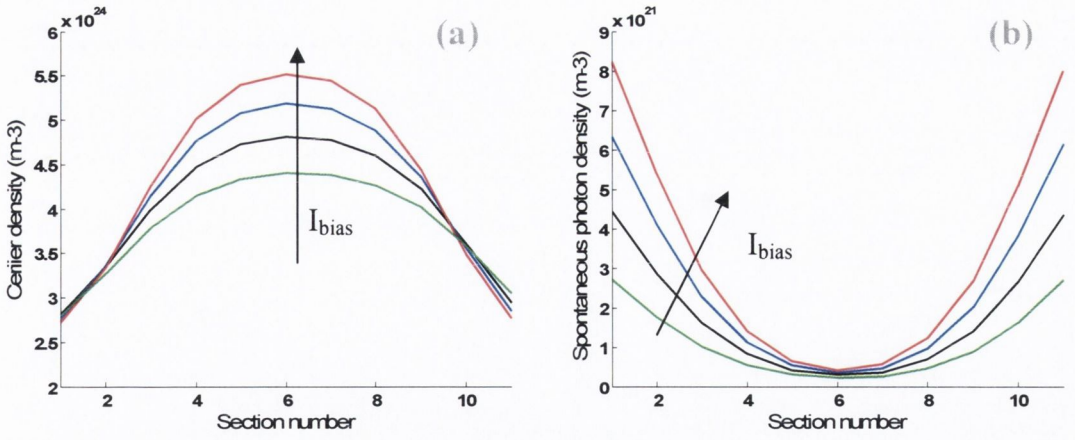

Figure 22. (a) Carrier density distribution along the device and (b) Spontaneous photon density distribution calculated for different values of bias current (50-200mA).

Further work was performed in order to model the carrier density as function of injection, with slightly different device parameters [39]. The signal is injected in the first section (m=1). As can be seen on figure 23 the carrier density distribution is symmetrical when no light is injected, as discussed before. The input signal causes a shift in the peak carrier density towards the input facet. As expected, injection of an optical signal causes a decrease of the carrier density due to stimulated emission. The effect is highest at the end of the device, where the input signal has been amplified and therefore causes higher carrier depletion. Perhaps more surprising is the increase of the carrier density with injection towards the input facet. As the input power is increased, the depletion towards the output of the device increases. This causes a decrease in the back-propagating ASE and thus a decrease in the depletion of the carriers by ASE towards the input facet [44, 45]. This is in agreement with the depletion of the ASE at the output of the device observed experimentally and discussed in section 9.2. For even higher input powers, the carrier density starts decreasing at the input facet as the depletion due to the injected signal dominates.

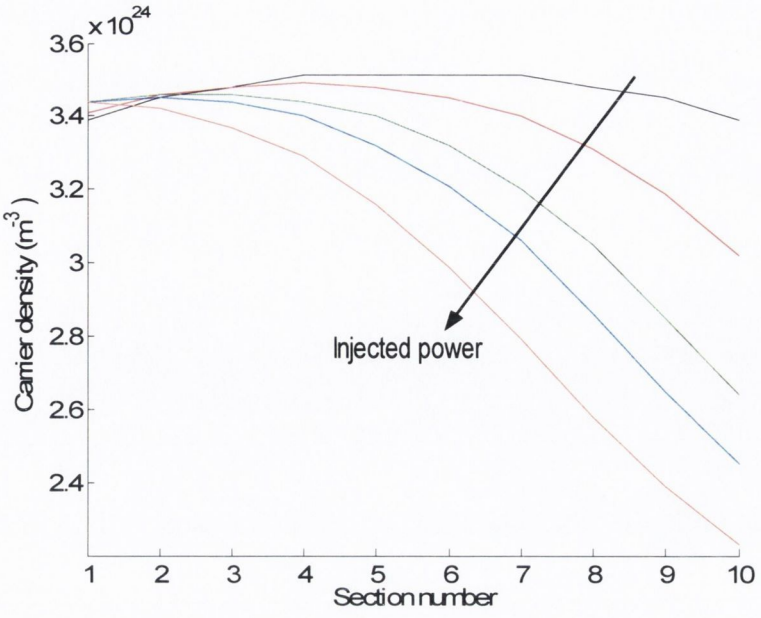

Figure 23. Carrier density distribution for different input powers (0 to 1mW).

The carrier distribution along the SOA is a function of the ASE and the injected signal. This is of critical importance for pump probe measurements, where the gain of one signal is dependent on the carrier distribution resulting from the propagation of a different signal. Moreover the experimental study presented in this work is performed in contra-propagation, therefore a different behaviour is expected under single beam injection, where carrier depletion is higher towards the output, than under two-beam injection, where carrier depletion is higher towards the input. Because of the different gain, refractive index and reflectivity experienced by the TE and TM modes, all the effects described in this section are expected to be polarisation dependent. Finally in the dynamic regime, non linear effects take place that are not included in this model and the gain experienced in each section will be influenced by the recovery of the other sections.

11. Conclusions

The basic principles behind optical amplification in SOAs, radiative processes in a two-level system and the creation of population inversion using p-n junctions, were first introduced. Then the technology used to manufacture travelling wave SOAs and reduce their polarisation sensitivity was presented, showing the critical importance of facet reflectivity, material gain, confinement factor and birefringence. The different mechanisms of carrier recombination, both radiative and non-radiative, were described, as well as the carrier dynamics following optical injection into the device. In particular, the terms of spectral hole burning and carrier heating, often used in relation to non-linear gain dynamics, were defined. The main characteristics of SOAs were then presented, together with the experimental characterization of the device under test, a bulk InGaAsP ridge waveguide. Finally a model based on the traveling wave description of the E-field in the amplifier cavity was described and used to show how the material gain relates to the experimental single-pass gain and emphasize the inhomogeneous distribution of carriers and photons in SOAs.

REFERENCES

[1] J. I. Pankove, *Optical Processes in Semiconductors*: Dover Publications, Inc, 1975.

[2] H. Ghafouri-Shiraz, *The Principles of Semiconductor Laser Diodes and Amplifiers, Analysis and Transmission Line Laser Modeling*: Imperial College Press, 2004.

[3] K. Kano, *Semiconductor devices*: Prentice-Hall, Inc, 1998.

[4] A. Yariv, *Quantum Electronics*, 3rd ed: John Wiley and Sons, 1989.

[5] M. J. Adams, *An Introduction to Optical Waveguides*: John Wiley and Sons, 1981.

[6] G. H. B. Thompson, *Physics of semiconductor devices*: John Wiley and Sons, 1980.

[7] G. P. Agrawal and N. K. Duta, *Long-wavelength semiconductor lasers*. New York: Van-Nostrad Reinhold, 1986.

[8] M. J. Connelly, *Semiconductor Optical Amplifiers*: Kluwer Academic Publishers, 2002.

[9] J. Eckner, *Semiconductor Optical Amplifiers: Optimization of Polarization and Monolithical Integration in Ridge Waveguide Bulk InGaAsP/InP. Series in Quantum Electronics. Volume 8*: Hartung-Gorre Verlag Konstanz, 1998.

[10] G. Guekos, *Photonic devices for telecommunications*: Springer-Verlag, 1999.

[11] Y. Z. Huang, Z. Pan, and R. H. Wu, "Analysis of the optical confinement factor in semiconductor lasers," *Journal of Applied Physics*, vol. 79 (8), 15 April 1996.

[12] T. D. Visser, H. Blok, B. Demeulenaere, and D. Lenstra, "Confinement factors and gain in optical amplifiers," *IEEE Journal of Quantum Electronics*, vol. 33, pp. 1763-1766, 1997.

[13] W. Wang, K. Allaart, and D. Lenstra, "Semiconductor optical amplifier gain anisotropy: confinement factor against material gain," *Electronics Letters*, vol. 40, pp. 1602-1603, 2004.

[14] T. D. Visser, B. Demeulenaere, J. Haes, D. Lenstra, R. Baets, and H. Blok, "Confinement and Modal Gain in Dielectric Waveguides," *Journal of Lightwave Technology*, vol. 14, no.5, may 1996.

[15] J. Mork, M. L. Nielsen, and T. W. Berg, "The Dynamics of Semiconductor Optical Amplifiers, Modeling and Applications," in *Optics & Photonics News*, July 2003.

[16] H. Dery, E. Benisty, A. Epstein, R. Alizon, V. Mikhelashvili, G. Eisenstein, R. Schwertberger, D. Gold, J. P. Reithmaier, and A. Forchel, "On the nature of quantum dash structures," *Journal of Applied Physics*, vol. 95, pp. 6103-6111, 2004.

[17] A. Somers, W. Kaiser, J. P. Reithmaier, A. Forchel, M. Gioaninni, and I. Montrosset, "Optical gain properties of InAs/InAlGaAs/InP quantum dash structures with a spectral gain bandwidth of more than 300 nm," *Applied Physics Letters*, vol. 89, pp. 061107, 2006.

[18] A. Bilenca, R. Alizon, V. Mikhelashhvili, D. Dahan, G. Eisenstein, R. Schwertberger, D. Gold, J. P. Reithmaier, and A. Forchel, "Broad-band wavelength conversion based on cross-gain modulation and four-wave mixing in InAs-InP quantum-dash semiconductor optical amplifiers operating at 1550 nm," *IEEE Photonics Technology Letters*, vol. 15, pp. 563-565, 2003.

[19] M. Van Der Poel, J. Mork, A. Somers, A. Forchel, J. P. Reithmaier, and G. Eisenstein, "Ultrafast gain and index dynamics of quantum dash structures emitting at 1.55mm," *Applied Physics Letters*, vol. 89, pp. 081102, 2006.

[20] E. P. O'Reilly and A. R. Adams, "Band-structure engineering in strained semiconductor lasers," *Quantum Electronics, IEEE Journal of*, vol. 30, pp. 366-379, 1994.

[21] E. Yablonovitch and E. O. Kane, "Band Structure Engineering of Semiconductor Lasers for Optical Communications," *Journal of Lightwave Technology*, vol. 6, no.8, pp. 1292-1299, August 1988.

[22] D. Lenstra, Y. Liu, M. T. Hill, G.-D. Khoe, and H. J. S. Dorren, "Nonlinear polarization rotation in semiconductor optical amplifiers: Theory and application to all-optical flip-flop memories," *IEEE Journal of Quantum Electronics*, vol. 39, pp. 141-148, 2003.

[23] J. B. D. Soole, C. Caneau, H. P. Leblanc, N. C. Andreadakis, A. Rajhel, C. Youtsey, and I. Adesida, "Suppression of Modal Birefringence in InP-InGaAsP Waveguides Through Use of Compensated Tensile Strain," *IEEE Photonics Technology Letters*, vol. 9, no.1, pp. 61-63, January 1997.

[24] G. Jones and E. P. O'Reilly, "Improved Performance of Long-Wavelength Strained Bulk-like Semiconductor Lasers," *IEEE Journal of Quantum Electronics*, vol. 39, no.5, pp. pp1344-1354, May 1993.

[25] T. Kakitsuka, Y. Shibata, M. Itoh, Y. Kadota, Y. Tohmori, and Y. Yoshikuni, "Influence of Buried Structure on Polarization Sensitivity in Strained Bulk Semiconductor Optical Amplifiers," *IEEE Journal of Quantum Electronics*, vol. 38, no.1, pp. 85-92, January 2002.

[26] T. Kakitsuka, Y. Shibata, M. Itoh, Y. Tohmori, and Y. Yoshikuni, "Numerical analysis of polarization sensitivity in strained bulk semiconductor optical amplifiers," *IEEE Proceedings 13th IPRM Naran, Japan*, pp. 485-488, 2001.

[27] C. Kittel, "Introduction to Solid State Physics," 7th ed: Wiley, 1996, pp. pp206-213.

[28] Y. Takahashi, A. Neogi, and H. Kawaguchi, "Polarization-dependent nonlinear gain in semiconductor lasers," *Quantum Electronics, IEEE Journal of*, vol. 34, pp. 1660-1672, 1998.

[29] X. Yang, D. Lenstra, G. D. Khoe, and H. J. S. Dorren, "Nonlinear polarization rotation induced by ultrashort optical pulses in a semiconductor optical amplifier," *Optics Communications*, vol. 223, pp. 169-179, 2003.

[30] J. Paul Callan, Albert M.-T. Kim, Christopher A. D. Roeser, and E. Mazur, "Ultrafast Dynamics and Phase Change in Highly Excited GaAs," in *Semiconductors and Semimetals: Ultrafast Physical Processes in Semiconductors*, vol. 67, K. T. Tsen, Ed.: Academic Press, 2001.

[31] B. N. Gomatam and A. P. DeFonzo, "Theory of hot carrier effects on nonlinear gain in GaAs-GaAlAs lasers and amplifiers," *IEEE Journal of Quantum Electronics*, vol. 26, pp. 1689-1704, 1990.

[32] A. D'Ottavi, E. Iannone, A. Mecozzi, S. Scotti, P. Spano, J. Landreau, A. Ouagazzaden, and J. C. Bouley, "Investigation of carrier heating and spectral hole burning in semiconductor amplifiers by highly nondegenerate four-wave mixing," *Applied Physics Letters*, vol. 64 (19), pp. 2492-2494, 9 May 1994.

[33] S. Hughes, "Carrier-carrier interaction and ultrashort pulse propagation in a highly excited semiconductor laser amplifier beyond the rate equation limit," *Physical Review A*, vol. 58, no3, pp. 2567-2576, September 1998.

[34] Yoshihiro Nambu and A. Tomita, "Spectral Hole Burning and Carrier-Heating Effect on the Transient Optical Nonlinearity of Highly Carrier-Injected Semiconductors," *IEEE Journal of Quantum Electronics*, vol. 30, no0, pp. 1981-1994, september 1994.

[35] T. P. Pearsall, *GaInAsP Alloy Semiconductors*: Wiley, 1982.

[36] J.-N. Fehr, M.-A. Dupertuis, T. P. Hessler, L. Kappei, D. Marti, F. Salleras, M. S. Nomura, B. Deveaud, J.-Y. Emery, and B. Dagens, "Hot phonons and auger

related carrier heating in semiconductor optical amplifiers," *IEEE Journal of Quantum Electronics*, vol. 38, pp. 674-681, 2002.

[37] J. Mark and J. Mork, "Subpicosecond Gain Dynamics in Ingaasp Optical Amplifiers - Experiment and Theory," *Applied Physics Letters*, vol. 61, pp. 2281-2283, 1992.

[38] P. Borri, S. Scaffetti, J. Mork, W. Langbein, J. M. Hvam, A. Mecozzi, and F. Martelli, "Measurement and calculation of the critical pulsewidth for gain saturation in semiconductor optical amplifiers," *Optics Communications*, vol. 164, pp. 51-55, 1999.

[39] B. F. Kennedy, "A Study of the Origin and Applications of Nonlinear Polarization Rotation in Semiconductor Optical Amplifiers," PhD thesis, Dublin City University, Electronic engineering, 2005.

[40] T. Durhuus, B. Mikkelsen, and K. E. Stubkjaer, "Detailed dynamic model for semiconductor optical amplifiers and their crosstalk and intermodulation distortion," *IEEE Journal of Lightwave Technology*, vol. 10(no.8), pp. 1056–1064, 1992.

[41] M. J. Connolly, "Wideband semiconductor optical amplifier steady-state numerical model," *IEEE Journal of Quantum Electronics*, vol. 37(no.3), pp. 439–447, 2001.

[42] L. Gillner, "Comparitive study of some travelling-wave semiconductor laser amplifier models," *IEE Proceedings in Optoelectronics*, vol. 139(no.5), pp. 339–347, 1992.

[43] I.D. Henning, M.J. Adams, and J. V. Collins, "Performance predictions from a new optical amplifier model," *IEEE Journal of Quantum Electronics*, vol. 21(no.6), pp. 609–613, 1985.

[44] S. Ruiz-Moreno and J. Guitart, "Practical method for modelling the nonlinear behaviour of a travelling wave semiconductor optical amplifier," *IEE Proceedings in Optoelectronics*, vol. 140(no.1), pp. 39–42, 1993.

[45] F. Salleras, M. S. Nomura, J. N. Fehr, M. A. Dupertuis, L. Kappei, D. Marti, B. Deveaud, J. Y. Emery, B. Dagens, and T. Shimura, "Longitudinal spatial hole burning in a gain clamped semiconductor optical amplifier," presented at Pacific Rim Conference on Lasers and Electro-Optics, CLEO - Technical Digest vol.1, 2002.

CHAPTER 3:
CHARACTERIZATION OF POLARISATION EFFECTS IN THE CONTINUOUS WAVE REGIME

1. Introduction

The main causes of the polarisation sensitivity in SOAs have been attributed to the inherent birefringence, i.e. different refractive indices in the TE and TM modes of the devices, the difference between the confinement factor [1] and material gain [2, 3] of the TE and TM modes. Some groups have looked at the underlying physical origins of non-linear polarisation rotation [4-7], but a full characterisation of the polarisation change has yet to be performed. In this chapter an experimental study of polarisation rotation in the continuous wave (CW) regime is undertaken. Firstly the principles of polarisation of light and means by which it can be described, measured and controlled are reviewed. Two techniques are then used to investigate the gain and birefringence along the two eigen modes of the component waveguide, with and without injection. The first method is based on the residual reflectivity of the facet mirrors. From the modulation depth of polarisation resolved spectra, we determine the gain and the refractive indices of these modes using the Hakki-Paoli method [1]. The second investigation takes into account the variation of the eigen mode gain and refractive indices as a function of the input power of a single injected CW beam.

2. Polarisation control and measurements

2.1 Polarised light

Polarisation is the phenomenon in which waves of light or other radiation are restricted in direction of vibration. More generally, polarisation is a characteristic of transverse waves and describes the direction of oscillation in the plane perpendicular to the direction of travel. The discovery of polarisation [8] is usually attributed to Bartholinus for his observation of double refraction in calcite. Working on the corpuscular theory of light, Newton suggested that the effect of double refraction

might indicate that particles of light were asymmetric. Malus used the idea to explain the double-refraction phenomenon by suggesting that the particles could be considered to initially be randomly oriented. Then as they passed through a double-refracting crystal they aligned and became ordered. In analogy to magnetic bodies Malus suggested that the particles had poles and called the oriented light 'polarized light'.

The state of polarisation of light is very sensitive to the optical properties of a medium. Sources of polarised light as well as ellipsometry are therefore used as tools in the study of material and interfaces optical properties, in spectroscopy, and in organic chemistry where many liquids show an ability to rotate the polarisation azimuth of a light wave called optical activity. The human eye sensitivity to the light state of polarisation, demonstrated by C.V. Raman [9] is restricted to high intensity in the blue-violet sector of the spectrum. This sensitivity however does not allow any precise measurements to be performed. For this reason different methods have been developed in order to characterize and measure polarisation.

2.2 Description and measurements

The description of light used in this thesis is based on Maxwell's approach in which light is described as an electromagnetic wave. Light waves require four basic field vectors for their complete description [10]: the electric field strength $\underline{E}$, the electric displacement density $\underline{D}$, the magnetic field strength $\underline{H}$ and the magnetic flux density $\underline{B}$. Of theses four vectors the electric field strength is chosen to define the state of polarisation of light waves. This choice is based on the fact that when light interacts with matter, the force exerted on the electrons by the electric field of the light wave is much greater than the force exerted by its magnetic field. In general once the polarisation of the electric field is known, the polarisation of the three remaining fields can be found using Maxwell's field equations and the associated material relations. Therefore in this work only the electric field component need be considered to describe the light.

The displacement of an electromagnetic wave is a vector quantity. Its polarisation specifies the magnitude and displacement of the wave. The direction of the displacement vector is called the direction of polarisation and the plane containing the direction of polarisation and the propagation vector is called the plane of polarisation.

The polarisation of light is usually defined by the behaviour of the electric vector, E with time, t, observed at a fixed point is space, z. There are different complementary methods [8, 11] of describing polarised light, including Jones vectors and the Poincaré sphere, however the main ones used here are based on the polarisation ellipse and the Stokes parameters.

2.2.1 Polarisation ellipse

Consider a plane wave propagating in the z direction and the electric field orientated in the x,y plane (or TE,TM plane). The electric field $\hat{E}$ propagating along the z direction as a function of time, t, can be expressed as:

$$\vec{E} = e^{i(\omega t - kz)}(\vec{E}_{0TE}e^{i\phi_{TE}} + \vec{E}_{0TM}e^{i\phi_{TM}}) \qquad (1)$$

Where w is the optical frequency, k the wave number, $\hat{E}_{0TE(0TM)}$ the $\hat{E}$ component in the TE(TM) direction and $\phi_{TE(TM)}$ its phase.

The phase difference between the two components is $\Delta\phi = \phi_{TM} - \phi_{TE}$ and the phase is related to the refractive index by:

$$\phi_{TE(TM)} = \frac{2\pi L n_{TE(TM)}}{\lambda} \qquad (2)$$

Where λ is the wavelength, L is the length of material travelled, and $n_{TE(TM)}$ its refractive index in the TE(TM) direction.

The equation for the electric field can also be written as:

$$\left(\frac{E_{TE}}{E_{0TE}}\right)^2 + \left(\frac{E_{TM}}{E_{0TM}}\right)^2 - \left(\frac{2E_{TE}E_{TM}}{E_{0TE}E_{0TM}}\right)\cos\Delta\phi = \sin^2\Delta\phi \qquad (3)$$

Which is the equation of an ellipse, called the polarization ellipse (Figure 1). The TE and TM coordinates of the electric field are bounded by $\pm E_{0TE}$ and $\pm E_{0TM}$.

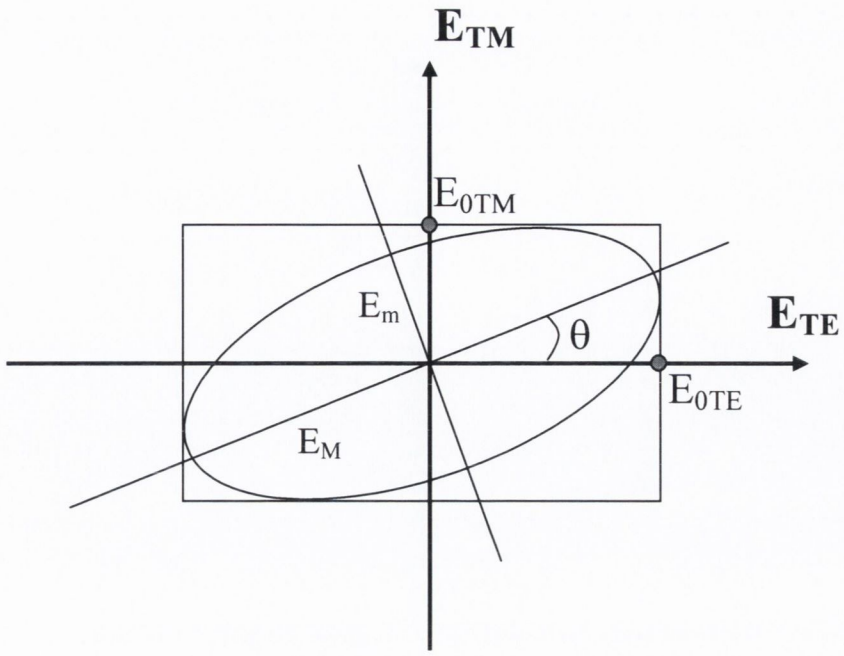

Figure 1. Polarisation ellipse.

The orientation of the ellipse with respect to the TE axis, θ, is

$$\tan 2\theta = \frac{2E_{0TE}E_{0TM}\cos\Delta\phi}{E_{0TE}^2 - E_{0TM}^2} \tag{4}$$

The ellipticity, e, of the ellipse is the ratio of the minor to the major axis and represents the amount of deviation of the ellipse from a circle. An ellipticity of 0 represents a linear polarisation and an ellipticity of 1 represents a circular polarisation. The sign of the ellipticity is defined by convention, negative for left-handed polarisation, positive for right-handed polarisation.

$$\tan e = \pm\frac{E_{0TE}\sin\phi_{TE}\sin\theta - E_{0TM}\sin\phi_{TM}\cos\theta}{E_{0TE}\cos\phi_{TE}\cos\theta + E_{0TM}\cos\phi_{TM}\sin\theta} \tag{5}$$

Therefore the tip of the electric field vector describes an ellipse in the plane normal to z and the wave polarisation is completely characterised by the two parameters (ellipticity and orientation) of the polarisation ellipse.

2.2.2 Jones vectors

The Jones vectors can be used to describe polarized light of known amplitude and phase with a small number of parameters. The Jones vector is defined as a 2-row column matrix consisting of two complex components in the TE and TM directions:

$$E = \begin{bmatrix} E_{0TE} \exp\{i(wt - k \cdot z + \phi_{TE}\} \\ E_{0TM} \exp\{i(wt - k \cdot z + \phi_{TM}\} \end{bmatrix} \qquad (6)$$

Where $E_{0TE(TM)}$ is the amplitude of the TE(TM) component and the other symbols have their usual meaning.

2.2.3 Stokes parameters and Mueller calculus

The polarimeter used to characterize the polarisation of the light signals is based on intensity measurements of the Stokes parameters.

The state of polarisation of an electromagnetic wave can be described by a Stokes vector. The Stokes vector is a 4x1 real matrix of Stokes parameters, which are measurable quantities and are defined as follow.

- **S0**: Total intensity. In our case the polarimeter output is normalised, therefore S_0=1.
- **S1**: Difference between intensity transmitted by a linear polariser oriented parallel to the TE axis and one oriented parallel to the TM axis.
- **S2:** Difference between intensity transmitted by a linear polariser oriented at 45° to the TE axis and one oriented at 135°.
- **S3**: Difference between intensity transmitted by a right-circular polariser and a left-circular polariser.

The equation for the electric field (1) contains no measurable quantities and must therefore be modified in order to establish the relationship between the polarisation

ellipse and the Stokes parameters. To simplify the calculation the amplitudes of the orthogonally polarized waves and their relative phase are assumes to be constants. The time average of (3) can be written as:

$$\frac{\langle E_{TE}{}^2 \rangle}{E_{0TE}} + \frac{\langle E_{TM}{}^2 \rangle}{E_{0TM}} - 2\frac{\langle E_{TE}E_{TM} \rangle}{E_{0TE}E_{0TM}}\cos\Delta\phi = \sin^2\Delta\phi \qquad (7)$$

Multiplying both sides by $(2E_{0TE}E_{0TM})^2$ gives:

$$4E_{0TM}^2\langle E_{0TE}^2 \rangle + 4E_{0TE}^2\langle E_{0TM}^2 \rangle - 8E_{0TE}E_{0TM}\langle E_{TE}E_{TM} \rangle\cos\Delta\phi = (2E_{0TE}E_{0TM}\sin\Delta\phi)^2 \qquad (8)$$

The time average of each term can be calculated [11] as:

$$\langle E_{TE}^2 \rangle = \frac{E_{0TE}^2}{2}, \langle E_{TM}^2 \rangle = \frac{E_{0TM}^2}{2}, \langle E_{TE}E_{TM} \rangle = \frac{1}{2}E_{0TE}E_{0TM}\cos\Delta\phi \qquad (9)$$

Substituting in (8) and adding $E^2{}_{0TE}+E^2{}_{0TM}$ on both sides, the equation can be rewritten as:

$$(E_{0TE}^2 + E_{0TM}^2)^2 - (E_{0TE}^2 - E_{0TM}^2)^2 - 2(E_{0TE}E_{0TM}\cos\Delta\phi)^2 = 2(E_{0TE}E_{0TM}\sin\Delta\phi)^2 \qquad (10)$$

Each term can be identified with a Stokes parameter. The amplitude and relative phase of the orthogonally polarized waves need not be constants if the Stokes parameters are defined as temporal averages and the terms become:

$$S_0 = \langle E_{0TE}^2 \rangle + \langle E_{0TM}^2 \rangle$$
$$S_1 = \langle E_{0TE}^2 \rangle - \langle E_{0TM}^2 \rangle$$
$$S_2 = \langle 2E_{0TE}E_{0TM}\cos\Delta\phi \rangle$$
$$S_3 = \langle 2E_{0TE}E_{0TM}\sin\Delta\phi \rangle$$

And equation (10) becomes $S^2_0 - S^2_1 - S^2_2 = S^2_3$, i.e. for a polarized wave only three of the Stokes parameters are independent. The Stokes parameters can be written in terms of parameters of the polarisation ellipse:

$$S_1 = S_0 \cos 2e \cos 2\theta$$
$$S_2 = S_0 \cos 2e \sin 2\theta$$
$$S_3 = S_0 \sin 2e$$

The Stokes parameters can be used to determine the degree of polarisation, defined as:

$$P = \frac{\sqrt{S_1^2 + S_2^2 + S_3^2}}{S_0}$$

Partially polarised light is represented as follows:

$$P\begin{vmatrix} S_0 \\ S_1 \\ S_2 \\ S_3 \end{vmatrix} + (1-P)\begin{vmatrix} S_0 \\ 0 \\ 0 \\ 0 \end{vmatrix}$$

The Poincaré sphere is a geometrical construction based on the Stokes parameters used to describe the state of polarisation of a light wave. The parameters S_1, S_2, S_3 are viewed as Cartesian coordinates of a point on a sphere of radius S_0, as shown on Figure 2. On the Poincaré sphere, right-handed polarisation is represented by points on the upper half surface. Linear polarisation is represented by points on the equator. Circular polarisation is represented by the poles. The Poincaré sphere was widely used in order to visualize the effect of an anisotropic medium on polarized light but its usefulness has decreased since it was discovered that the Stokes parameters could be treated as elements of a column matrix and Mueller calculus could be used. From the intensity measurements of the polarimeter used in the following experiments and the associated software, the Stokes parameters, degree of polarisation, polarisation ellipse and Poincaré sphere representation are available.

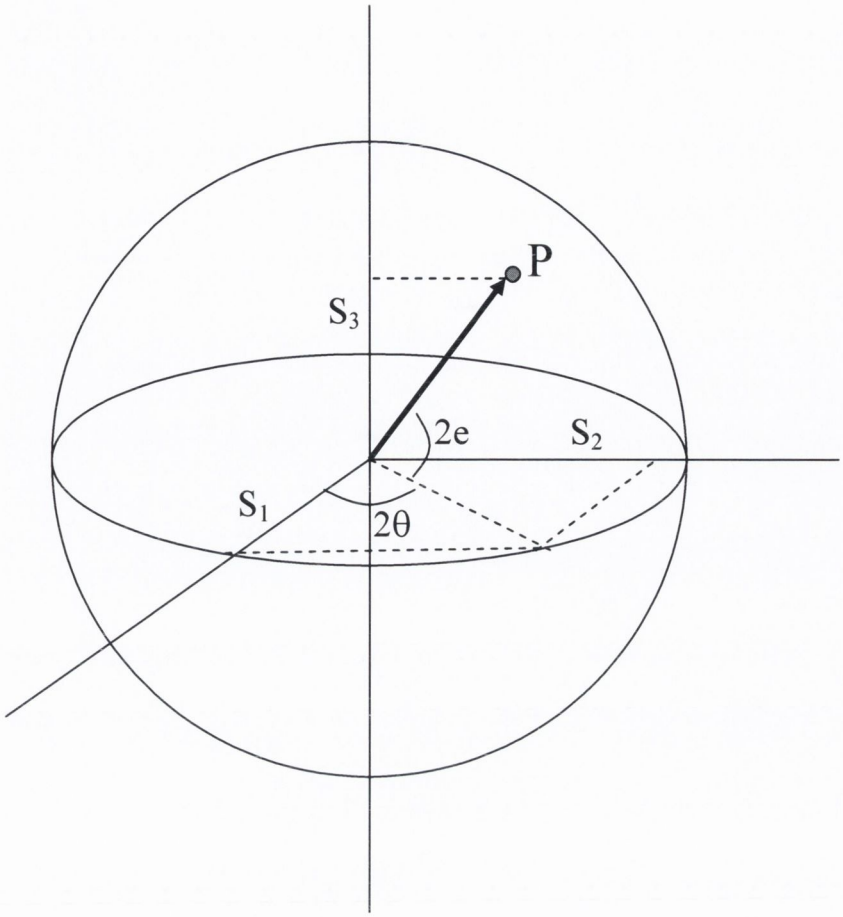

Figure 2. Poincaré sphere.

When light is represented as a Stokes vector S, the effect of an optical component (e.g. beamsplitter, mirror, and polarizer) transforming the incoming polarisation state S into S' can be represented by M, a 4x4 Mueller matrix so that S'=MS or:

$$\begin{vmatrix} S_0' \\ S_1' \\ S_2' \\ S_3' \end{vmatrix} = \begin{vmatrix} m_{11} & m_{12} & m_{13} & m_{14} \\ m_{21} & m_{22} & m_{23} & m_{24} \\ m_{31} & m_{32} & m_{33} & m_{34} \\ m_{41} & m_{42} & m_{43} & m_{44} \end{vmatrix} \begin{vmatrix} S_0 \\ S_1 \\ S_2 \\ S_3 \end{vmatrix}$$

Here M is the Mueller matrix of the optical device that transforms S, the input signal Stokes vector, into S', the output signal Stokes vector.

2.2.4 Comparison between Jones and Mueller matrices

The fundamental difference is that the physical parameters of the Jones formalism are amplitude and phase while those of the Mueller formalism are intensities [12]. The main advantage of the Stokes parameters and Mueller matrices is that their elements are directly measurable. Unlike the Stokes vector, the Jones vector is a theoretical description and cannot handle unpolarised or partially polarised light. However the Jones matrix is derived from the Maxwell's equations and as such presents a mathematical rigour that the Mueller matrix lacks, since it arises from the assumption that the incident Stoke vector is linearly related to the emergent one. As the Stokes parameters are measurable quantities they are mores suited to the present experimental study.

2.3 Control

2.3.1 Polarizer

Polarizers transmit a beam of light whose electric field vector oscillates in a plane that contains the beam axis. Incident light whose electric field vector has a component perpendicular to the transmission direction of the polarizer have that component absorbed, reflected, or deflected, depending on the type of polarizer used. For extremely precise measurements, as is the case in this work, it is important to keep in mind that some polarizers are not homogeneous along the beam axis [8]. In fact if polarization takes place in the middle of the polarizer, the light may be depolarized by imperfections as it leaves. Since the light emerges from a different face depending on the direction of propagation, the performance of the polarizer may vary. Therefore the component should be tested so that the best configuration is used. Another problem affecting the performance is that some polarizers are not homogeneous along their polarizing axis, causing the performance to vary as the polarizer is rotated. In practice this was found to have a greater influence than the lack of homogeneity along the beam axis and the only way to avoid errors due to the polarizer performance is to make sure the beam is precisely perpendicular to the polarizing axis and centred on the polarizer axis of rotation.

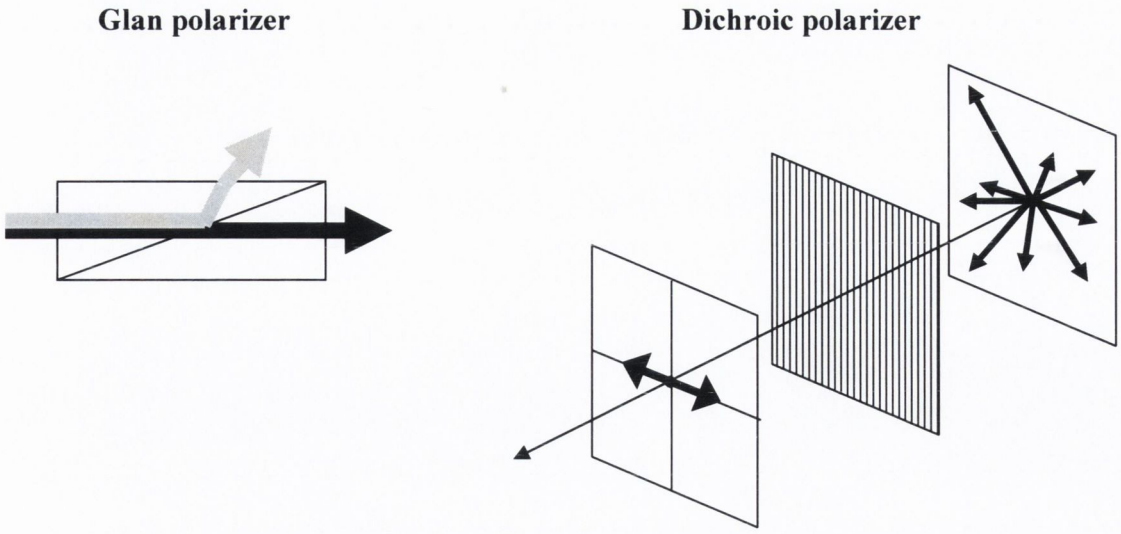

Figure 3. Two types of polarizer used in the experimental set-up.

Figure 3 shows the two different types of polarizer used in the following experiments: birefringence polarizers and dichroic polarizers [8]. Birefringence polarizers take advantage of double refraction in uniaxial crystals. A compound prism is used to create a situation where, over a small range of angles, one polarisation undergoes total internal reflection while the other is transmitted. While the main advantage of these birefringence polarizers is their high extinction ratio, they are also able to handle high energy beams and some are fabricated so that the component removed from the transmitted beam is also available in a second beam. Dichroic polarizers take advantage of linear dichroism which corresponds to the absorption of one of the two orthogonally polarized components of the incident beam. Molecules in a plastic sheet are oriented so that their transition dipole moments are aligned along a particular axis. Light polarized along this axis is then absorbed, whereas light polarized perpendicularly is transmitted [13]. A major advantage of dichroic polarizers is their lower cost but what proved invaluable in the following experiments is their small thickness which minimised the perturbation of the experimental set-up alignment. Their extinction ratio and power handling capacity were found to be sufficient. As a result the birefringence polarizers were gradually removed as the complexity of the set-up increased and alignment became more of an issue.

2.3.2 Retarder

Retarders allow the phase of two orthogonal polarization components of light to be varied with respect to one another. Two different retarders are used in the set-up, a quarter wave plate and a half wave plate. Retardation is an effect of the refractive index, as light passes from a vacuum to a transparent body, the speed of light is reduced by a factor that is the reciprocal of the refractive index [8]. Since the frequency of light remains constant, the phase angle of the light changes more rapidly with position inside the body than it did in the vacuum. As a consequence the phase of light required to traverse the body is increased compared to what it would have been to traverse the same distance in vacuum. In birefringent plate retarders a phase difference between the two linearly polarized components of light is introduced, when the phase shift introduced is 90° the retarder is called a quarter wave plate and when the phase shift is 180° it is call a half wave plate. The retardance of birefringent plates is strongly dependent on the wavelength of light. Commercial retarders are available for 1550nm wavelengths and as the input beams used here have a wavelength of 1580nm, both a half wave plate and a quarter wave plate are needed in order to rotate the input polarization.

3. Underlying properties - Spectral analysis

The device is first studied without any light injection in order to determine the inherent polarisation dependence of the device. A bias current is applied and the amplified spontaneous emission (ASE) is measured using a polarimeter and an optical spectrum analyzer (OSA).

3.1 ASE state of polarisation

Measuring the ASE state of polarisation with the polarimeter, the polarisation ellipse shown on Figure 4(a) appears predominantly TM due to the waveguiding properties of the device. However looking more closely at the degree of polarisation it is actually largely unpolarised, as can be seen on Figure 4(b) where the bias current dependence of the degree of polarisation is given. At lower bias, the degree of polarisation

increases with bias current, reaching a maximum of 22% at 250mA and then starts decreasing. At our working point of 350mA the ASE is 13% polarized.

(a) Polarimeter response for the ASE (300mA bias)

(b) Bias Current Dependence

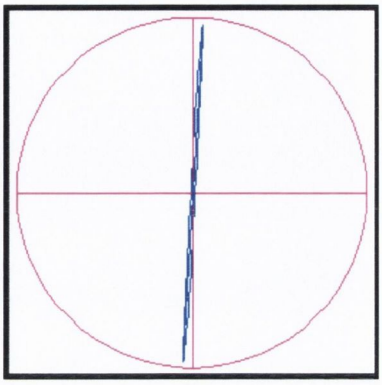

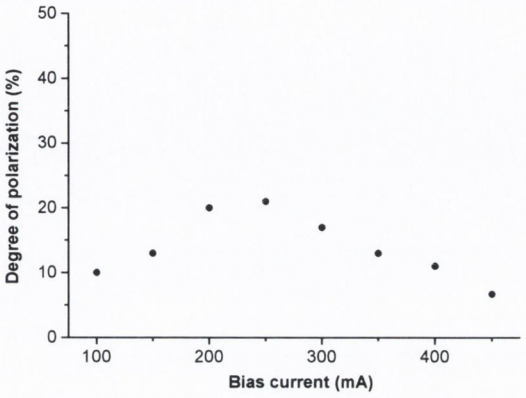

Figure 4. State of polarization of the ASE, (a) Measured at I_{bias} = 300mA (ellipticity = 0.01, orientation = 86°), (b) Degree of polarization of the ASE as a function of bias current.

3.2 Measurement of ASE spectra

The polarisation resolved amplified spontaneous emission (ASE) spectra, Figure 6, are recorded for both eigen modes using an optical spectrum analyser (OSA). The SOA is temperature controlled at 20°C with a Peltier cooler. The output of the SOA is collected and collimated using a microscope objective. Then a Glan polarizer selects either the TE or TM component of the output before it is coupled into a single mode fibre using a second objective lens and sent into an OSA, as shown on Figure 5. The best wavelength resolution available is used, 0.07nm and averaging is used during the acquisition in order to minimise the effect of vibrations and temperature drift. Indeed the sensitivity of the device to changes in temperature was found to be critical, with changes as low as 0.01° at the thermistor leading to up to 1dB decrease in the output ASE level in the gain region. Therefore a PID controller is used in conjunction with the Peltier cooler and the set-up is left to stabilise for approximately an hour each time the bias current is changed.

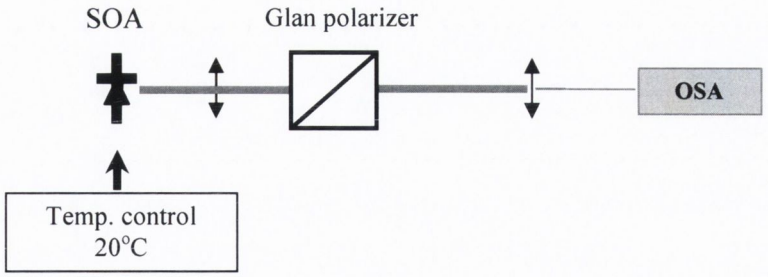

Figure 5. Experimental set-up for ASE spectral measurements.

Figure 6 shows one of the polarisation resolved spectra measured. A modulation due to Fabry-Perot resonances is clearly observed at high bias currents, despite the anti-reflection coating of the facets. The ASE signal power is about 3 to 5mW and the low power displayed on the OSA trace is due to the large losses of the coupling into the single mode fibre. The ripples can be seen to go in and out of phase as the wavelength changes, showing inherent birefringence of the device.

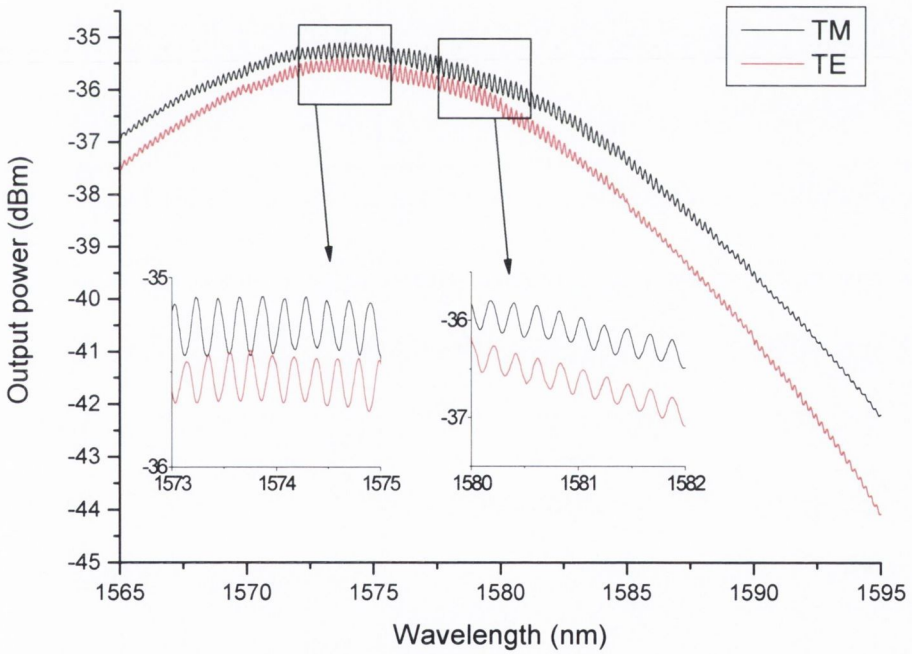

Figure 6. Polarisation resolved ASE spectra of the TE and TM modes for I_{bias}=400mA.

3.3 Single pass gain calculation

From the modulation depth of the ripples, we can determine the wavelength dependence of the gain [1, 14] and the refractive indices for TE and TM modes. The so-called Hakki-Paoli method was first used to study lasers but due to residual reflections at the facets it is possible to perform similar gain measurements in travelling wave SOAs. The only limitation is a smaller range of wavelengths and bias currents over which the depth of modulation is high enough for precise measurements. For this reason the spectra were measured at bias currents over 300mA and wavelength between 1565nm and 1595nm. Outside this range the modulation depth of the ripples is too shallow to yield accurate results.

A Matlab based program is used to extract the gain spectra from the ASE spectra. The maxima and minima of the Fabry-Perot resonances are stored, as well as the wavelength at which they are measured. The gain reflectivity product spectrum,γ, is calculated from the formula:

$$\gamma(\lambda) = \frac{\sqrt{r(\lambda)} - 1}{\sqrt{r(\lambda)} + 1} \qquad (11)$$

where r the modulation depth around the troughs is given by:

$$r_i = \frac{P_i^{\max} + P_{i+1}^{\max}}{2P_i^{\min}} \qquad (12)$$

P^{max} i and $i+1$ represent neighbouring peak modulation power values and P^{min} the minimum power between these peaks. γ is linked to the single pass gain, G by:

$$\gamma = \sqrt{R_1(\lambda)R_2(\lambda)}G(\lambda) \qquad (13)$$

where R_1 and R_2 are the reflectivities of the output facets. We assume that the R_1 and R_2 are equal and constant over the spectral range of our study, in accordance with reference [15]. The single pass gain is calculated from the TE and TM spectra, as shown in Figure 6, using Eqs. (11) to (13).

3.4 Results

Figure 7 shows the calculated TM and TE single pass gain spectra for a range of bias. As the current increases, the peak value of the gain increases for both modes. It is interesting to note that for bias currents from 350mA to 450mA and wavelengths between 1575 and 1580, where the gain is maximal, the single pass gains in TE and TM are approximately equal, as quoted by the manufacturer.

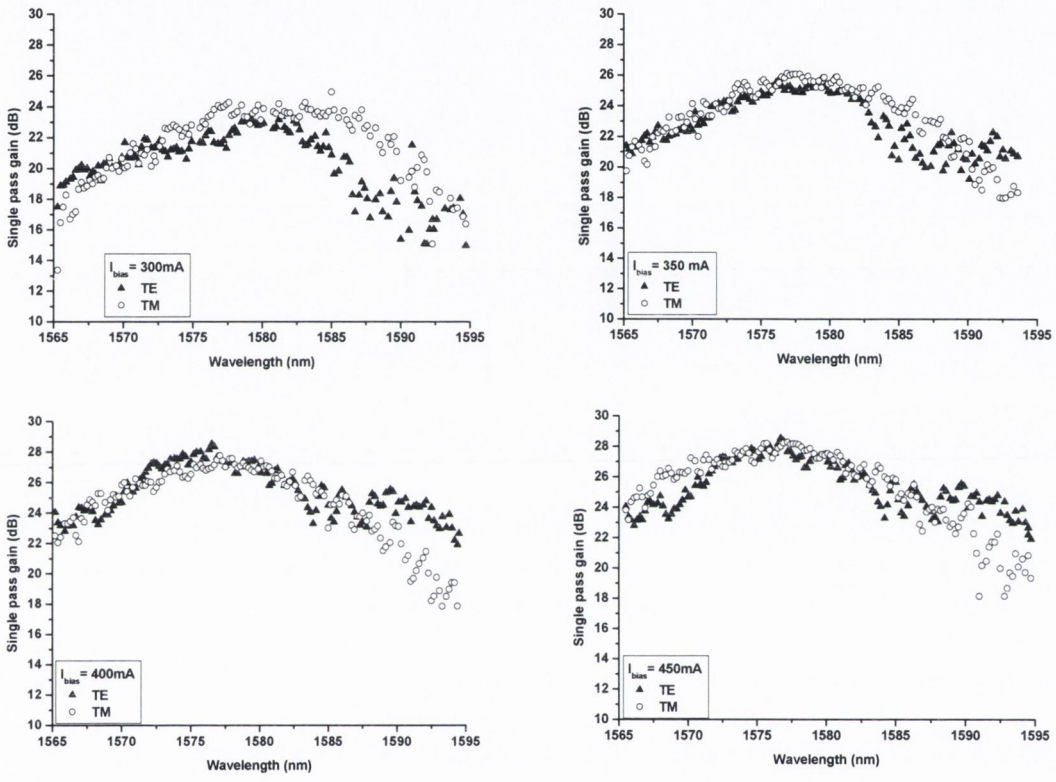

Figure 7. Polarisation resolved gain spectra calculated from the ASE spectra for a range of bias currents.

3.5 Birefringence

Birefringence has also been mentioned as an effect responsible for non-linear polarisation rotation [7, 16]. In order to observe and quantify this effect, the refractive index is calculated for both the TE and TM modes. If there is a birefringent effect in the device then the period of the modulation ripples is different for both polarisations since light travels at different speeds for each mode. In other words, the ripples in the ASE spectrum go in and out of phase with respect to each other, due to the small but

finite difference in the periods of the ripple [17]. These effects can be seen in the insets of Figure 6. Both modulations are in phase at 1581nm, however, at 1574nm they are out of phase. This means that there are different refractive indices for the TE and TM modes, indicating birefringence in the device. The refractive index is measured using the ASE spectra recorded for the gain calculations. Using the definition of the free-spectral range in a Fabry-Perot resonator, the refractive index for both modes can be calculated:

$$\Delta\lambda = \frac{2n_{g,eff}L}{k} - \frac{2n_{g,eff}L}{k+1} = \frac{2n_{g,eff}L}{k(k+1)} \approx \frac{\lambda^2}{2n_{g,eff}L} \qquad (3)$$

where λ is the wavelength, $n_{g,eff}$ is the effective group refractive index, L is the length of the device and k is the wavevector. Using this equation we can extract $n_{g,eff}$ as a function of wavelength. $\Delta\lambda$ is the trough to trough wavelength separation, as measured from the ripples on the ASE spectra in Figure 6 and λ is taken as the central wavelength from trough to trough. In this way a refractive index can be calculated for each central wavelength. Figure 8 (a) and (b) show the effective refractive index dependence from 1560nm to 1590nm at 400mA for the TE and TM modes respectively.

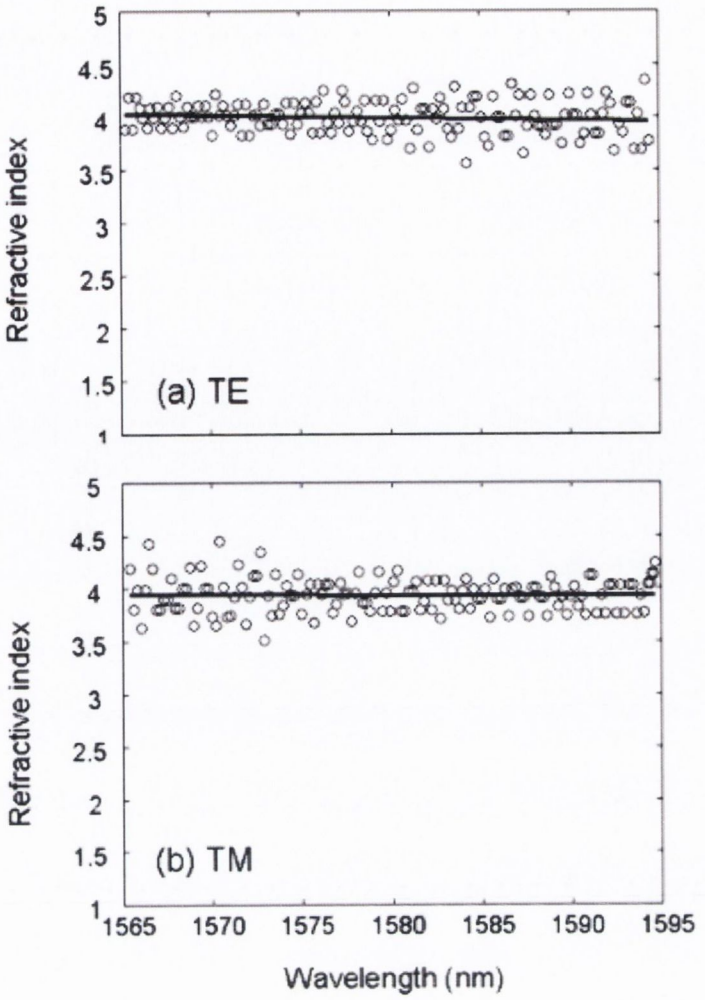

Figure 8. Refractive index calculated from the Fabry-Perot ripples at 400mA bias current for (a) the TE mode and (b) the TM mode

The effective refractive index is found to be 4.03 for the TE mode and 3.95 in the TM mode, where the refractive index was averaged over the complete range of wavelengths, from 1560nm to 1590nm, providing experimental evidence of the birefringence of the device under study. While these values are consistent with previously documented results [15], Figure 8 clearly shows that the scattering of the data is larger than the calculated difference in refractive indices. Therefore quantitative characterisation of the device birefringence cannot be achieved with this method.

Furthermore we can consider the dispersive nature of the semiconductor material and the dispersion parameter for each mode can be extracted using the following expression:

$$n_{g,eff} = n_{eff} - \lambda \frac{dn}{d\lambda} \qquad (4)$$

Where $n_{g,eff}$ corresponds to the refractive index found from the free spectral range, n_{eff} is effective wavelength independent refractive index and $dn/d\lambda$ the dispersive term. It is found that the scatter of the refractive index data, in Figure 8, is too large to extract a meaningful quantitative value. However it is clear from the slope that the dispersion parameter for the TE mode is less than that of TM, in agreement with the results from [15]. Therefore the TE refractive index is higher than the TM refractive index and this difference between refractive indices decreases slightly with increasing wavelength. This birefringence is a second possible origin of the NPR in the SOA.

In conclusion, without injected light the single-pass gain in the TE and TM modes were found to be close, with less than 2dB difference at 1580nm, and a small birefringence was measured.

4. Single beam injection

The behaviour of the SOA is now investigated under continuous wave (CW) injection. The changes in polarisation undergone by a single CW beam are studied as a function of different parameters of the SOA and input signal [4].

4.1 Experimental set-up

The SOA is biased at 350mA and temperature controlled at 20^0C by means of a Peltier cooler. Figure 9 shows the one beam injection set-up. The probe signal is provided by a HP8168F tuneable laser source. The polarisation of the free space signal is controlled by several components. Firstly by a polarizer in order to achieve a linearly polarised signal, secondly by a half-wave plate in order to rotate the linearly polarised signal and lastly by a quarter-wave plate to compensate the mismatch between the operating wavelength of the device and the operating wavelength of the plates. The optical signal is then launched into the SOA using a 0.25NA AR

microscope objective. The launching conditions are optimised using the two mirrors and micro-control lens mounts. The SOA output is then collected and collimated using a second microscope objective. Different possibilities are used at the detection end of the set-up: a photodiode is used for alignment purposes, a fibre coupler and an OSA are used for optimisation of the light injection. For polarisation measurements, a band-pass filter centred at 1580nm with a bandwidth of 10nm is placed in front of the polarimeter to reduce the influence of the random polarisation of the ASE.

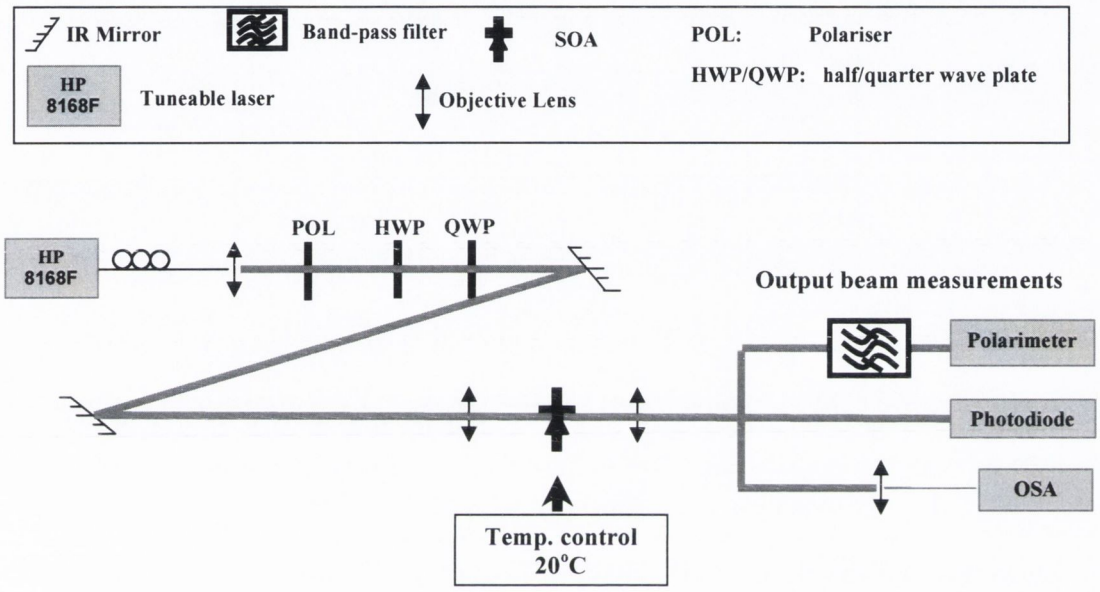

Figure 9. One beam injection set-up.

4.2 Characterization of non-linear polarisation rotation

The state of polarisation of the input beam is set as linear and its orientation rotated between 0° and 90°. For each orientation the output state of polarisation is recorded for a range of injected powers at a bias current of 350mA and an injection wavelength of 1580nm. This wavelength was specifically chosen since it corresponds to the peak gain of the TE and TM modes as shown in Figure 7. The parameters of the polarisation ellipse, orientation and ellipticity, are shown on Figure 10 and Figure 11. When light is injected along the eigen modes of the device (θ_{in}=0° and θ_{in}=90°), the output orientation remains mostly unchanged and the ellipticity close to 0, showing that no significant modification of the principal axis of the device are detected over

the range of power injected. The largest changes in orientation and ellipticity seem to occur between 40° and 60° injection. As the power of the input beam is increased, the behaviour seems more linear. In other words the change in the state of polarisation is less dramatic, with the ellipticity getting closer to 0 and the output orientation staying closer to the input orientation.

As the injection angle increases the ellipticity decreases, reaching a minimum at 48°, independently of input power. A minimum of –0.94 is achieved at 48° injection for 166μW of injected power. At the minimum of ellipticity curves, the output is approaching a circular polarisation. The fact that the minimum is reached at an input angle greater than 45° indicates that the TE gain must be greater than the TM gain. For example at an input orientation of 48°, there will be more light injected into the TM mode than the TE mode and in order for the output to approach a circular polarisation the gain in TE mode must compensate for the lower injected power. The negative sign shows that the output polarisation is of left-handed rotation, which is consistent with the TE axis being slower than the TM axis ($\phi_{TE} > \phi_{TM}$), as was measured in the spectral analysis. At 90° the ellipticity is zero, the linear input is injected along the TM mode, propagates and is amplified along this mode. This indicates that there is no measurable modification of the principal axes over this power range.

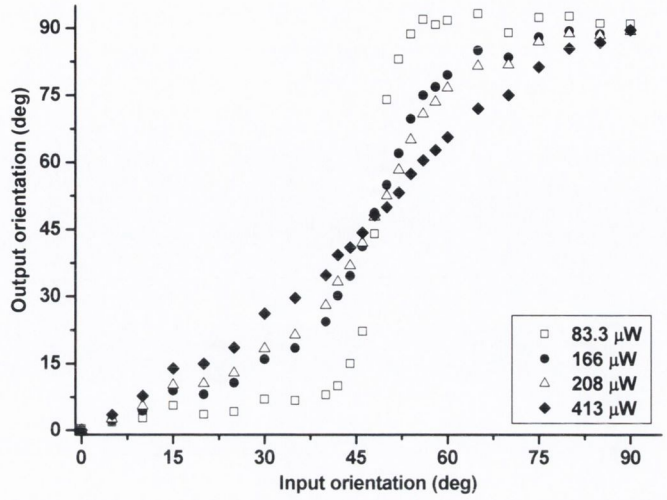

Figure 10. Output orientation as a function of input orientation for different input powers. I_{bias} = 350mA, Input linearly polarised, λ = 1580nm.

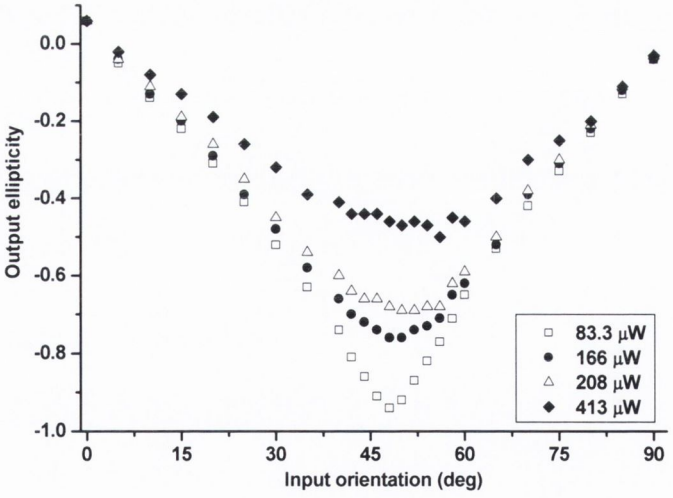

Figure 11. Output ellipticity as a function of input orientation for different input powers. I_{bias} = 350mA, Input linearly polarised, λ = 1580nm.

4.3 Modelling

4.3.1 Principle

In order to develop a more quantitative understanding of the experiment, a Matlab based model was written. It is based on a propagating electric field, Ê, having two components aligned along the modes of the waveguide. The two components are assumed to travel independently through the SOA, experiencing different refractive indices and gain, before being recombined at the output.

$$\vec{E} = e^{i(\omega t - kz)}(\vec{E}_{0TE}e^{i\phi_{TE}} + \vec{E}_{0TM}e^{i\phi_{TM}})$$

where, $\hat{E}_{0TE(TM)}$ is the $\hat{E}$ component at the output of the device corresponding to the TE (TM) direction and its phase is $\phi_{TE(TM)}$. $\hat{E}_{0TE}$ and $\hat{E}_{0TM}$ are expressed as:

$$\begin{cases} \vec{E}_{0TE} = \rho E\cos(\theta_{in})\vec{u}_{TE} \\ \vec{E}_{0TM} = E\sin(\theta_{in})\vec{u}_{TM} \end{cases}$$

where, ρ is the ratio of the single pass gain in the TE mode to the one in the TM, θ_{in} is the input angle and $\hat{u}_{TE(TM)}$ is the unit vector along the horizontal (vertical) axis. The amplitude E of the input field is taken to be unity in our model. The phases ϕ_{TE} and ϕ_{TM} are defined as follows:

$$\phi_{TE(TM)} = \frac{2\pi L n_{TE(TM)}}{\lambda}$$

Where L is the length of the device, $n_{TE(TM)}$ is the refractive index of the TE(TM) mode and λ the wavelength of the input signal.

There are two input parameters to the model, the gain ratio ρ related to the different gain experienced by each component, and the relative phase $\Delta\phi$ related to the different refractive index experienced by each component. The program calculates both components, E_{TE} and E_{TM}, of the electric field, and traces the polarisation ellipse. Both the ellipticity, e, and the orientation θ_{out} are then extracted. One example of the

calculated output polarisation ellipse can be seen in Figure 12. The ellipticity is found by dividing the minimum amplitude A_{MIN} of the E field by its maximum A_{MAX}. The orientation is calculated by using the equation given on the figure.

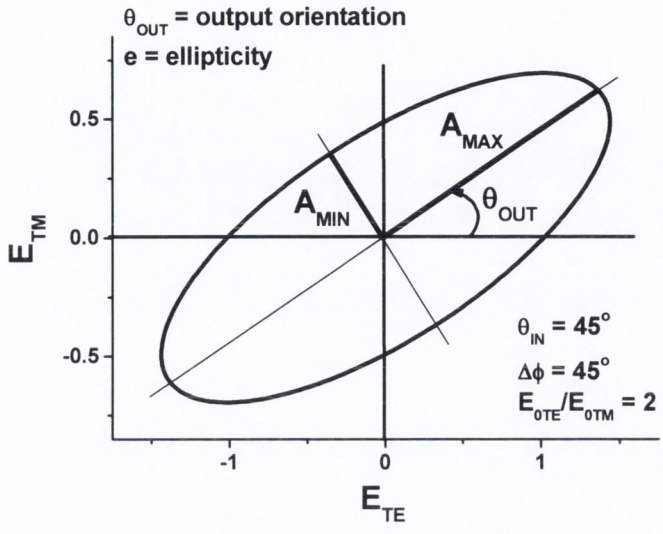

$$|e| = A_{MIN}/A_{MAX}$$

$$\theta_{OUT} = \frac{1}{2}\tan^{-1}\left(\frac{2E_{0TE}E_{0TM}\cos\Delta\phi}{E_{0TE}^2 - E_{0TM}^2}\right)$$

Figure 12. Calculated output polarisation ellipse for input parameters $\rho = 2$ and $\Delta\phi = 45°$, and equations used to calculate its ellipticity and orientation.

This is repeated for each input orientation. The output ellipticity and orientation curves are plotted as a function on the input orientation. The input parameters are then adjusted so that the calculated curves fit the experimental data as well as possible. This allows the phase shift and gain ratio introduced by the device to be followed as a function of the input power. It is important to note here that the output ellipticity and output orientation are parameters of the same ellipse and are only presented in separate curves for more clarity.

4.3.2 Parameters

The effects of the input parameters on the output ellipticity and orientation curves are shown on Figure 13. The curves are given for different values of one of the parameters while the other one is fixed (ρ=1 or $\Delta\phi$=45°). Looking first at the effect of the phase parameter on the ellipticity (a), the minimum reached by the ellipticity decreases from a linear output when $\Delta\phi$=0 to a circular output when $\Delta\phi$=-90° and

θ_{in}=45°. If we kept decreasing the phase from -90° to -180°, the minimum value would increase back to 0. Keeping the phase parameter constant and varying the gain parameter, (b), causes the input orientation for which the ellipticity reaches its minimum value to change. If the gain is higher in TM than in TE the minimum occurs at input angles below 45° and if it is higher in TE than in TM, the minimum occurs above 45°. Looking now at the effect of the same parameter, ρ, on the orientation (d) the input angle at which the output orientation reached 45° increases with the TE to TM gain ratio. Finally varying the phase parameter affects the linearity of the orientation curves (c), with a linear dependence on the input orientation when $\Delta\phi$=0 to a step-like variation when $\Delta\phi$=-90°.

One limitation of this model is that the sign of the ellipticity and quadrant of the phase shift are not determined directly from the program. Because of the use of the tangent and cosine functions and the ambiguity of the sign of the ellipticity, different phase shifts can give the same results. The simplest way to determine the quadrant where the phase shift lies is to look at the experimental data as well, then from the addition of a sine and cosine functions:

If	$0°<\theta_{out}<90°$	and	$e>0$,	$0°<\Delta\phi<90°$.
If	$-90°<\theta_{out}<0°$	and	$e>0$,	$90°<\Delta\phi<180°$.
If	$-90°<\theta_{out}<0°$	and	$e<0$,	$-180°<\Delta\phi<-90°$.
If	$0°<\theta_{out}<90°$	and	$e<0$,	$-90°<\Delta\phi<0°$.

Since the measured output orientation was positive and the ellipticity negative, the phase shift in our case is between -90° and 0° (mod 2π).

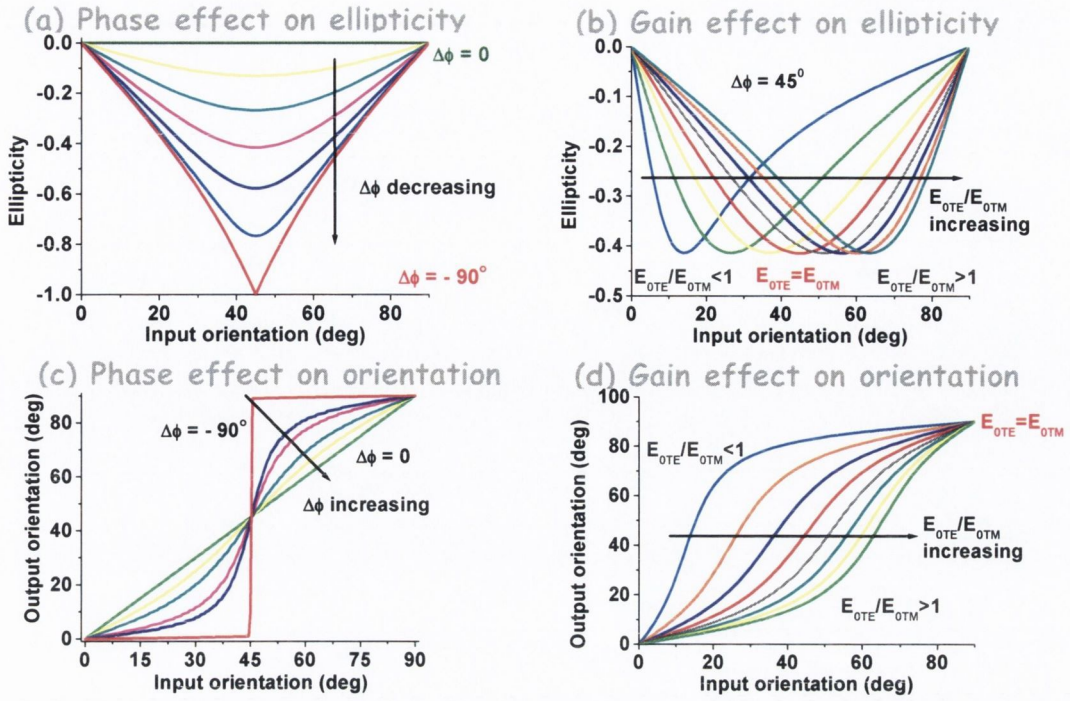

Figure 13. Effect of the model parameters on the output ellipticity and output orientation versus input orientation curves.(a) Phase parameter effect on ellipticity, ρ=1, $\Delta\Phi$ varied between 0° and -90°. (b) Gain parameter effect on ellipticity, $\Delta\Phi$=45°, ρ varied between 0.125 and 4. (c) Phase parameter effect on orientation, ρ=1, $\Delta\Phi$ varied between -90° and 0°. (d) Gain parameter effect on orientation, $\Delta\Phi$=45°, ρ varied between 0.125 and 4.

Another limitation of the model is that it only gives relative values, i.e. a phase shift and a gain ratio and thus do not allow us to access directly the values of the TE and TM gains and refractive indices.

4.4 Analysis

The model was then applied to fit the experimental data. As shown in Figure 14, a good correspondence can be achieved and the parameters ρ and the phase difference $\Delta\phi = \phi_{TM} - \phi_{TE}$ can be extracted for each injected power. Furthermore the same parameters give good agreement when applied to fitting the output orientation as a function of input orientation over a range of injected power showing that the birefringence and gain effects does not depend on the input polarisation angle for our experimental conditions. The fit of the ellipticity data is better than that of the

orientation data. However the best fit parameters for the ellipticity were found to be the same as the best fit parameters for the orientation. An offset of 4° can be seen on the orientation curves, especially away from the eigen modes of the device. Its origin is not clearly understood, although the preferential TM polarisation of the ASE, a small rotation of the eigen modes and optical feedback effects in the set-up can be contributing factors. Optical feedback is due to reflections at lens surfaces and at the tip of the launching fibre, causing a small part of the injected beam to travel back into the set-up. Further measurements taken after replacing the microscope objectives by achromatic lenses showed that the effect was reduced, without affecting the ellipticity data and best fit parameters. Further investigation of the offset will be presented below.

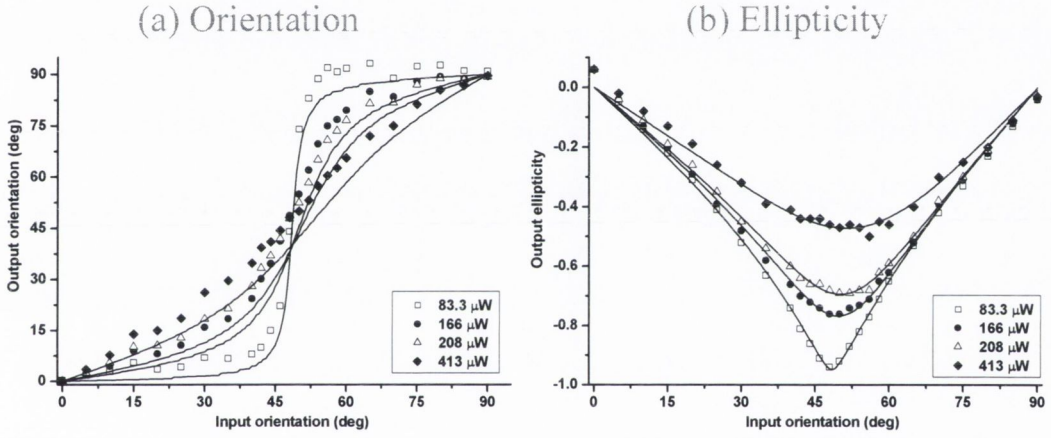

Figure 14. One beam injection: polarisation data fit.

Figure 15 illustrates the power dependences of the best fit gain and phase parameters. Within the range of injected power, the gain ratio increases up to a value of 1.25 for an injected power of *413 μW*. Indicating that the single pass TE gain becomes increasingly greater than the single pass TM gain. This is consistent with the saturation effect observed in chapter 2, where the saturation power for the TM mode was found to be smaller than that of the TE mode. As the injected power is decreased towards zero, ρ converges towards 1 indicating the single pass TE gain approximates to the single pass TM gain. This is consistent with the results of Figure 7, where the gain spectra are obtained under conditions of no injection.

The phase difference $\Delta\phi$ is negative, meaning that the $\hat{E}$ field rotates counter clockwise. As the phase is defined mod 2π it is not possible to relate it directly to the refractive indices. This approach is limited since only relative gain and phase difference values can be extracted. However it is obviously a powerful technique for determining the polarisation sensitivity of the SOA devices and also identify which mode is more susceptible to gain saturation. As mentioned earlier the sample under test is sold commercially as a low polarisation sensitivity device, but here we can clearly see a change in polarisation under standard operating conditions. This indicates that SOAs hold potential for the exploitation of these polarisation effects.

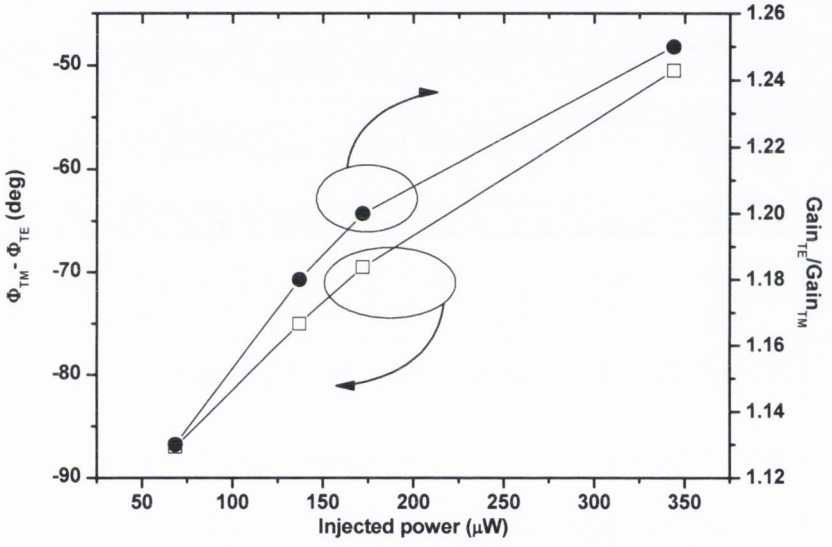

Figure 15. Best fit parameters as a function of injected power.

4.5 Rotation of the principal axis.

As discussed before when light is injected along one of the principal axis, TE or TM, its polarization remains mostly unchanged. Because of that in the previous experiment the phase shift and relative gain can be determined by rotating the input polarisation over 90°. However a small change can sometimes be measured and output ellipticities between 0 and 0.02° and orientations up to 3° were recorded for a TE polarised input. This alteration of the state of polarisation when injecting along the principal axes is not expected and is dependent on injected power and bias current. It has been suggested that this modification is due to modes other than the fundamental propagating through the SOA [16, 18]. Under injection of an optical beam, the refractive index variation, due to the change in carrier density [19], modifies the confinement factor of the waveguide. For large optical power, this can lead to higher order modes being supported by the waveguide [20].

Using the same experimental set-up as before, but replacing the objective lenses by anti-reflection coated aspheric lenses in order to reduce the offset in the orientation data, a rotation of the principal axes should cause an asymmetry in the data recorded between -90° and 0° and those recorded between 0° and 90°. This rotation can then be quantified by introducing a rotation of the principal axis in the model before fitting the curves with the gain and phase parameters. The rotation given here is the difference between the horizontal direction and the TE axis. An example of the fit obtained with and without introducing the rotation is shown on Figure 16. Once again the ellipticity data are used to find the best fit parameters: the TE axis oriented at 5° from the horizontal, a phase difference $\Delta\phi$ of -77° and a relative gain ρ of 1.2. It follows that the rotation of the eigen axes contributed to the disparity between experimental data and best fit curves in the previous section. However as can be seen on Figure 16, the effect of this rotation on the orientation curves does not account for an offset of 4° for all data points and therefore the effect of optical feedback cannot be ruled out.

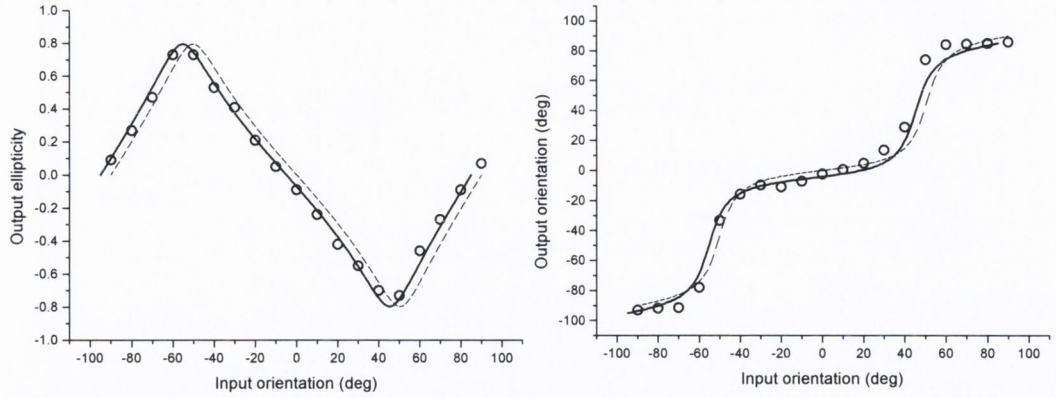

Figure 16. Fitting used to determine the rotation of the principal axes of the SOA. o: data points, solid line: best fit obtained with TE oriented 5° from the horizontal, dash line: best fit obtained without introducing the rotation (the same parameters are used in both cases, $\rho = 1.2$, $\Delta\phi = -77°$). I_{bias} =350mA, λ = 1580nm, P_{in} = 208μW.

This rotation is dependent on the power of the input beam, varying from 2° at lower powers to a maximum of 5°, as well as on the bias current injected and can therefore not be attributed to the way the SOA is mounted or the orientation of the device. It is associated with the underlying physical properties of the SOA device. While this method does not give any information on the origin of the rotation, it is a powerful tool to measure it in the continuous wave regime and could potentially be used to study its dependence on input beam and device parameters.

5. Conclusion

The origin of the non-linear polarisation rotation in semiconductor optical amplifiers was studied using two different techniques. Two phenomena were considered as sources of the NRP: the asymmetric gain between the TE and TM modes and the birefringence. In the first experiment, without injected signal, the underlying properties of the waveguide are probed. Polarisation resolved ASE spectra were recorded and the gain and refractive index for the two eigen modes of the SOA waveguide were calculated. It was found using this method, that a difference in the refractive indices of the two modes could be determined, with the refractive index along the TE axis greater than that along the TM axis. Furthermore estimations of

effective refractive indices of the two modes could be extracted. The values obtained are in agreement with the literature.

In the second experiment, a new approach has been developed to investigate the gain and refractive index differences of the two eigen modes. The change in polarisation state of an injected signal at the output of the device is measured using a polarimeter. From the fit of the experimental results, with a basic electric field propagation model, we are able to measure the TE and TM gain ratio and the birefringence as a function of injected power. It is found that even though the TE and TM gains are close under low optical injection, consistent with the gain extracted from the analysis of the ASE spectra, the difference in gain between the two modes increases with increasing injected power. The phase difference between TE and TM modes was found to get closer to zero as the injected power is increased, causing the maximum ellipticity to decrease and the orientation curves to become more linear. Finally by measuring the change of polarisation of the input beam over a larger range of input orientation (-90° to 90°), a small rotation of the principal axes, to a maximum of 5°, was observed.

REFERENCES

[1] B. Hakki and T. Paoli, "Gain spectra in GaAs double-heterostructure injection lasers," *Journal of Applied Physics*, vol. 46 (6), pp. 1299-1306, 1975.

[2] T. D. Visser, H. Blok, B. Demeulenaere, and D. Lenstra, "Confinement factors and gain in optical amplifiers," *IEEE Journal of Quantum Electronics*, vol. 33, pp. 1763-1766, 1997.

[3] W. Wang, K. Allaart, and D. Lenstra, "Semiconductor optical amplifier gain anisotropy: Confinement factor against material gain," *Electronics Letters*, vol. 40, pp. 1602-1603, 2004.

[4] B. F. Kennedy, S. Philippe, P. Landais, A. L. Bradley, and H. Soto, "Experimental investigation of polarisation rotation in semiconductor optical amplifiers," *Optoelectronics, IEE Proceedings-*, vol. 151, pp. 114-118, 2004.

[5] D. Lenstra, Y. Liu, M. T. Hill, G.-D. Khoe, and H. J. S. Dorren, "Nonlinear polarization rotation in semiconductor optical amplifiers: Theory and application to all-optical flip-flop memories," *IEEE Journal of Quantum Electronics*, vol. 39, pp. 141-148, 2003.

[6] Y. Liu, M. T. Hill, E. Tangdiongga, H. De Waardt, N. Calabretta, G. D. Khoe, and H. J. S. Dorren, "Wavelength conversion using nonlinear polarization rotation in a single semiconductor optical amplifier," *IEEE Photonics Technology Letters*, vol. 15, pp. 90-92, 2003.

[7] R. J. Manning, A. Antonopoulos, R. Le Roux, and A. E. Kelly, "Experimental measurement of nonlinear polarisation rotation in semiconductor optical amplifiers," *Electronics Letters*, vol. 37, pp. 229-231, 2001.

[8] D. S. Kigler, J. W. Lewis, and C. Einterz Randall, *Polarized light in optics and spectroscopy*: Boston Academic Press, c1990.

[9] Y. P. Svirko and N. I. Zheludev, *Polarization of Light in Nonlinear Optics*: John Wiley & Sons, 1998.

[10] R. M. A. Azzam and N. M. Bashara, *Ellipsometry and Polarized Light*: North-Holland Publishing Company, 1997.

[11] R. Guenther, *Modern Optics*: John Wiley & Sons, Inc, 1990.

[12] C. Brosseau, *Fundamentals of polarized light: a statistical optics approach*: John Wiley, 1998.

[13] E. Hecht, *Theory and Problems of Optics*: McGraw-Hill Book Company, 1975.

[14] S. A. Meritt, C. Dauga, S. Fox, I.-F. Wu, and M. Dagenais, "Measurement of the facet modal reflectivity spectrum in high quality semiconductor travelling wave amplifiers," *Journal of Lightwave Technology*, vol. 13, (3), pp. 430-433, 1995.

[15] G. Guekos, *Photonic devices for telecommunications*: Springer-Verlag, 1999.

[16] H. Soto, J. C. Dominguez, Erasme D., and G. Guekos, "Demonstration of an all-optical switch using cross-polarization modulation in semiconductor optical amplifiers," *Microwave and Optics Technology Letters*, vol. 29, (3), pp. 205-209, 2001.

[17] S. Diez, C. Schimt, R. Ludwig, H. G. Weber, P. Doussiere, and T. Duceiller, "Effect of birefringence in bulk semiconductor optical amplifier on FWM," *IEEE Photonics Technology Letters*, vol. 10, (2), pp. 212-214, 1998.

[18] H. Soto, D. Erasme, and G. Guekos, "Cross-polarization modulation in semiconductor optical amplifiers," *IEEE Photonics Technology Letters*, vol. 11, pp. 970-972, 1999.

[19] J. Mark and J. Mork, "Subpicosecond Gain Dynamics in Ingaasp Optical Amplifiers - Experiment and Theory," *Applied Physics Letters*, vol. 61, pp. 2281-2283, 1992.

[20] E. Alvarez, H. Soto, and J. Torres, "Investigation of the carrier density dependence on the confinement factor in a bulk semiconductor optical amplifier with a ridge waveguide," *Optics Communications*, vol. 222, pp. 161-167, 2003.

CHAPTER 4 :
CONTINUOUS WAVE PUMP-PROBE MEASUREMENTS

1. Introduction

Pump-probe studies are needed in order to assess the potential of non-linear polarisation rotation for optical switching applications. Some polarisation pump probe measurements have been performed by other groups [1, 2] using a fiberised SOA output and polarisation analyser. However the following data were obtained using free space optics only, so as not to disturb the polarisation state of the output beam. For ultrafast switching applications, modulated continuous wave (CW) or pulsed sources are necessary [3]. However depending on the average power and repetition rate of those sources, it can be difficult to characterise the polarisation at the output of the SOA due to the relatively large ASE noise. Using un-modulated CW sources allows us to accurately measure the states of polarisation with a polarimeter. While the information concerning the fast effects, like spectral hole burning and carrier heating, is lost when using CW, the implementation of the set-up is much simpler and the expected extinction ratio due to the slower carrier pulsation effects can be extracted. In addition the change in probe polarisation due to injection of a second (pump) beam can be characterized as a function of pump parameters (power and polarisation) and bias current.

In the following experiments, two beams are injected into the device. The probe is a low intensity beam so that it affects the waveguide as little as possible, but the output probe signal must be high enough to be accurately measured. The pump beam is a higher intensity beam, which changes the properties of the device as it travels through it and thereby affecting the probe output. The output polarisation of the probe beam is monitored as a function of pumping parameters and of the SOA bias current.

2. Experimental set-up

A free space contra-propagation set-up, as shown on Figure 1, is used as free space filters do not allow for the wavelength resolution required to separate the two signals in a co-propagation configuration and fiberised filters, while offering good wavelength resolution, modify the polarisation states of the signals. Furthermore in this configuration we have the possibility to pump and probe at the same wavelength, in this case at the peak of the gain region. Two beamsplitters are used, one on each side of the SOA, in order to isolate the pump and probe outputs. The continuous wave (CW) input signals are generated by two HP8168F tuneable laser sources, with the probe signal set at 1580nm and the pump signal at 1575nm. The states of polarisation of the pump and probe signals are controlled independently using a polarizer, a half-wave plate and a quarter-wave plate. A 1580nm interference filter is then used to cut-off most of the noise created by the ASE and the optical feedback, before detecting the output probe signal. The SOA is temperature regulated at 20^0 by means of a Peltier cooler.

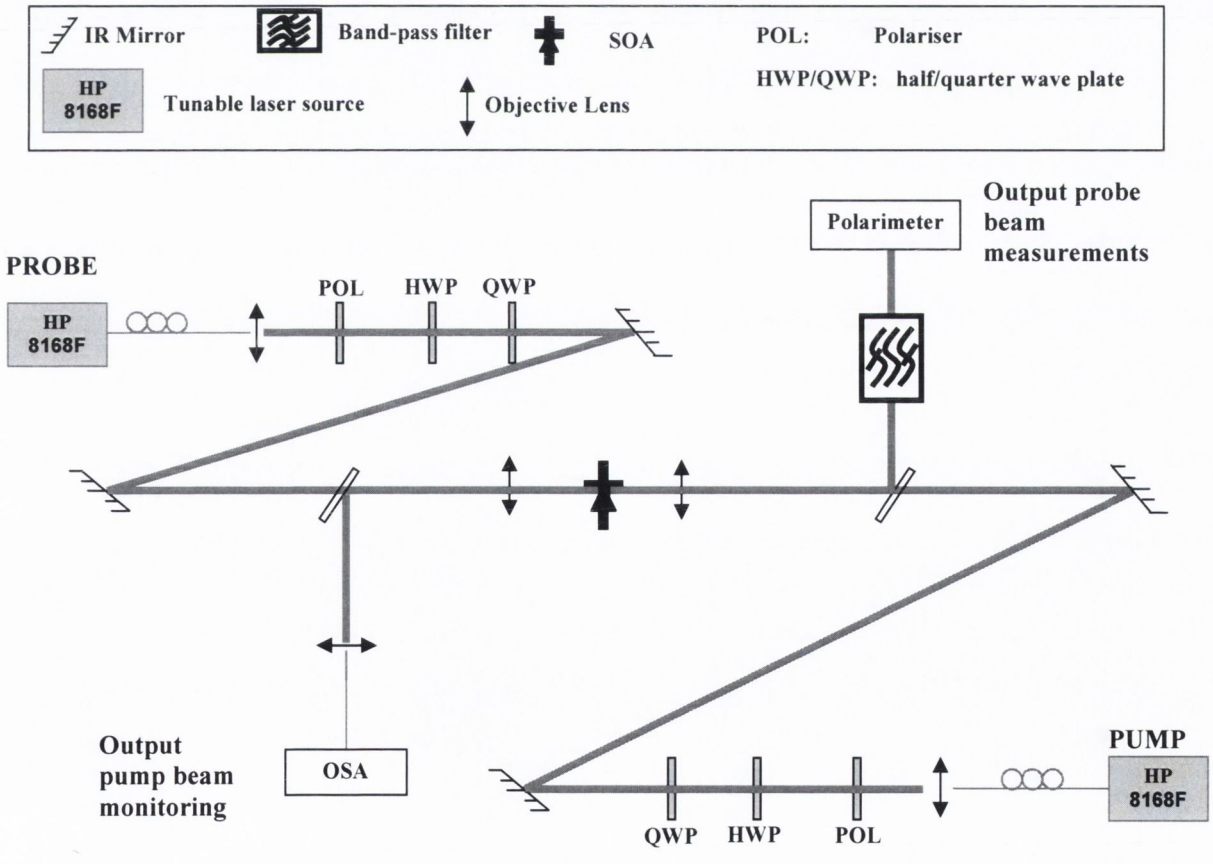

Figure 1. Continuous wave pump probe set-up.

3. Pump signal parameters

The output probe signal ellipticity and orientation are first measured as a function of the pump power for different pump state of polarisation. As can be seen in Figure 2 the evolution of the state of polarisation of the probe at the output is relatively independent of the state of polarisation of the pump, with the effect of the TE polarised pump slightly stronger than the TM polarised pump and the data obtained with the pump linearly polarised at 45° lying in between. However, there is modification of both the ellipticity and orientation of the probe polarisation as the injected pump power increases. In the example shown below for an input probe beam with a linear polarisation state at 45°, the ellipticity of the output probe signal is strongly dependent on the pump power. At low pump power the probe state of polarisation is approximately circular and as the pump power increases the probe state of polarisation tends toward a linear state of polarisation. The orientation of the probe state of polarisation changes initially and then remains relatively constant. However the change in orientation observed at lower pump power is not highly significant considering the high ellipticity measured. One possibility for the modification of the probe polarisation as a function of the pump power is that the waveguide is being modified due to intensity dependent refractive index and gain effects. Since gain saturation and refractive index changes are different for the TE and TM modes, the effect of the pump on the probe gain and polarisation is dependent on pump polarisation.

The probe gain is dependent on the injected pump power, the higher the pump power the fewer carriers are available for probe gain. A reduction in the carrier density can also be achieved by reducing the bias current and the dependence of the probe state of polarisation on the bias current in the presence and absence of a pump signal is presented in the next section.

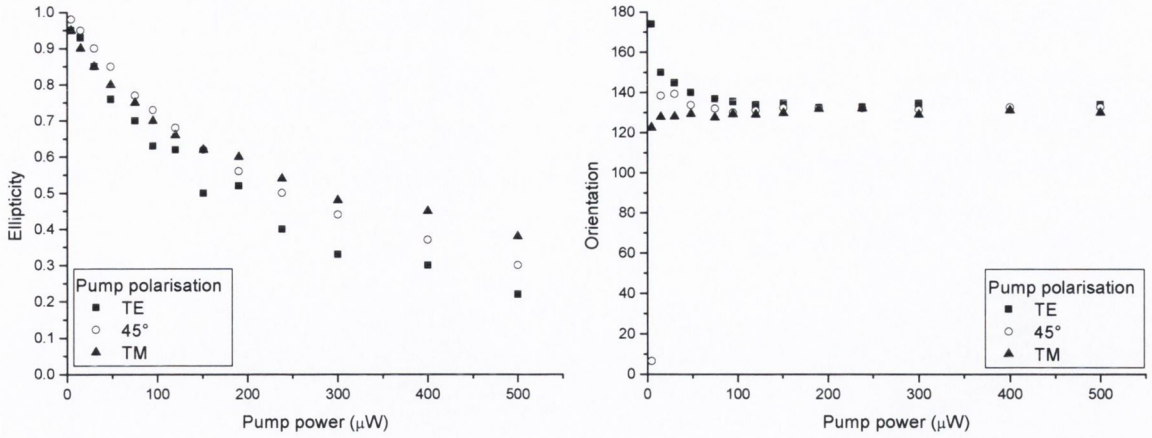

Figure 2. Probe output ellipticity and orientation as a function of pump input power for different orientations of the pump state of polarisation. Probe input linear at 45°, I_{bias} = 350mA, P_{probe} = 30μW, λ_{probe} = 1580nm, λ_{pump} = 1575nm.

4. Bias current

4.1 Experimental results

In this experiment, the effect of the SOA bias current is investigated. The pump signal is set at 1575nm, 258μW and in a TE polarisation state. The probe signal is set at 1580nm, 30μW and in a linear polarisation state of orientation 40°, 45°, 50° and 55°. The ellipticity and orientation of the output probe signal are measured for the pump on and off states. The results are plotted in Figure 3 for 40° and 55° where it can clearly be seen that the effect of the pump is strongly dependent on the bias current and varies with the input probe orientation. Over this range of probe polarisation, the maximum variation in ellipticity and orientation of the output probe polarisation ellipse as the pump is switched on is found to decrease as the orientation of the probe polarisation is increased. With the pump off the probe ellipticity increases with bias current to reach a maximum around 375mA and then falls off, while with the pump on the probe ellipticity increases over the whole range of bias current. Both the orientation of the pump on and pump off data decrease with bias current, although the decrease is faster when the pump is on. It is interesting to note that the maximum rotation between the pump off and pump on states (at high bias currents) occurs for the lowest change in ellipticity and similarly the largest change in ellipticity (at lower bias currents) occurs when the rotation is the

smallest. Clearly a trade-off between rotation and change in the ellipticity has to be found in order to get a good extinction ratio for switching applications. It is already known from the single beam experiment that both the birefringence and the relative gain of the TE and TM modes change with input power. When a pump beam is injected, the probe signal gain also varies: as the pump is switched on, fewer carriers are available for probe amplification but the carrier concentration increases with bias current. Therefore we could expect the change in probe polarisation caused by injection of the pump to be reversed by an increase in bias current. For example Figure 3 (a) at a bias current of 300mA, the probe ellipticity changes from 0.4 to 0 as the pump is switched on, and reaches 0.4 again as the bias current is increased to 400mA. However this is not supported by all the data, in particular no decrease in the probe orientation with bias current is observed when the pump is on, while it is clearly the case when the pump is off. We later try to model these effects but first the effect of the beamsplitter on the output polarisation is characterised.

Indeed the experimental polarisation data do not take into account the effect of the reflection [4, 5] at the beamsplitter, which changes the sign of the ellipticity and of the TE component and also rotates the orientation by an additional angle, between 2^{o} and 5^{o}. In order to determine the state of polarisation of the probe directly at the output of the device, the change in probe polarisation induced by the beamsplitter must be known and will be dealt with later. However these data are strongly relevant since the design of this set-up (Figure 1) is a possible configuration for switching applications. The beamsplitter would be part of the practical switch design, and has been used before in a fiberised set up [6]. The data presented in Figure 3 can therefore be analysed in order to obtain the conditions corresponding to the optimum extinction ratio in the absence and presence of the pump signal and therefore the optimum switching conditions.

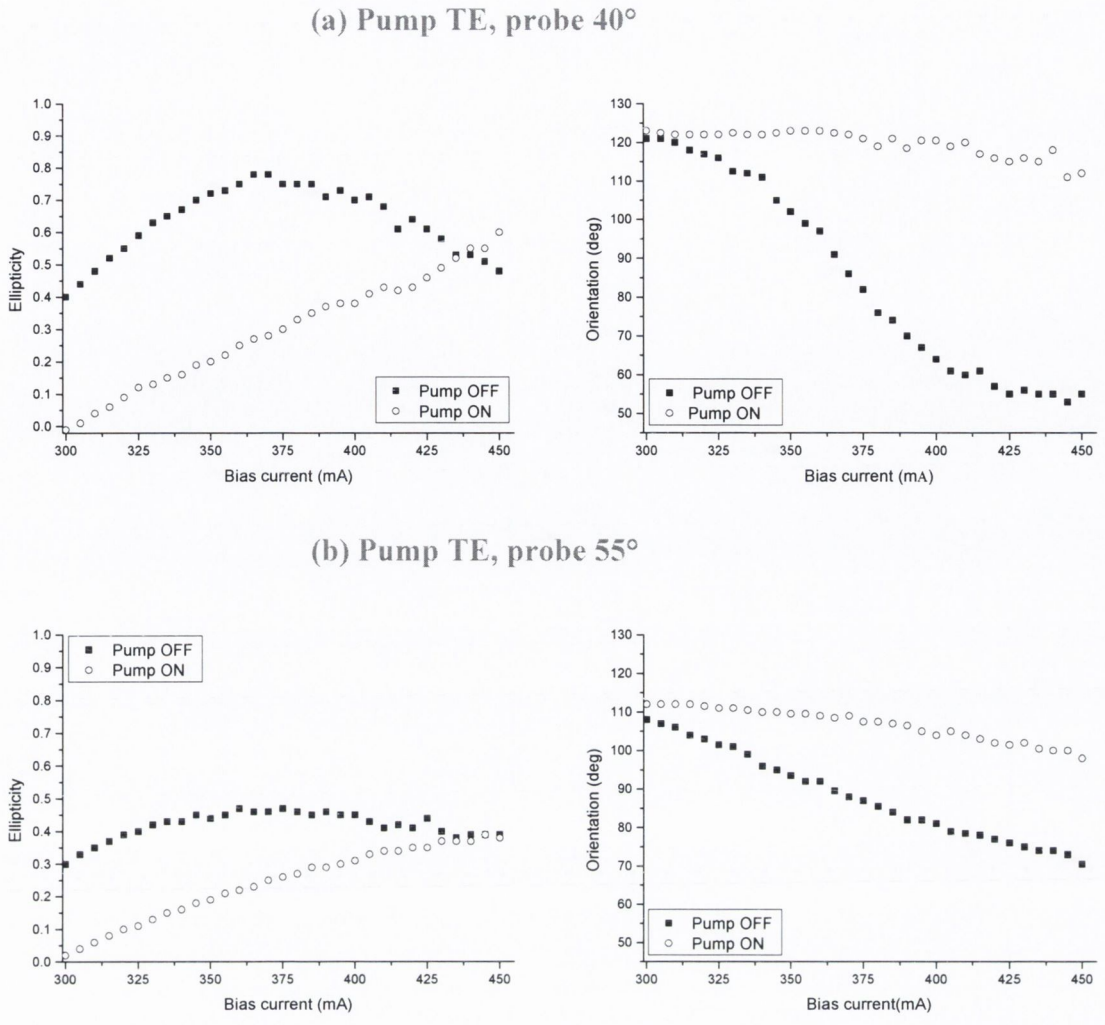

Figure 3.Output probe ellipticity and orientation vs. bias current for both pump OFF and pump ON conditions, λ_{probe}=1580nm, λ_{pump}=1575nm, P_{probe}=30mW, P_{pump}=258mW, Pump TE polarised. (a) Probe linearly polarised at 40°, (b) probe linearly polarised at 55°.

4.2 Extinction ratio

As discussed before a trade-off between the change in ellipticity and the change in orientation as the pump is switch on has to be found in order to determine the optimum switching conditions. This could easily be measured experimentally by placing a polarizer in the output probe signal path (after the beamsplitter) and recording the probe output intensity as a function of polarizer angle for the pump on, I_{ON}, and pump off, I_{OFF}, conditions. The extinction ration (ER) is then found as follows:

$$ER = \frac{I_{ON}}{I_{OFF}}$$

However this would be very time consuming, instead a Matlab program was written in order to calculate the ER that could be achieved if a polarizer was placed in front of a photodetector. The effect of the polarizer can be modelled using Mueller calculus [7] and the theoretical polarizer can be orientated for all possible angles of the polarising axis. The Stokes vectors measured with the polarimeter are normalised and must first be scaled by the intensity, as it is the intensity transmitted by the polarizer in front of the photodetector which is the parameter determining the ER. As discussed before, this intensity changes when the pump is switched on because of the probe gain compression due to carrier depletion by the pump signal, as shown on Figure 4(a). The scaling is achieved by integrating the signal spectrum measured with the OSA, with and without the pump input. The gain compression measured in these experimental conditions, without the polarizer, was found to be 5.5dB, i.e. switching the pump signal on decreases the probe output level by 5.5dB, which corresponds to an ER of -5.5dB due to gain switching only. This value is consistent with the slow gain compression found in the polarisation resolved dynamics, chapter 5, when pumping in TE (probe TE or TM) or pumping and probing at 45°, where values of 4dB to 7dB are measured.
Mueller calculus is then used to find the output intensity after the polarizer. The Mueller matrix of a linear polarizer at an angle θ is [7]:

$$M = \frac{1}{2}\begin{vmatrix} 1 & \cos(2\theta) & \sin(2\theta) & 0 \\ \cos(2\theta) & \cos^2(2\theta) & \cos(2\theta)\sin(2\theta) & 0 \\ \sin(2\theta) & \cos(2\theta) & \sin^2(2\theta) & 0 \\ 0 & 0 & 0 & 0 \end{vmatrix}$$

This is repeated at the different bias currents for all angles of the polarizer, using steps of 1°, and for pump on and off. The achievable extinction ratio can then be found. The extinction ratio as a function of polarizer angle is plotted for each bias current and the curve obtained at 400mA is shown on Figure 4(b). The ER is always negative because of the gain compression due to the pump. The best ER was found to be –7.5 dB, for an input signal polarisation of 40°, a 400mA bias current and at a polarizer angle of 39°. This is low compared to results obtained in fiberised set-ups, where ERs of more than 20dB [6] have been achieved. However fiberised set-ups tend to modify the states of polarisation and the change of polarisation is not only due to propagation through the

SOA but also through the polarisation controllers, half wave plates or polarizers that are often placed before detection, at the output of the device. The ER measured in our case is different since the output probe is detected directly after the SOA and thus only the changes in intensity and polarisation due to the device are taken into account. For example, using the same set-up, if when the pump is off a retarder is used to linearise the output probe polarisation and followed by a polarizer blocking the signal so that $I_{OFF} \approx 0$, then as the pump is switched on the output polarisation changes and some light is transmitted through the polarizer. In that case the ER is positive, and can reach a high value even if the transmitted intensity is low, depending on how well the signal is blocked when the pump is off. However the output states of polarisation are not known and the best results are usually obtained by trial and error. Therefore the method presented here is useful to determine the best working point and improve fiberised set-ups as well as other switching methods like cross-gain modulation. Figure 4(b) shows that under these conditions, using polarisation switching by including only a polarizer at the output can improve the extinction ratio obtained by gain switching by up to 2dB, or deteriorate it by up to 1.5dB depending on the orientation of the polarizer.

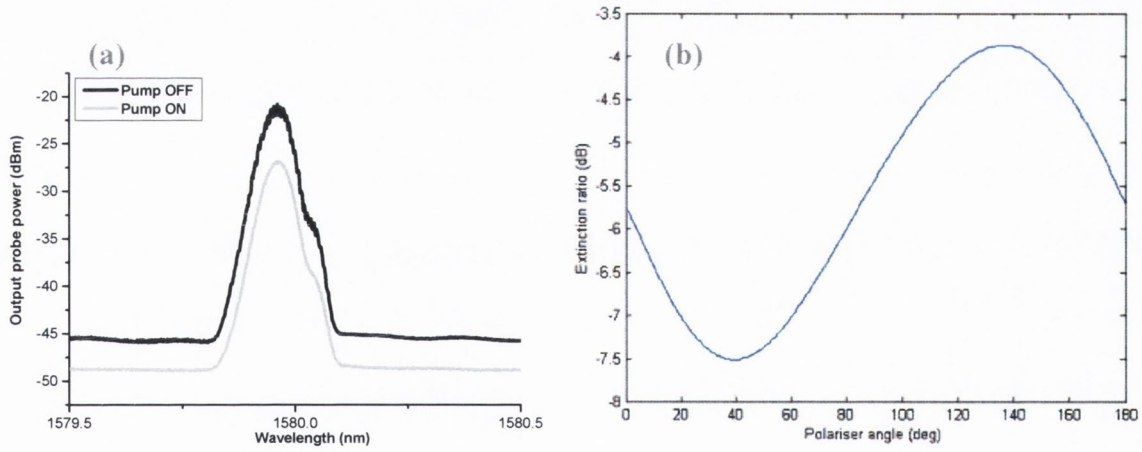

Figure 4. (a) Probe output spectrum for pump OFF and pump ON conditions, showing probe gain compression due to injection of the pump signal, (b) Calculated extinction ratio vs. polarizer angle I_{bias}=400mA for an input probe polarisation linear at 40° and pump TE polarised, λ_{probe}=1580nm, P_{probe}=30μW, λ_{pump}=1575nm, P_{pump}=258μW.

5. Characterisation of the change in probe polarisation

5.1 Influence of the beamsplitter

As mentioned above, the output probe polarisation is modified by the beamsplitter used to isolate the probe from the pump signal. In order to study the polarisation effects and to use the model presented in the previous chapter, the effect of the beamsplitter on the state of polarisation of an incident beam as it is reflected has to be characterized. Finding the Mueller matrix of the beamsplitter would be particularly interesting as it directly relates the Stokes parameters of the incident beam to the reflected beam. The beamsplitter can be thought of as a mirror reflecting half the intensity. In that case the Mueller matrix of the beamsplitter is that of a perfect mirror [4] multiplied by 0.5, as follows:

$$M = \frac{1}{2}\begin{vmatrix} 1 & 0 & 0 & 0 \\ 0 & 1 & 0 & 0 \\ 0 & 0 & 1 & 0 \\ 0 & 0 & 0 & -1 \end{vmatrix}$$

The effect of a perfect mirror on the polarisation of the incident beam is to reverse the electric field direction of rotation. Because the Mueller matrix is based on the measurable Stokes parameters, its accuracy can easily be checked. An additional rotation and change in ellipticity is observed experimentally showing that the use of this ideal representation of the beamsplitter does not lead the accuracy required for this work. Since a Mueller matrix assumes a linear relationship between the incident and reflected Stokes vector, it can be determined experimentally by measuring four sets of incident, S, and reflected, S', Stokes vectors and solving the corresponding linear equations:

$$\begin{aligned} S_1' &= m_{11}S_1 + m_{12}S_2 + m_{13}S_3 + m_{14}S_4 \\ S_2' &= m_{21}S_1 + m_{22}S_2 + m_{23}S_3 + m_{24}S_4 \\ S_3' &= m_{31}S_1 + m_{32}S_2 + m_{33}S_3 + m_{34}S_4 \\ S_4' &= m_{41}S_1 + m_{42}S_2 + m_{43}S_3 + m_{44}S_4 \end{aligned}$$

The Mueller matrix found with this method presented complex elements and could therefore not be used. The reason for the limitations of this approach can be found in the physical realizability conditions of Mueller matrices [4] and is probably linked in this case to the polarising properties of the beamsplitter i.e. the reflection is not only polarisation dependent but also introduces extra polarisation. Since only the polarised part of the signal was taken into account, this results in an erroneous calculated degree of polarisation greater than one. Although in general this can be corrected by post-multiplying the Mueller matrix for the ideal case by another Mueller matrix, another approach is possible.

A different method is therefore implemented where instead of relating the incident and reflected Stokes vector via the Mueller matrix of the beamsplitter, the relative gain and phase shift between the TE and TM components of the incident beam introduced by the beamsplitter are found. This method is based on the model presented in the previous chapter and can be implemented in two ways. Firstly the linear incident state of polarisation is rotated over 90° as before, and the reflected state of polarisation measured. The results are then fitted and the relative gain and phase shift introduced by the beamsplitter are found, as can be seen on Figure 5. A second way is to rotate the input probe signal over 90° and to measure the output probe signal (pump off) before and after reflection by the beamsplitter. The results are then fitted with the model as before and the difference between the best fit parameters before and after reflection give the phase shift and relative gain introduced by the beamsplitter. The same results were obtained with both methods, with a phase shift of -161±1° and relative gain of 0.77 ±0.05. Therefore the effect of the beamsplitter on the electric field is characterised and the reflected polarisation data can still be fitted using the model developed in chapter 3.

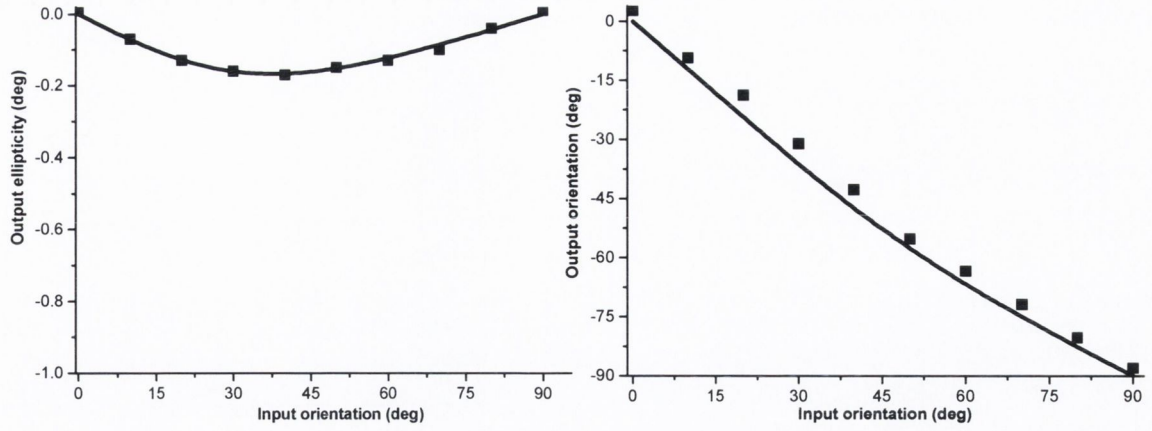

Figure 5. State of polarisation (ellipticity and orientation) of the beam reflected by the beamsplitter as the linear incident beam polarisation is rotated. Measured data points and best fit obtained with the model described in chapter 3. Best fit parameters: $\rho = 0.77$, $\Delta\phi = -161°$.

5.2 Results

In this experiment the change in probe polarisation is characterised under pumping condition. The pump is TE polarised with a 1575nm wavelength. The input probe (λ=1580nm) linear state of polarisation is rotated from 0° to 90° and the model described in the previous chapter is used to fit the data recorded for different values of pump and probe input powers. Figure 6 shows the measured data as well as the best fit curves for two bias currents. Looking first at the ellipticity, Figure 6(a), clearly a break down of the model is observed as it becomes impossible to fit all the data with only two parameters (relative gain and phase difference). While the model is able to cope at higher bias currents and low probe powers, the fitting gets worse as the bias current is decreased, or as the probe power is increased. The data shown here were taken with the pump TE polarised and the fit seems worse for the data points corresponding to probe input polarisation orientation closer to TE, however data taken with the pump TM polarised show the same trend.

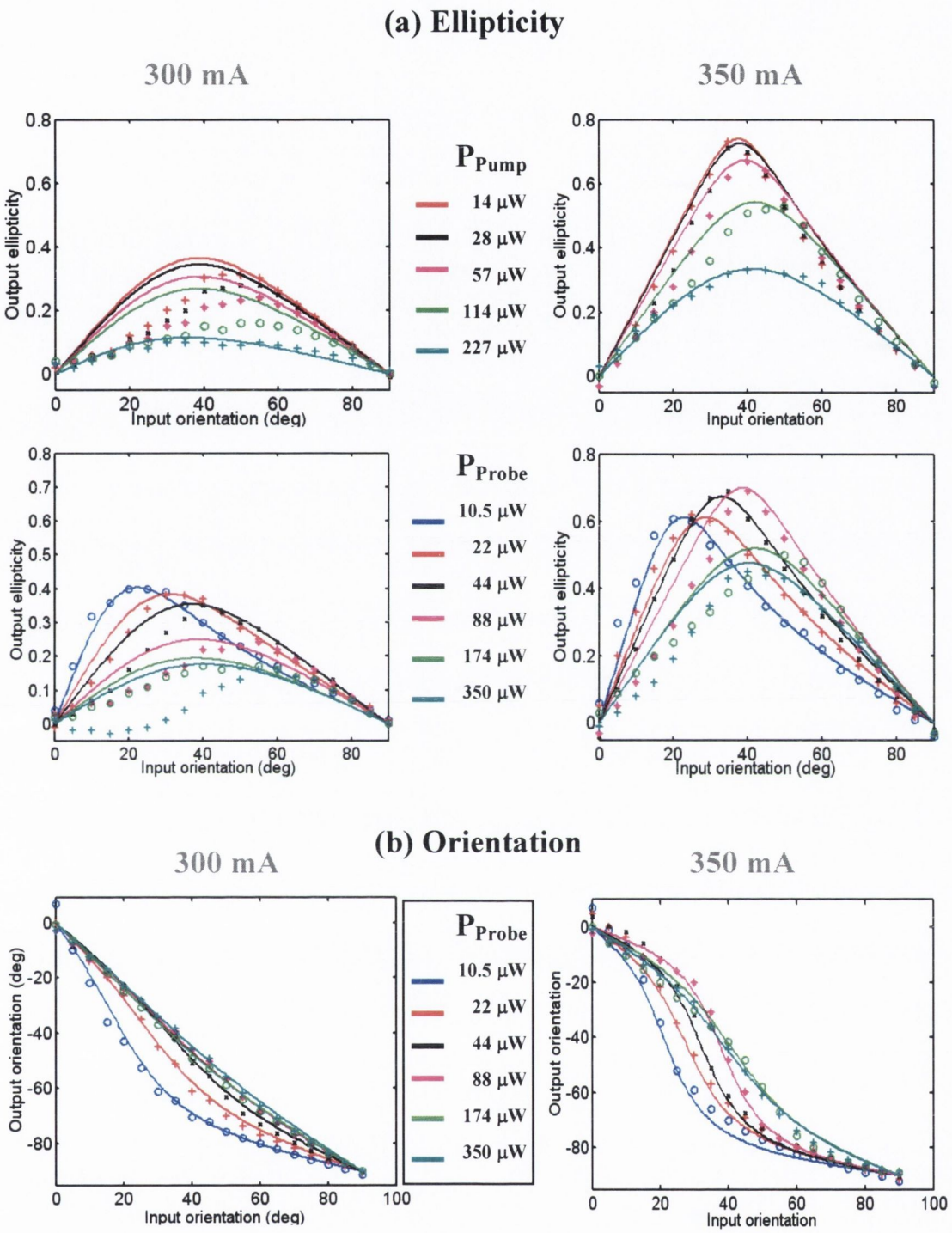

Figure 6. Characterisation of the probe change of polarisation: CW pump-probe data and best fit curves at two different bias current, 300mA and 350m. (a) Ellipticity data for different pump (P_{probe}= 22μW) and probe input powers (P_{pump}= 44μW), (b) orientation data for different probe input powers (P_{pump}= 44μW).

On the other hand the fit of the orientation data, Figure 6(b), appears much better than that of the ellipticity data. In fact the orientation can always be fitted well with the same model for all values of probe and pump power as well as all bias currents. As was the case in the single beam experiment, the output orientation curves become more linear as the probe power is increased. The same effect is observed as the pump power is increased. In the results given here, the best fit of the orientation and ellipticity is obtained using the same relative gain and phase difference inputs in the model, as they are parameters of the same polarisation ellipse. However the ellipticity parameter is more sensitive to the polarisation and power dependence of the pump probe experimental data.

The fact that the polarisation data in this case cannot all be fitted using the gain and phase parameters shows that when two beams are injected the gain and birefringence experienced by the probe is dependent on the probe state of polarisation. This is due to the modification of the longitudinal carrier distribution [8-10] which is dependent on the relative states of polarisation of the pump and probe signals. As discussed in the next chapter, for the same input power different gain compression is achieved depending on the pump and probe states of polarisation due to the different carrier densities available for TE and TM transitions. It implies that the gain experienced by each component of the electric field is now dependent on the pump and probe states of polarisation since it is directly related to the carrier densities. Moreover, as demonstrated in chapter 5, coupling is achieved between the TE and TM modes via the light hole valence band and conduction band. Therefore the assumption that the electric field can be considered as two independent orthogonal components is not strictly true and leads to inaccurate modelling of pump probe experiments. However the fact that a good fit of the experimental data is obtained in the previous chapter suggests that this assumption can be used to study polarisation effects under a single CW beam condition, although a break down of the model could be expected at higher optical injection. Unlike in the pump probe experiment, the carrier distribution encountered by the probe along the waveguide is gradually modified by the probe signal only. Another contributing factor could be the polarisation dependent carrier heating due to Auger recombination that has been observed experimentally in the CW regime [11].

6. Conclusion

The output probe state of polarisation is found to be strongly dependent on input pump power and bias current while the variation observed with pump polarisation is smaller. The ellipticity decreases with pump power while both the ellipticity and orientation are modified as the bias current is changed. This change in polarisation is always present unless light is injected with a linear polarisation oriented along the eigen modes of the device. As such it should be taken into account for any switching application. Using polarisation switching by placing a polarizer at the output of the device can lead to an improvement of the extinction ratio, compared to gain switching only, by 2dB or decrease it by 1.5dB depending on the polarizer orientation. This however is not a limitation of the set-up but rather reflects the change in polarisation experienced by the probe when the pump is switched on. The ER could easily be improved by adding extra polarisation controlling components in order to block out the output probe signal when the pump is on.

As the injected power of either the probe or pump signal is increased, the change in probe polarisation becomes more linear, with a more constant rotation and a smaller output ellipticity. The modification of the electric field by the output beamsplitter can be characterized by a phase shift of -161 and a gain ratio of 0.77 and therefore is not a limiting factor in the characterization of the nonlinear polarisation rotation. A breakdown of the model developed in the previous chapter is observed when fitting the experimental polarisation data under pumping condition, showing that the gain and birefringence effects are now dependent on the input probe state of polarisation. The ellipticity data are more sensitive to the presence of the pump. In all the experiments conducted in the CW regime, the ellipticity was found to be a critical parameter of the polarisation sensitivity in SOAs, while the polarisation rotation is mostly observed at low injected powers and is larger at low bias current.

REFERENCES

[1] H. Soto, D. Erasme, and G. Guekos, "Cross-polarization modulation in semiconductor optical amplifiers," *IEEE Photonics Technology Letters*, vol. 11, pp. 970-972, 1999.

[2] C. S. Wong and H. K. Tsang, "Polarization-independent wavelength conversion at 10 Gb/s using birefringence switching in a semiconductor optical amplifier," *IEEE Photonics Technology Letters*, vol. 15, pp. 87-89, 2003.

[3] D. Cotter, R. J. Manning, K. J. Blow, A. D. Ellis, A. E. Kelly, D. Nesset, I. D. Phillips, A. J. Poustie, and D. C. Rogers, "Nonlinear Optics for High-Speed Digital Information Processing," *Science*, pp. 1523-1528, 19 November 1999.

[4] C. Brosseau, *Fundamentals of polarized light: a statistical optics approach*: John Wiley, 1998.

[5] R. Guenther, *Modern Optics*: John Wiley & Sons, Inc, 1990.

[6] Y. Liu, M. T. Hill, E. Tangdiongga, H. De Waardt, N. Calabretta, G. D. Khoe, and H. J. S. Dorren, "Wavelength conversion using nonlinear polarization rotation in a single semiconductor optical amplifier," *IEEE Photonics Technology Letters*, vol. 15, pp. 90-92, 2003.

[7] D. S. Kigler, J. W. Lewis, and C. Einterz Randall, *Polarized light in optics and spectroscopy*: Boston Academic Press, c1990.

[8] F. Salleras, M. S. Nomura, J. N. Fehr, M. A. Dupertuis, L. Kappei, D. Marti, B. Deveaud, J. Y. Emery, B. Dagens, and T. Shimura, "Longitudinal spatial hole burning in a gain clamped semiconductor optical amplifier," presented at Pacific Rim Conference on Lasers and Electro-Optics, CLEO - Technical Digest vol.1, 2002.

[9] J. L. Pleumeekers, M. A. Dupertuis, T. Hessler, P. E. Selbmann, S. Haacke, and B. Deveaud, "Longitudinal spatial hole burning and associated nonlinear gain in gain-clamped semiconductor optical amplifiers," *IEEE Journal of Quantum Electronics*, vol. 34, pp. 879-886, 1998.

[10] J. N. Fehr, M. A. Dupertuis, T. P. Hessler, L. Kappei, D. Marti, P. E. Selbmann, B. Deveaud, J. L. Pleumeekers, J. Y. Emery, and B. Dagens, "Direct observation of longitudinal spatial hole burning in semiconductor optical amplifiers with injection," *Applied Physics Letters*, vol. 78, pp. 4079, 2001.

[11] J.-N. Fehr, M.-A. Dupertuis, T. P. Hessler, L. Kappei, D. Marti, F. Salleras, M. S. Nomura, B. Deveaud, J.-Y. Emery, and B. Dagens, "Hot phonons and auger related carrier heating in semiconductor optical amplifiers," *IEEE Journal of Quantum Electronics*, vol. 38, pp. 674-681, 2002.

CHAPTER 5 :
POLARISATION DEPENDENT DYNAMICS

1. Introduction

There are two ways of investigating the polarization dependence of the SOA dynamics using pump-probe experiments. Monitoring the output probe intensity for different pump and probe input states of polarisation allows us to study the polarisation dependence of the device response, while rotating a polarizer in front of the photodiode allows us to characterize the change in polarisation induced by the device. The former is the subject of the present chapter while the latter is dealt with in the next one. These studies are complementary as the device response to different input states of polarisation gives information on the actual underlying physics of the dynamics and how to optimise them. On the other hand the polarisation dependent detection helps differentiate between pure gain effects and coupled gain and polarisation effects. Both studies combined provide a direct assessment of the performance that can be expected for switching applications as well as a better understanding of gain and polarisation effects in SOAs.

2. Experimental technique

2.1 Pump-probe experiments

The pump-probe method is used to measure ultrafast phenomena in a material. The material is excited by a high energy pulse, the pump pulse, while monitoring a low energy pulse, the probe pulse, as a function of the time delay between the pump and probe pulses. The energy of the weaker probe pulse is chosen below the gain saturation so that the probe travels through the SOA without disturbing the waveguide. The higher energy pump pulse induces a change in the optical properties of the material, which modifies the state of the output probe pulse. This modification, in our case the intensity of the output probe signal, is recorded for different positions of the delay line corresponding to different positions of the pump and probe pulses overlap.

2.2 Choice of pump-probe configuration

2.2.1 Free space

Various configurations have been implemented for all-optical wavelength conversion, based on cross-gain and cross-phase modulation [1-9]. Most of the applications proposed use at least partially fiberised set-ups, where the polarisation state of the light is random or modified as it travels through the fibres. This makes it very difficult both to set the polarisation to a known state and to measure how it is modified. Polarization maintaining fibres have been used in previous studies of non-linear polarization rotation but while it helps to set and preserve a signal polarization, it is strictly restricted to linear states of polarization. In fact the output of such a fibre is always linear and thus injecting elliptically polarized light or even light linearly polarized with an orientation at an angle with the polarization maintaining fibre axis will lead to losses. Moreover any variation in the input polarization will lead to fluctuations in the output intensity. Therefore the set-up used here is totally free space and although such a system demands more complex alignment procedures and presents stability problems due to the number of mechanical elements and degrees of freedom, it allows for complete control and preservation of the signals state of polarization.

2.2.2 Counter-propagation

In a wavelength conversion system, a high intensity laser beam (pump) modifies properties (transmission, polarisation and phase) of a low intensity laser beam (probe). Pump-probe techniques can be used to investigate the timescales over which the probe is modified by the pump, by monitoring the probe output as a function of time delay between the pump and the probe pulses. The resolution of such experiments is mainly determined by the width of the pulses. In a conventional pump-probe set-up, the pump and probe pulses travel collinearly and in the same direction through the SOA and one is delayed with respect to the other. When the pump and probe are at the same wavelength the only way to separate them is via the polarization, the most common method being to launch cross-polarised pump and probe pulses and to separate them at the output with a polarizer. In the context of a polarization study this would obviously limit the measurements that could be undertaken. Not only do the pump and probe have to be cross-polarised but their state of polarization must be preserved as they travel

through the SOA. Practically this means they have to be polarised along the eigen modes of the device, leaving only two possible combinations, probe TE pump TM and probe TM pump TE. Although a more complicated heterodyne detection [10] has been proposed, a simpler and more flexible method to study the polarisation dependence of pump-probe measurements is to use a counter-propagation configuration where the pump and probe pulses travel in opposite directions. Then the beams can simply be separated using a beamsplitter, whatever their polarisation may be. The main disadvantage of this configuration is the longer fall time. In contra-propagation it corresponds to the pulses overlapping at different positions inside the device and is strongly dependent on the length of the SOA, whereas in co-propagation it corresponds to the pulses overlapping each other, and depends mostly on the pulsewidth. The analysis and modelling of the experimental data is not as straightforward since the probe experiences different regimes as it travels through the SOA. For one pump probe delay, part of the SOA could be saturated by the pump signal while another section could have recovered already.

2.2.3 Picosecond regime

Experimental studies in the femtosecond regime [11-15] are able to resolve the different ultrafast effects and determine their contributions and time constants. They also give valuable information about the structure of the material under test. The response of the SOA to femtosecond pulses is dominated by intraband effects. While operating in this regime allows investigation of the underlying physics, it cannot be used for switching applications. A large amount of work has also been done in the 10ps to 100ps regime, in particular on switching applications [16-22]. The response of SOAs to those signals is dominated by interband effects. But for optical telecommunications applications of polarization rotation effects it is interesting to study the dynamics of the effects in the picosecond regime in order to assess the switching capacity for data rates over 100Gb/s. In that case both interband and intraband effects are observed.

Different laser sources were used to perform the following experiments, the first one is an optical parametric oscillator (OPO) system. This bulky system was found to necessitate numerous time consuming adjustments and problems of stability of the output intensity, wavelength, and pulsewidth were encountered. As a result all the final

data presented here were taken using a fibre-based femtosecond laser. This laser has a fiberised output and the pulsewidth after dispersion in the patch fibre is 2.5ps.

2.2.4 Experimental set-up

A free space contra-propagation configuration is used, allowing total control and preservation of the state of polarisation of the injected and collected signals, as shown on Figure 1. The 1580 nm pulsed input is produced using a fibre based femtosecond laser, with a repetition rate of 82 MHz. The pulse width after dispersion in the fiberised output is 2.5ps and a grating filter with a 1nm spectral width is used. The pulses are coherent and one is delayed with respect to the other using a variable delay stage. The polarisation of each beam is controlled independently with a quarter wave plate (QWP) and a half wave plate (HWP). Two beamsplitters allow us to monitor the input and output of each beam. The light is coupled in and out of the SOA by two anti reflection-coated aspheric lenses mounted on micro-control 3D translation stages. The device under test is a commercially available 1.5mm long bulk InGaAsP/InP travelling wave SOA biased at 350mA and temperature regulated at 20°C by means of a Peltier cooler. An interference filter is used to isolate the 1580nm probe signal from the broad ASE at 1580 nm and the signal is detected using an infrared photodiode and a lock-in detection technique. The displacement of the delay line by a stepper motor as well as the signal acquisition are automated and controlled via a Labview based program.

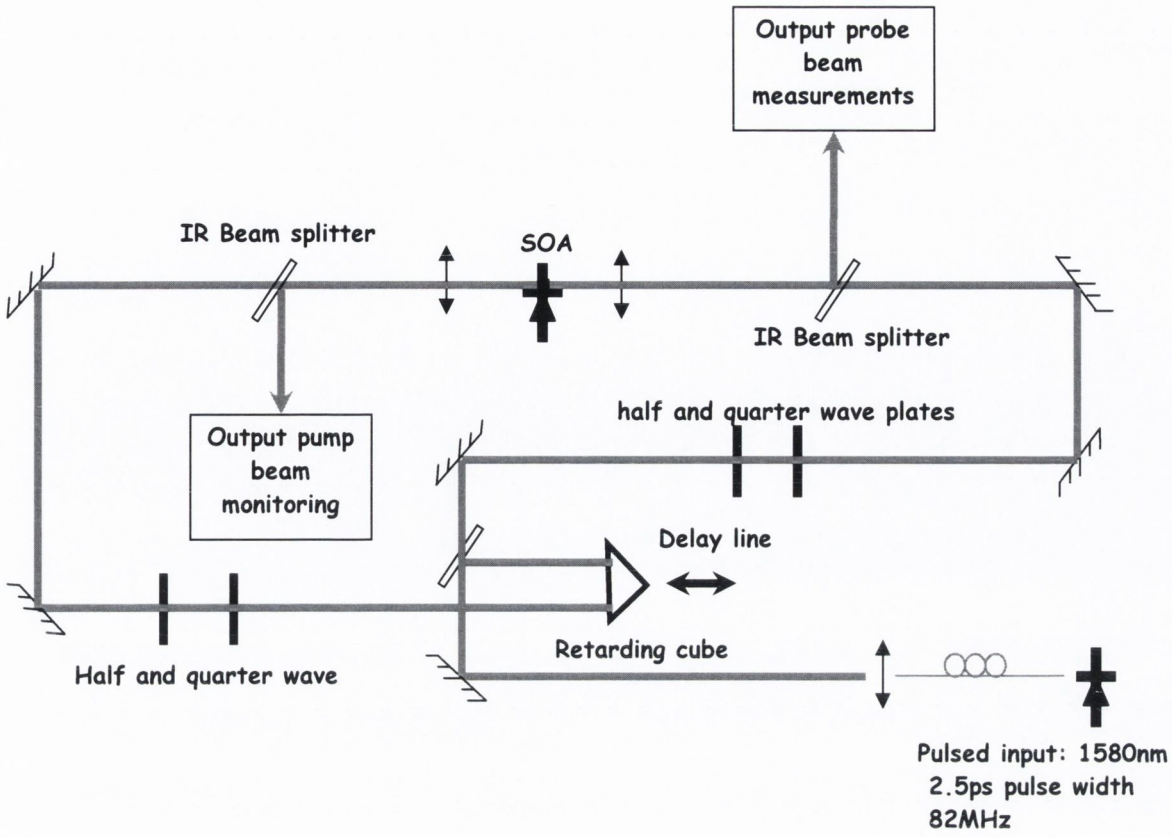

Figure 1. Free space contra-propagation pump probe experimental set-up.

2.3 Lock-in detection

Lock-in detection is commonly used to recover signals in the presence of high background noise [23]. Figure 2 shows the block diagram of a typical lock-in amplifier. Its basic function is to provide a DC output proportional to the AC signal under investigation. The average probe power injected into the SOA is typically under 1μW while the output ASE power at 350mA bias current reaches 5mW. An optical band pass filter is used to reduce the ASE noise, as well as a polarizer when possible, but still the noise level can be several orders of magnitude above the signal level. In those conditions it is not possible to measure the intensity or polarization of the output probe signal directly.

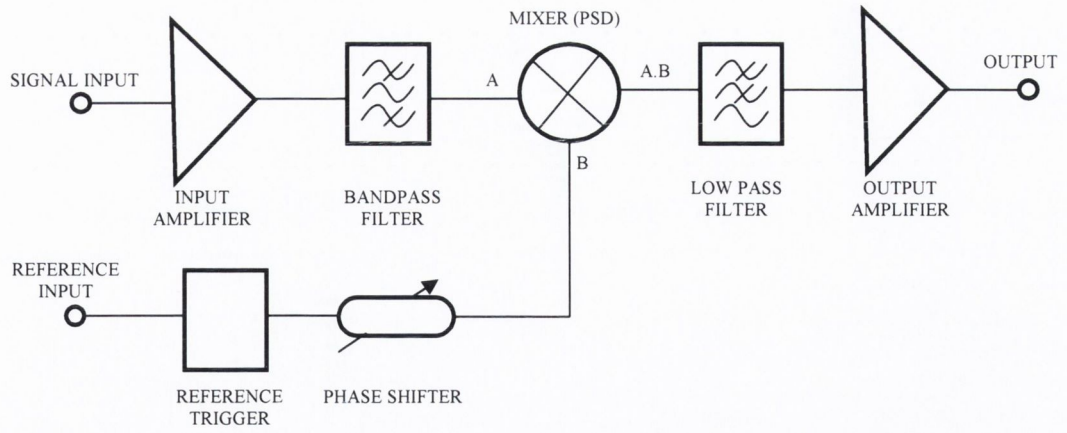

Figure 2. Block diagram of a typical lock-in amplifier.

The probe input signal is chopped mechanically using an optical chopper of high frequency stability and this reference frequency is fed to the reference input of the lock-in amplifier. The input signal, including noise is amplified by an adjustable-gain amplifier in order to match it more closely to the optimum input signal range of the phase-sensitive detector (PSD) and then filtered in order to reduce the bandwidth of the noise voltages. The reference signal is passed through a phase shifter to compensate for phase differences introduced between the signal and reference inputs by the experiment. The reference and signal channels are then applied to the PSD. The PSD is a special rectifier that performs the AC to DC conversion. Only the part of the signal at the same frequency as the reference is properly rectified and so converted to a DC level, while the errors due to rectified noise components appear at the PSD output as an AC fluctuation. This AC can easily be filtered out with a low-pass filter and the DC output further amplified.

3. Data acquisition and analysis

3.1 Main features of a typical decay curve

A typical probe intensity signal obtained in counter-propagation is shown in Figure 3. This curve is part of the early data collected using the OPO system and an artefact, probably due to temporal instability of the pulses can be seen on the recovery of the device. This was never observed with the fibre laser. However this figure illustrates well the importance of the stability of the input source for accurate data analysis. At high

resolutions, a small interference pattern due to reflections at the facets of the device as well as at the coupling lenses can be seen. The lock-in amplifier output, proportional to the probe intensity is usually normalised by the probe signal level that is achieved in the absence of the pump pulse in order to give transmission values. The displacement of the delay line is converted to a relative time delay. As discussed above there is not a single value of time delay (t=0) when the pump and probe overlap, but rather the position of the pump and probe pulses overlap changes with time delay. Therefore the relative time delay is set to zero when the influence of the pump is the greatest.

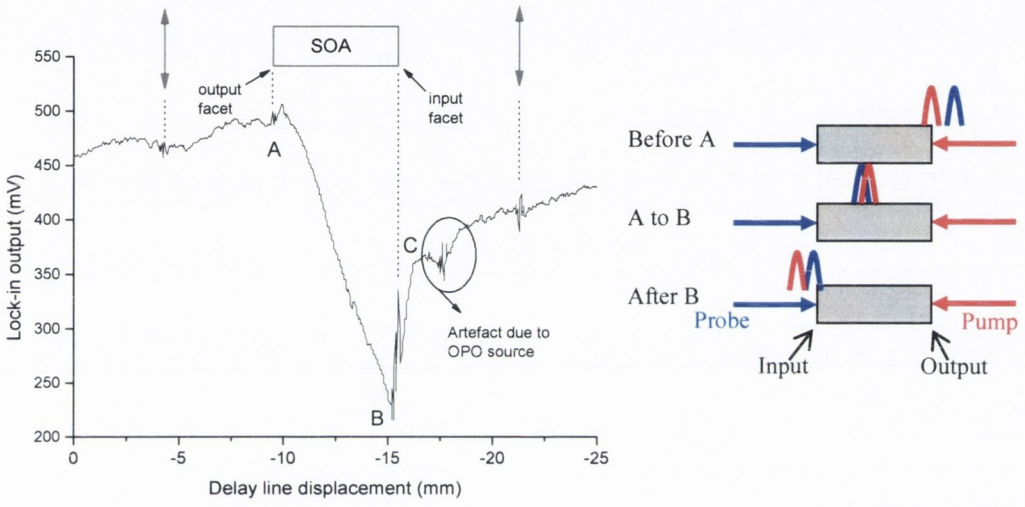

Figure 3. Main features of a decay curve (raw data) and corresponding positions of pump and probe pulse overlap.

We refer to the probe input facet (pump output facet) as the SOA input and the probe output facet (pump input facet) as the SOA output. Before A, the probe leaves the SOA before the pump enters it and its transmission is left unchanged. At A, the pump and probe pulses overlap at the output of the SOA. Between A and B the pulses overlap inside the SOA, and as is expected the gain experienced by the probe is reduced and therefore the intensity of the amplified probe signal decreases. It is important to note here that since a contra-propagation configuration is used, the range of pump-probe delays over which the pump and probe pulses overlap inside the SOA corresponds to twice the length of the device divided by the velocity of light in the amplifier. A minimum is reached at B, where the pulses overlap at the input of the SOA. This

minimum can be expected, as it is at this delay that the pump has affected the entire length of the SOA, with no time for any recovery before the probe arrives. After that point the pump leaves the SOA before the probe enters it and the device has started to recover before the arrival of the probe. As the delay is further increased the amplified probe signal will continue to increase and the recovery time of the device is monitored. Two components can be seen in the recovery of the probe transmission at positive delays. The fast component, between B and C, corresponds to the recovery of the gain compression due to carrier heating and spectral hole-burning by intraband carrier recombination while the slower recovery is associated with interband recombination [24]. As the pump pulse duration decreases the contribution of intraband effects to the gain compression increases and with picosecond pulsewidths we expect significant contributions of both interband and intraband effects [25]. Even though the timescales for the intraband effects (typically < 500 fs) cannot be resolved within the time resolution of the 2.5ps pulses, the polarization dependence of the intra and interband dynamics can be determined by examining the relative contributions of the fast and slow components to the probe transmission as a function of delay.

3.2 Coherent artefact

Under specific experimental conditions: very small steps of delay line displacement, low pass filter disconnected and no averaging at lock-in output, oscillations of the transmitted probe intensity can be observed near the delay corresponding to the maximum gain compression, when the pump and probe overlap at the input of the amplifier. These oscillations, shown on Figure 4, could be attributed to two different phenomena, the interference between the probe pulse and the pump pulse reflected at the SOA input facet or a coherent artefact.

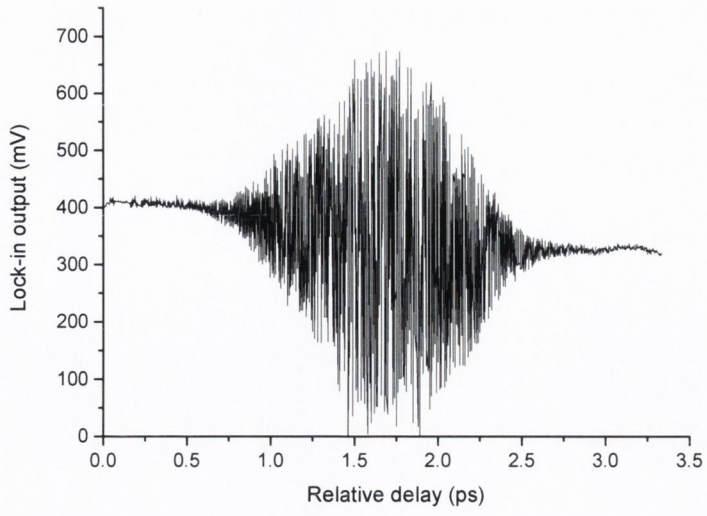

Figure 4. Variations in the lock-in amplifier for co-polarised pump probe signals as a function of relative pump-probe delay.

A coherent artefact has been reported in experimental studies [12] and a theoretical analysis of ultrafast pump probe experiments in SOAs predicts strong oscillatory structures in the probe signal [26]. The predicted oscillations are not due to direct interference but are a consequence of the coherent interaction of the pulses with the gain medium. They oscillate with half of the optical period and should still be observed with cross-polarised pump probe signals [26]. However this prediction is based on the assumption that linear states couple to the same bands, which is not strictly the case in our device where low coupling between cross-polarised beams are measured, as discussed below. While transitions for the TE and TM mode both involve the conduction band, the TE transitions involve mostly the heavy hole valence band and the TM transitions the light hole valence band. On the other hand interferences are not expected for cross-polarised signals and should oscillate at the optical period. Unfortunately the set-up used here does not have the mechanical stability necessary for interferometric precision measurements at 1580nm, however further investigation shows that the oscillations are still present with cross-polarised pump probe signals but with much lower amplitude, as can be seen on Figure 5.

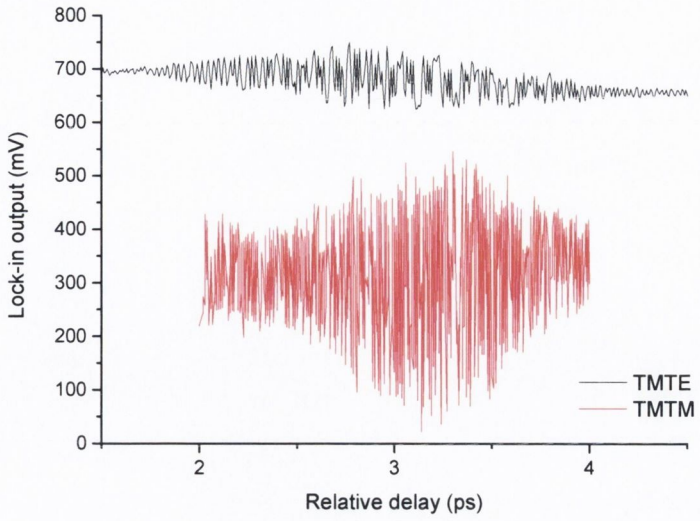

Figure 5. Oscillations of output probe signal near zero time delay in the co and cross-polarised cases.

Although this is consistent with a coherent interaction with the gain medium, interferences cannot be ruled out completely unless the pump and probe are cross linearly polarised along the eigen modes of the device. As discussed below, there is evidence of interferences between probe pulse and pump reflections at the coupling lenses and at the output facet of the device. The fact that the oscillations observed when pump and probe overlap at the SOA input have a much higher amplitude suggest that both interference and coherent artefact are present.

The oscillations are much localised over a small delay range and of less than 2ps, furthermore they are only observed for specific experimental conditions that are different from the optimised conditions usually used (longer displacement steps, between 0.25ps and 0.5ps, low-pass filter with a long time constant and small averaging at the output). These optimised conditions are specifically chosen so as to reduce the noise without degrading the temporal response of the decays. Moreover with our contra-propagation set-up they are not observed on the recovery part of the decay. Therefore the error introduced by the oscillatory structure remains small in typical experimental conditions.

3.3 Gain compression

Different gain compression parameters are measured, giving information on the relative importance of intraband and interband effects as a function of the input states of polarisation and injected pump energy. Figure 6 shows the three different gain compression parameters that are extracted from the transmission curves. The maximum gain compression, measured between A and B, is linked to the extinction ratio. The slow gain compression, measured between A and C, corresponds to the part of the signal recovering by slower interband effects. And the additional fast gain compression, measured by subtracting the slow gain compression from the maximum gain compression, corresponds to the part of the signal that recovers by faster intraband effects.

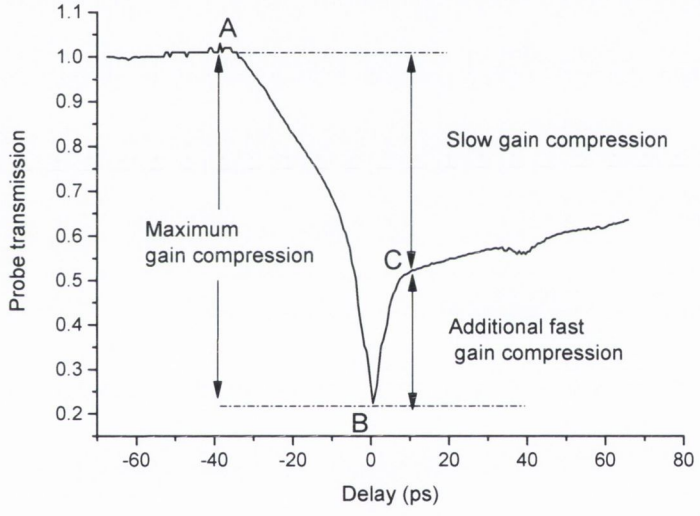

Figure 6. Gain compression measurements definitions.

3.4 Timescales

Although the pulsewidth of 2.5ps used here does not allow resolving the different ultrafast dynamics involved and their time constants, their combined effects on the probe signal can be observed. Timescales can also be extracted from the transmission curves, as shown on Figure 7. We define the *fall time* (t_f) as the 10% to 90% fall time between A and B, and the fast *recovery time* (t_r) as the 10% to 90% rise time between B and C. The *slow timescale* cannot be measured directly due to limitations of the delay

line displacement and is found by an exponential fit of the slow recovery recorded after C.

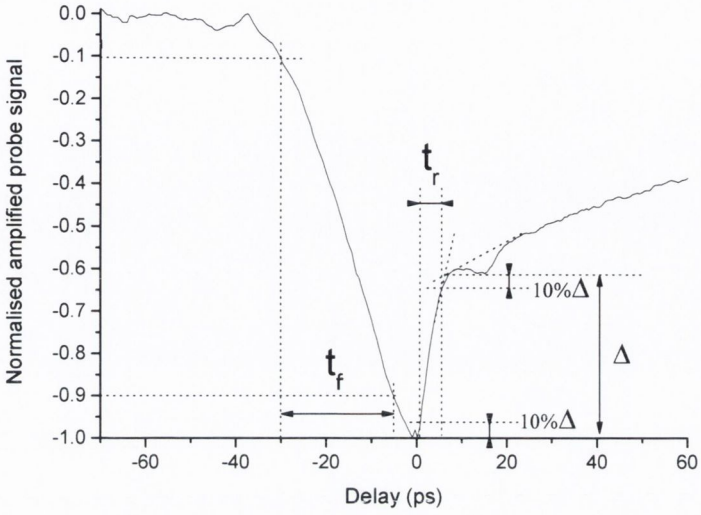

Figure 7. Timescale measurements definitions. The decay is normalised between 0 for no effect of the pump and -1 for the maximum effect of the pump.

4. Injection along the eigen modes of the device

The pump and probe wavelength are set at 1580nm at the peak of the SOA gain spectrum. The probe transmission is recorded as a function of pump probe delay for a range of pump pulse energies (6fJ-975fJ), while the probe pulse energy is kept constant at 12fJ, below the gain saturation energy. The data are taken for the different combinations of probe and pump states of polarisation [27], probe and pump TE polarised (TETE), probe and pump TM polarised (TMTM), probe TE pump TM (TETM) and probe TM pump TE (TMTE). As the pump and probe are set along the eigen modes of the device, they travel through it with their polarisation unchanged. Therefore in all cases the output polarizer is aligned with the input probe polarisation in order to reduce the noise due to the ASE. The legend of each figure gives the probe state of polarization, followed by that of the pump.

4.1. Input state of polarisation dependence

The results for two values of the pump pulse energy can be seen on Figure 8 and show a clear dependence of the probe transmission on the input signals polarisation. As discussed before the oscillations [26] around 0ps delay are only observed at negative delays and do not account for the polarization dependence of the gain compression as may be the case in co-propagation [12].

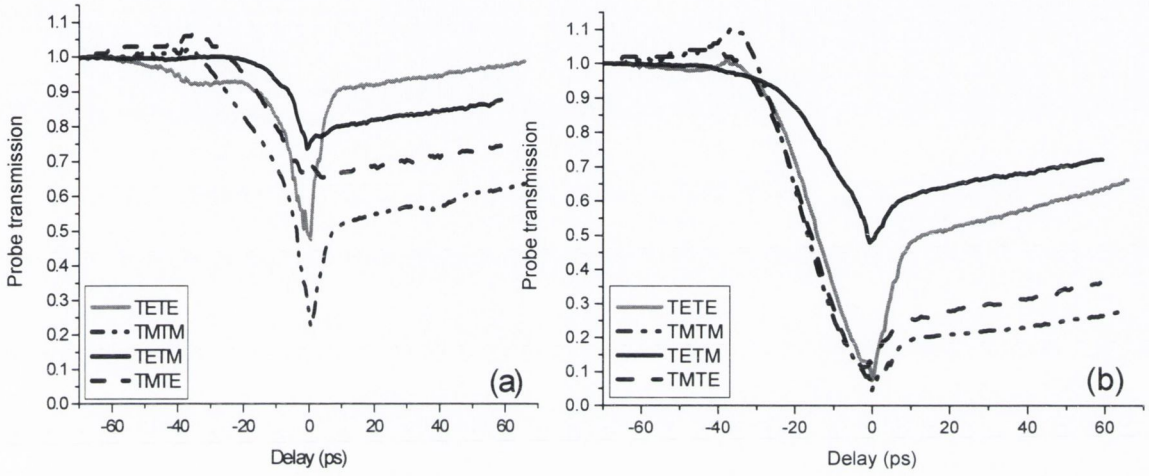

Figure 8. Transmitted pump signals as a function of delay for the different co and cross polarised cases. Eprobe=12fJ, (a) Epump=24fJ, (b) Epump=732fJ.

At lower powers the onset of the decrease in the probe transmission occurs at earlier time delays for the co-polarized pump and probe pulses due to the fact that the effect of the pump is greater and therefore it has to traverse less of the SOA to induce gain compression of the probe signal. An additional feature is observed around -30ps delay when the pump and probe pulses overlap close to the output facet of the SOA. It can also be noted that this feature is strongly polarisation dependent. For high pump powers there is an increase in the probe transmission in the TMTM case, whereas the feature is absent in the TETM case at all pump energies. Modelling is under way to study the origin of this effect, which most likely arises from modification of the carrier distribution along the device [28]. The depletion of carriers at a given position inside the device can lead to a decrease in the amount of ASE travelling from that position and thus increase the carrier density at other positions along the SOA.

4.2 Pump pulse energy dependence

In all cases, the decrease in probe transmission gets larger as the pump energy is increased, as shown on Figure 9 to Figure 12. The additional feature observed at -30ps is mainly observed in the co-polarised cases and is power dependent. The device saturation can clearly be seen in the TMTM case. The fast recovery component is always present in TETE and can also be observed in TMTM, but in that case it gets smaller at higher pump energies. In the cross-polarised cases it is only observed at high pump energies and has smaller amplitude.

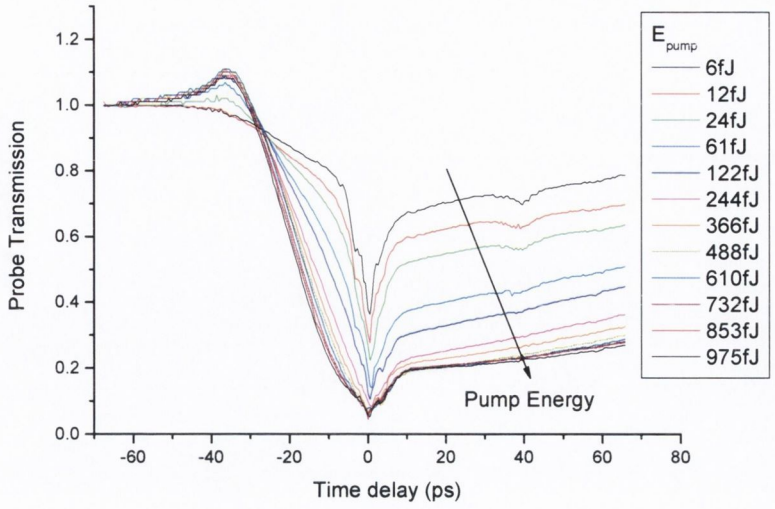

Figure 9. Decay curves of the TM co-polarised case for different values of pump pulse energies (6fJ-975fJ).

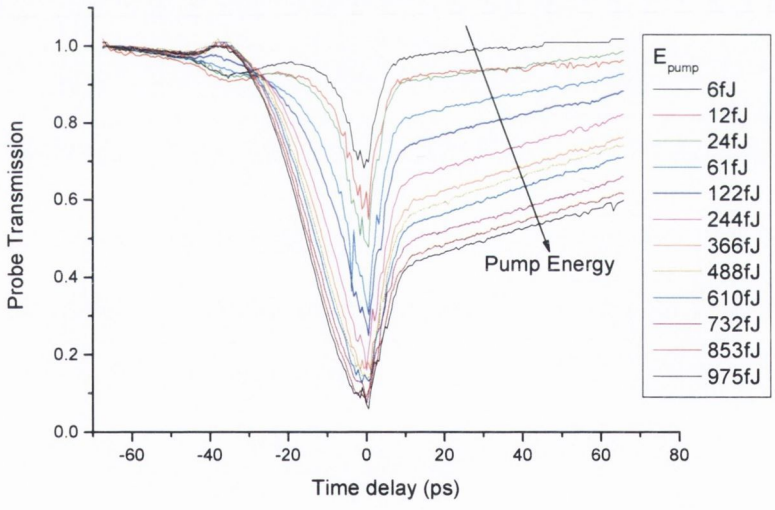

Figure 10. Decay curves of the TE co-polarised case for different values of pump pulse energies (6fJ-975fJ).

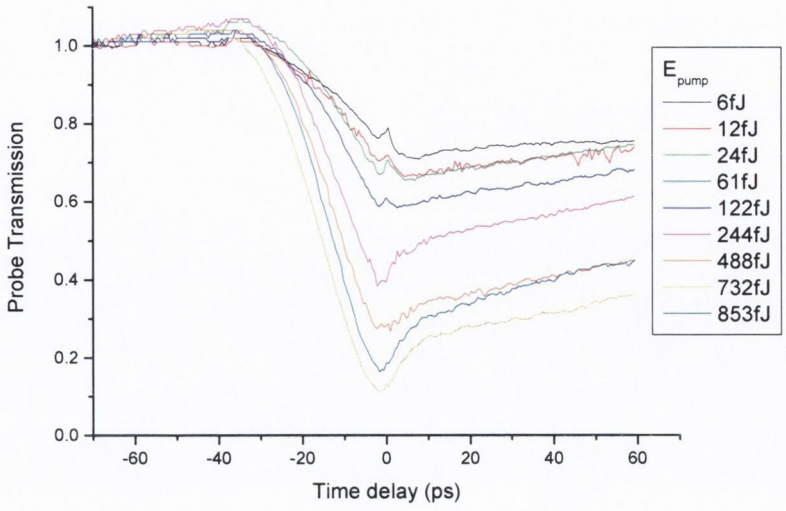

Figure 11. Decay curves of the cross-polarised case probe TM, pump TE, for different values of pump pulse energies (6fJ-854fJ).

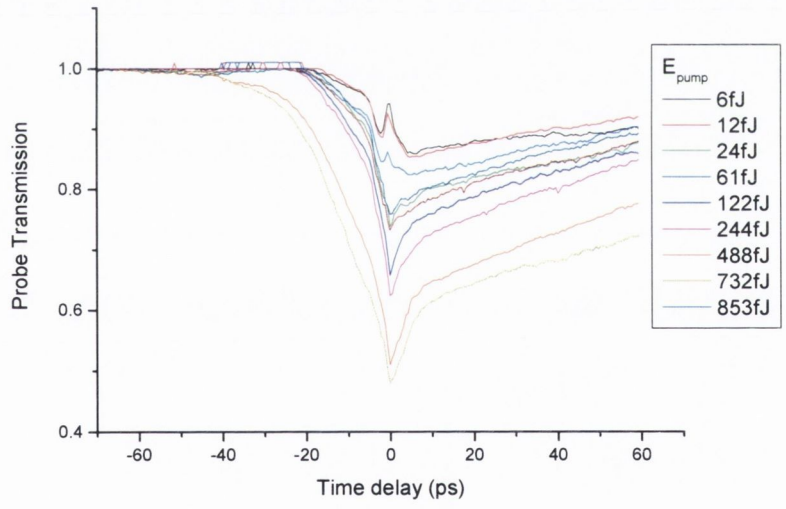

Figure 12. Decay curves of the cross-polarised case probe TE, pump TM, for different values of pump pulse energies (6fJ-854fJ).

4.3 Maximum gain compression

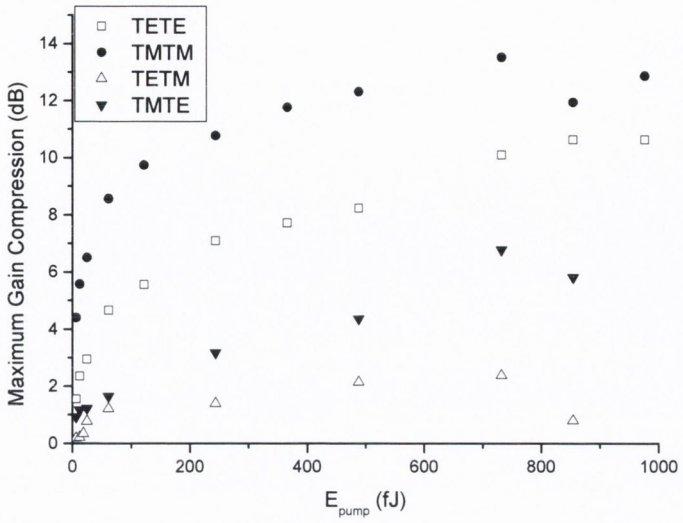

Figure 13. Maximum gain compression as a function of pump pulse energy for the different input polarization cases.

The maximum gain compression (measured between A and B) at zero time delay for each case is shown on Figure 13 as a function of pump energy. As the pump energy increases the gain compression increases, as would be expected from carrier depletion effects. At higher pump energies the gain compression stabilises in the co-polarised cases and starts to decrease in the cross-polarised cases. A higher gain compression is achieved by pumping and probing the same eigen mode. When pumping orthogonal to the probed mode, much higher pump energy is needed to reach the same gain compression. For the probe TM polarised, a gain compression of ~7dB can be achieved by either injecting a 24fJ TM polarised pump or a 732fJ TE polarised pump, giving a cross-gain compression coefficient of 3.3%. Similarly, for the probe TE polarised, a gain compression of ~2.5dB is obtained with a 12fJ TE polarised pump or a 732fJ TM polarised pump, giving a cross-gain compression coefficient of 1.6%. Therefore cross-gain compression from one mode to the other is low, due to the low cross-saturation coefficient [29], but increases with pump energy. Cross-gain compression from TE (pump) to TM (probe) is higher than TM to TE.

4.5 Fast component

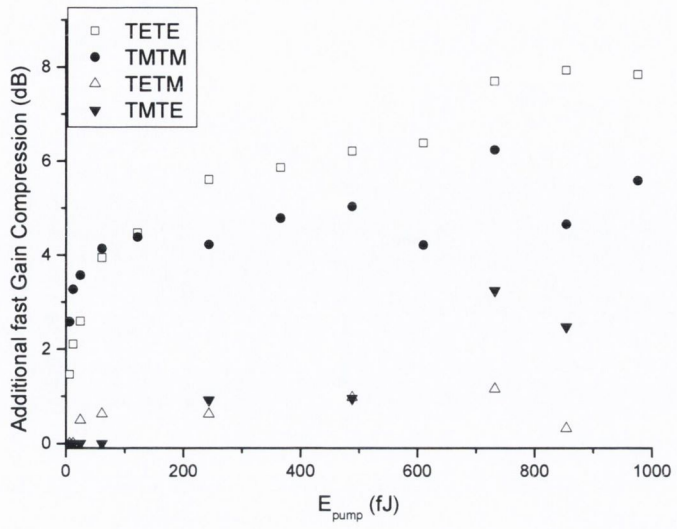

Figure 14. Additional fast gain compression as a function of pump pulse energy for the different input polarization cases.

At lower pump energies the fast recovery component, due to intraband effects is only significant in the co-polarized cases, as shown on Figure 14. It can also be observed in the cross-polarized case at higher pump energy but its amplitude, is only significant in the TMTE case. The fast recovery dominates the probe transmission recovery for the TETE case, where only a small level of slow gain compression remains. A fast component is also evident for the TMTM case but there is a greater contribution of the slow gain compression in that case.

The fast recovery component is usually attributed to spectral hole burning and carrier heating effects and at 2.5ps pulsewidth carrier heating is the main contribution [25]. Carrier heating effects can have different sources [30]; injection heating is due to the injected carriers having a high energy in order to reach the active layer. It depends on bias current but not on pump probe time delay. Stimulated emission depletes (stimulated recombination) lower energy carriers in both the conduction and valence bands and leaves those with higher than average energy. Auger recombination, where the energy released during an electron-hole recombination is absorbed by another carrier, which is excited to a higher energy level. In InGaAsP, main Auger processes gives energy to valence band (CHHS, CHHL) and has been suggested as the main carrier heating mechanism in SOAs under continuous wave injection [31]. However the Auger

recombination rate is proportional to the cube of the carrier density, thus decreasing quickly as the carrier density decreases, and this behaviour is not observed in the present experimental data. Free carrier absorption has also been suggested as the main mechanism of carrier heating [32], and in particular free hole absorption is a major contributor to free carrier absorption in InGaAsP [33]. Another source of carrier heating mentioned in earlier work is two-photon absorption [34]. Although stimulated emission is the largest contributor, other carrier heating mechanisms, like free carrier absorption and TPA, result in the creation of high energy carriers and thus could contribute significantly to carrier heating, despite the lower probability of them happening. Most work only takes into account carrier heating in the conduction band where it is independent of the direction optical polarization [29, 32]. From the experimental data, the fast effect is mainly observed when pump and probe are co-polarised, i.e. when pump and probe interact with the same valence band. This shows that the fast recovery observed is mostly due to hot hole recombination, as hot electron would have the same effect in the cross-polarised cases. At higher power the fast gain compression is higher for TMTE than TETM due to the role of light holes in both TE and TM transitions as is also the case for the slow gain compression. Fast gain compression values are close for TETE and TMTM cases. TETE seems slightly larger by about 1dB but this is within the resolution of the experiment at these low transmission values. However the maximum gain compression was higher in the TMTM case, meaning that a smaller proportion of carrier density has recovered by carrier cooling than in the TETE case. This is consistent with a lower density of states of the light hole valence band, as scattering is not as important as in the heavy hole valence band. It could also be attributed to the role of LO phonons in light hole recombination, while heavy holes tend to cool by acoustic phonon scattering [35]. LO phonon emission happens with a timescale of the order of 100fs while acoustic phonon scattering happens on a longer timescale. As the pulse duration used in the experiment is 2.5ps, carrier recombination happening with a 100fs timescale may not be observed. Picosecond dynamics have been attributed to nonthermal heavy holes in previous work performed in the femtosecond regime [35].

4.4 Slow gain compression

Considering now the slow gain compression, Figure 15, different behaviors are observed for each pump probe polarization combination. The discrepancy between the

TM mode gain compression and the TE mode gain compression is most likely due to strain effects [36, 37] . This is commonly present in heterostructures, even for a negligible lattice mismatch [36] and has the consequence of removing the degeneracy of the light and heavy hole valence bands. The transitions associated with TE and TM modes are different [38] with TM transitions involving light holes while TE transitions involve a mixture of light (25%) and heavy (75%) holes [2]. As a consequence in all cases an increase in gain compression with pump energy is observed, as the conduction band is depleted by the pump, whatever its polarization may be. However the amount of gain compression differs due to the different transitions involved for each eigen mode from the conduction band to the heavy hole and light hole valence bands.

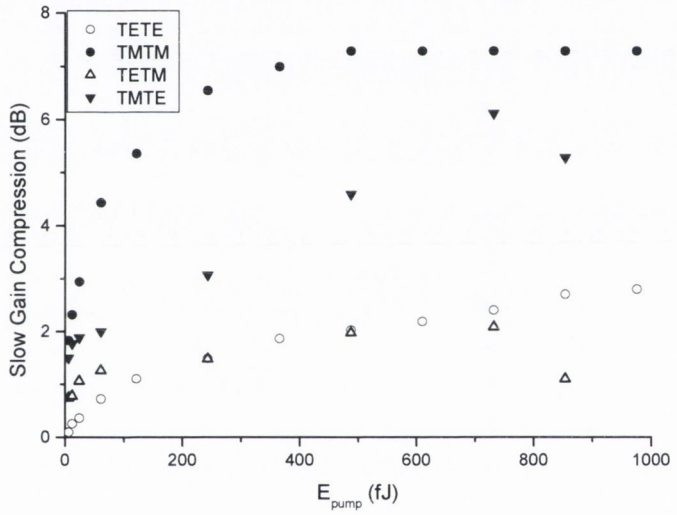

Figure 15. Slow gain compression as a function of pump pulse energy for the different input polarization cases.

In the co-polarised cases, the pump signal depletes the carriers by the same transitions used for probe amplification. The slow gain compression is much higher in the TM mode than in TE mode. As can be seen on Figure 15, the pump energy needed to reach the same gain compression is lower for TM than for TE, this is consistent with the carrier density of the heavy holes valence band (TE) being higher than that of the light holes (TM). The TM slow gain compression reaches a constant value of 7dB above 400fJ pump energy while the TE slow gain compression keeps increasing slowly with pump energy but only reaches 2.8dB. One possible explanation is that the saturation is

mainly experienced by the light hole valence band so in the TMTM case a high gain compression occurs whereas in the TETE case the saturation only affects 25% of the transitions, and while both conduction band and heavy hole band are also depleted, enough carriers remain for signal amplification.

In the cross-polarised cases, a greater cross saturation effect from TE (pump) to TM (probe) than TM to TE is observed. The TE transitions involve mainly heavy holes but also 25% light holes which can lead to a significant reduction of light hole concentration at high pump powers, and a decrease in the TM probe gain. On the other hand the decrease in light hole concentration due to a TM pump will only concern at most 25% of the holes associated with the TE probe transitions.

For a given probe polarisation, we expect a higher gain compression in the co-polarised case than in the cross-polarised case. As can be seen for the TM probe, the slow gain compression is always higher when pumping in TM than in TE, the difference increases rapidly with the pump energy as the light holes are quickly depleted by the TM pump. The difference then decreases after saturation of the light hole valence band is reached for the pump TM polarised but not for the TE polarised where only a minority of the transitions involve the light hole valence band. However the behaviour observed when the probe is TE polarised is different, the slow gain compression reached with a pump TE or TM polarised are very similar, suggesting again that the gain compression due to interband effects is dominated by the saturation of the light hole valence band consistent with a lower carrier density. At low input pump energies the slow gain compression is higher for TETM than TETE, as the light holes are depleted by the TM pump while the TE pump energy is not high enough to deplete significantly the light hole valence bands. As the pump power is increased, both the TE and TM pumps saturate the light hole valence band, reaching the same gain compression. But unlike for the TM pump case, the slow gain compression then keeps slowly increasing when the pump is TE polarised as the number of carriers depleted by transitions between conduction band heavy hole valence band increases.

4.6 Timescales

The fall time corresponds to the pump and probe pulses overlapping inside the SOA and is shown on Figure 16. At lower input pulse power, the difference between the co-polarized cases is due to the additional feature observed at -30ps. While the TETE decay curves show a decrease in transmission the TMTM signal increases so that the point at which the transmission has decreased by 10% happens at earlier time delays in TETE than in TMTM. In all cases, the difference in fall times is mainly due to the polarization dependence of the onset of the gain compression. Both cross-polarized cases exhibit lower fall times than the co-polarized case at lower pump energies because the pump pulse has to travel through a longer distance in the SOA in order to have an effect on the probe transmission. Similarly the fall time of the TETM is shorter than the TMTE due to the TE pump affecting more of the TM transitions. At higher pump energies the fall time stabilizes around 22ps, except in the TETM case where the probe is less affected by the pump and fluctuations are observed.

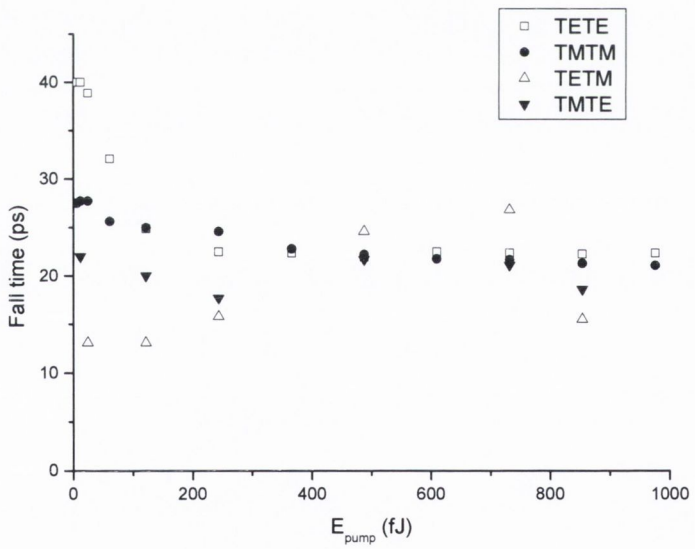

Figure 16. Average fall time as a function of pump pulse energy for co and cross polarised cases.

Figure 17 shows the fast recovery time for the co-polarised cases where the fast component represents a significant part of the device recovery. The fast recovery time

increases with pump energy and is slightly lower in TM than in TE, with a minimum of 4.4ps at 6fJ in TM and a maximum of 7.2ps at 975fJ in TE. The dependence of the gain recovery on pulse energy does not necessarily mean a change in the time constants of the intraband effects as the gain recovery dynamics also depend on the amount of gain compression [1]. Comparing Figure 13 and Figure 17, it can be seen that the range of energies over which the fast recovery time increases corresponds to the increase in gain compression. As the fast component corresponds to a convolution of the fast and slower effects and the slow timescale measured in the TETE case is slightly higher than in the TMTM, a slightly slower fast recovery time in TETE can be expected even for equal time constants of the intraband effects.

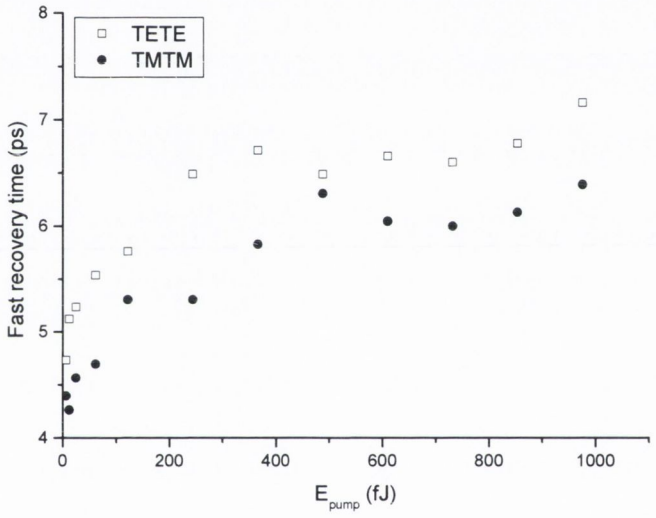

Figure 17. Fast recovery time as a function of pump pulse energy for co-polarised cases.

The slow timescale decreases rapidly with energy at low pump energies and stabilises above 200fJ to values between 100ps to 300ps depending on pump and probe polarisation. A decrease of the recovery time with injected optical power has been observed by other groups [19, 39] and attributed to the effect of the ASE on gain dynamics. The trend for the slow timescale follows the opposite trend of the slow gain compression (Figure 15). At lower pump energies, around 100fJ, the TMTM has the highest slow gain compression and the shortest slow timescale, while the other cases have similar gain compression and slow timescale. At higher pump powers, above

700fJ, the slow gain compression increases from TETM to TETE to TMTE to TMTM while the slow timescale decreases in the same order.

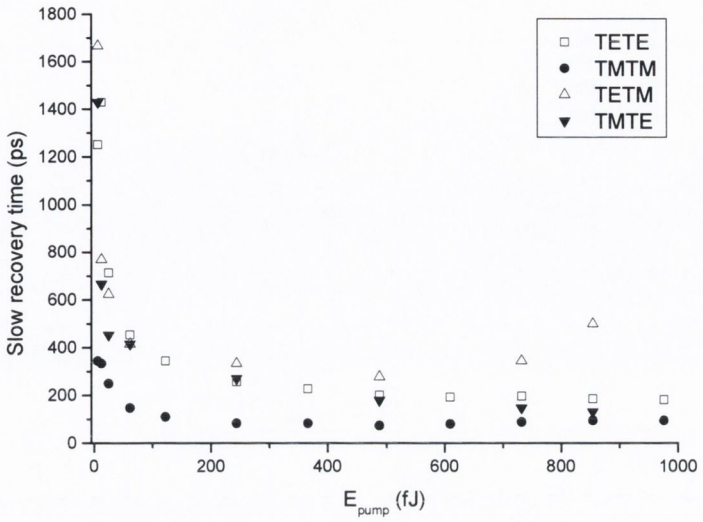

Figure 18. Slow recovery time as a function of pump pulse energy for different pump and probe input states of polarization.

4.7 Implications for gain switching

For gain switching applications the polarisation dependence of the cross gain modulation has to be taken into account. The pump and probe beams are generally set along the eigen modes of the device and travel through it with their polarisation unchanged. However as was discussed above the performance of the switch would be greatly affected by the state of polarisation of the input signals. It is obvious from Figure 14 that the co-polarised configuration is most interesting with a faster component present even at lower pump energies and a higher gain compression. Although the TMTM case displays a higher total gain compression and would therefore give a higher extinction ratio it is dominated by the slower interband effects. Therefore under our experimental conditions pumping and probing along the TE mode would give the best performances for ultrafast gain switching.

5. Injection at 45°

As discussed before the dynamic behaviour for the four different cases where light is injected along the eigen modes of the device is polarization dependent, while the probe polarization remains unchanged. For polarization switching the probe input state of polarization is usually set around 45° orientation so that it is altered as the signal travels through the SOA. In this section the dynamics are studied for signals linearly polarized at 45° (and -45°) orientation so that the same amount of power is injected in each mode. Since a contra-propagation configuration is used the cross-polarised case is probe 45°, pump 45° while probe 45° and pump -45° is co-polarised. The co/cross polarization only refers to input signals since the states of polarization vary with time delay and position inside the SOA. Figure 19 and Figure 20 show the decays recorded for a range of input pump pulse energies. Clearly the effect of the pump on the probe transmission is different in the co and cross polarised cases, with a stronger depletion in the cross-polarised case. This result is unexpected, since half the signal power is injected along each eigen mode, one could expect a similar combination of the TE and TM dynamics for injection at 45° or -45°. In fact, as the polarization of the input beams changes from linear to elliptical due to gain and birefringence effects, the photons acquire angular momentum, thus affecting the transitions probabilities [40].

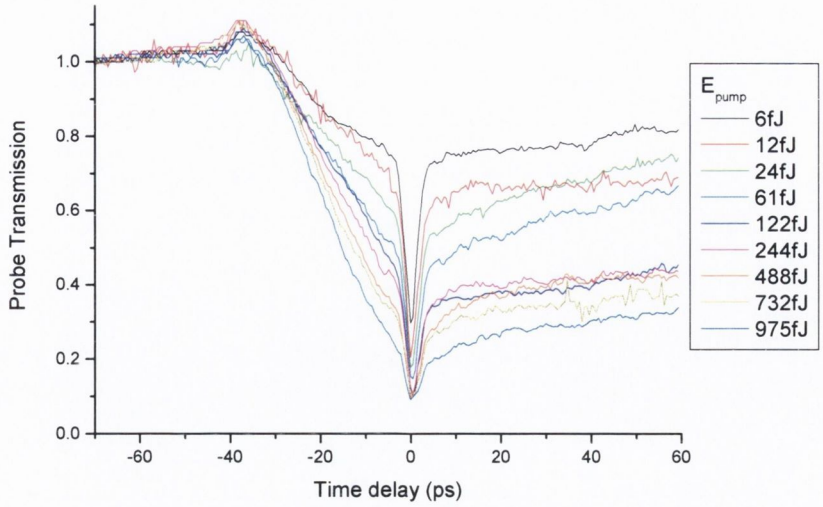

Figure 19. Decay curves of the cross-polarised case probe and pump linear at 45° for different values of pump pulse energies (6fJ-975fJ).

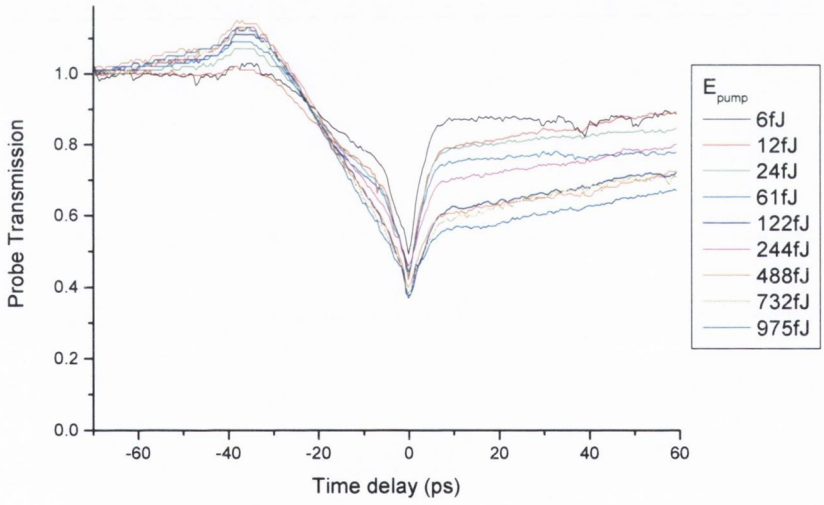

Figure 20. Decay curves of the co-polarised case probe linear 45° and pump linear at -45° for different values of pump pulse energies (6fJ-975fJ).

5.1 Gain compression

The maximum gain compression, shown on Figure 21, increases rapidly with pump energy in the cross-polarised case and stabilises around 10dB, while it stays almost constant at 4dB in the co-polarised case. Looking at the contribution of interband and intraband effects, Figure 23 and Figure 24, the gain compression is always larger in the cross-polarised case. The slow gain compression increases with pump energy, due to carrier depletion, while the additional fast gain compression decreases slightly. In both cases, pumping at 45° and -45°, intraband effects and interband effects contribute similarly to the gain compression without one dominating it.

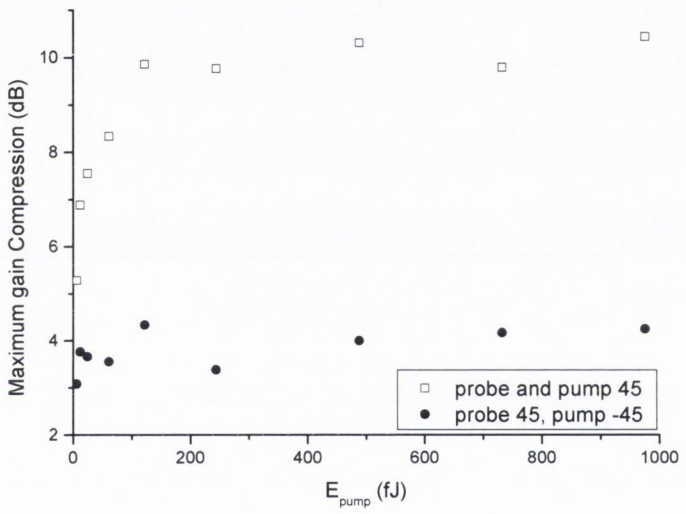

Figure 21. Maximum gain compression as a function of pump pulse energy, probe linearly polarised at 45°, pump linearly polarised at 45° and -45°.

Comparing these results with those obtained for light injected along the eigen modes of the device, the cross-polarised case (probe 45°, pump 45°) shows maximum and fast gain compression values similar to the co-polarised cases (TETE and TMTM) and slow gain compression values close to the TMTM case. The co-polarised (probe 45°, pump -45°) maximum gain compression values are closer to the TETM and TMTE cross-polarised cases, while the slow gain compression is closer to the TE polarised probe

data (TETE and TETM) and the fast component is present even at low pump energies, as was the case for TETE and TMTM but with a lower amplitude.

It has been shown [35] that when circular states of polarization are used in a pump probe experiment the spin systems become decoupled and the allowed transitions depend on the photon spin of the pump and probe signals. Therefore different gain compressions are expected for co-circular and counter-circular configurations.

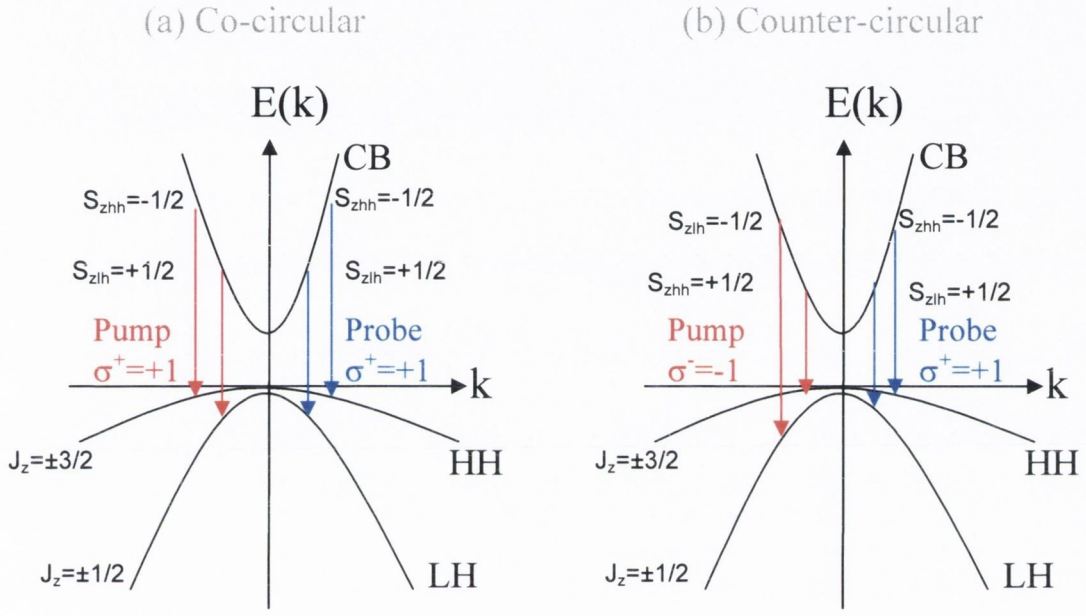

Figure 22. Band structure diagram including the conduction band (CB), heavy hole (HH) and light hole (LH) bands. Direct transitions for pump and probe signals for (a) the co-circular and (b) counter-circular pump probe configurations.

If both pump and probe are circularly polarised with a photon spin +1 the transitions bleached by the pump signal are the same as the ones used for probe amplification, as shown on Figure 22 (a). In the co-circular case, both the light hole (J_z=±½) and the electron populations (S_{zlh}=+½) involved in the probe gain compression are depleted by the conduction band to light hole band transitions of the pump. As can be seen on Figure 22 (b), in the counter-circular case, pump circularly polarised with a photon spin -1 and probe with a photon spin +1, the transitions affected by the pump are different from those used for probe amplification. Therefore a higher gain compression is expected in the co-circular case than in the counter-circular case.

In our case the state of polarisation of both pump and probe change at they travel through the SOA, thus at different positions inside the device we have different combinations of co-polarised, cross-polarised, circular and elliptical polarizations. The experimental data suggest that in the cross-polarised case, probe and pump at 45°, the elliptical states of polarisation of the probe and pump tend to rotate co-circularly while in the co-polarised case, probe 45° pump -45° they tend to rotate counter-circularly. Therefore in addition to the combination of the TE and TM dynamic behaviour, a contribution due to angular momentum is observed when injecting at 45.

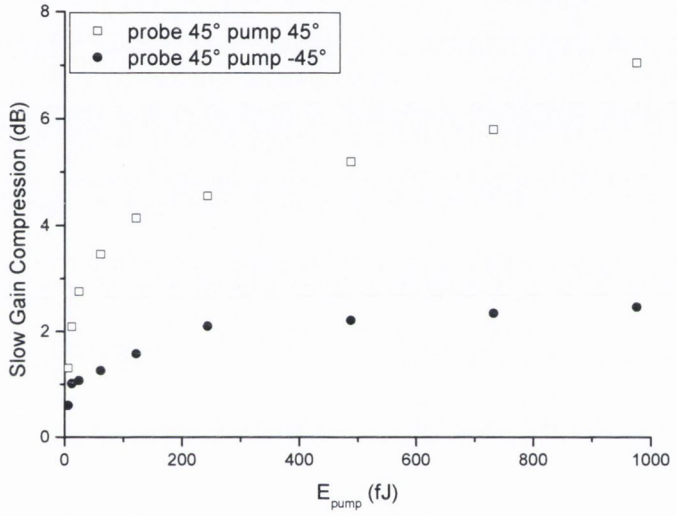

Figure 23. Slow gain compression as a function of pump pulse energy, probe linearly polarized at 45°, pump linearly polarized at 45° and -45°.

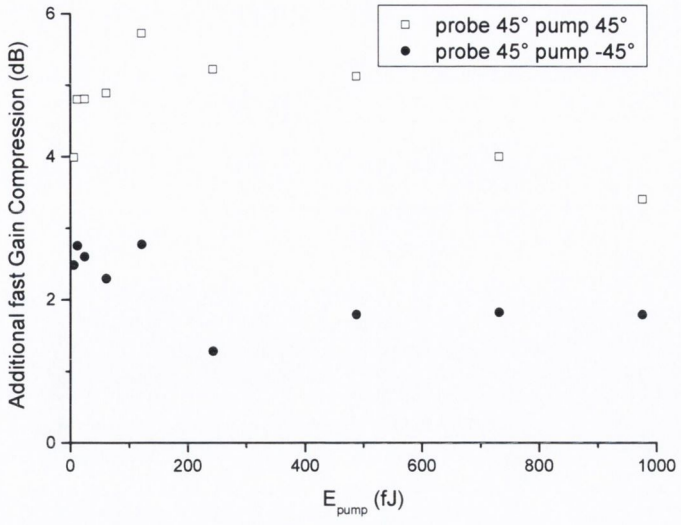

Figure 24. Additional fast gain compression as a function of pump pulse energy, probe linearly polarized at 45°, pump linearly polarized at 45° and -45°.

5.2 Timescales

As can be seen on Figure 25 the fall time for both cases does not vary much with pump energy and is slightly longer when probe and pump are cross-polarised, around 27ps than when they are co-polarised, around 23ps. This is consistent with the cross-polarised case having more of an effect on the waveguide so that the pump has to travel a shorter distance inside the device in order to change the probe transmission.

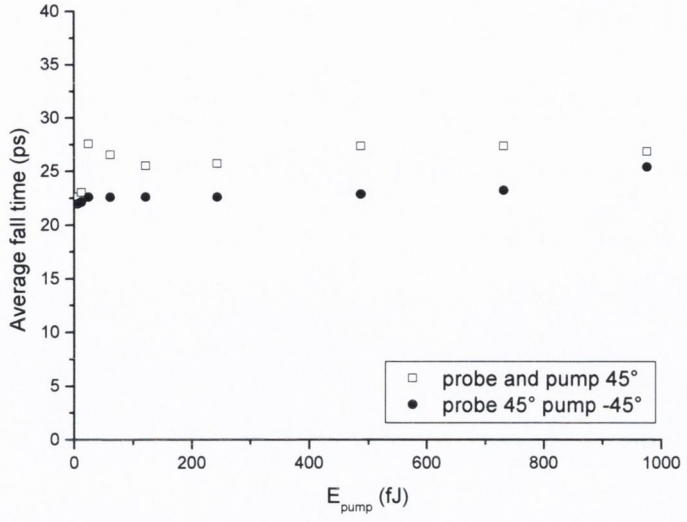

Figure 25. Average fall time as a function of pump energy, probe 45° pump 45° and -45°

The fast recovery time, shown on Figure 26, also stays constant as the pump energy is increased. It is shorter in the cross-polarised (probe and pump 45°) case than in the co-polarised case, at about 2.5ps and 4.5ps respectively. The 4.5ps fast recovery time corresponds to additional fast gain compression values close to what is observed at low pump energy when injecting along the eigen modes of the device. However 2.5ps is lower than any timescale measured in the previous experiment. As this corresponds to the pulsewidth used in the experiment it could actually be an even faster component that we are unable to resolve. One example would be the role of LO phonons in light hole recombination, but at 45° injection the slower contribution of heavy hole recombination is still expected. Unlike the difference between the TETE and TMTM fast recovery times, it cannot be explained by the convolution with the slow timescale.

As was the case when injecting along the eigen modes of the device, the slow timescale, shown on Figure 27, decrease rapidly with pump energy and reaches a steady state value of about 200ps at 122fJ for both co and cross-polarised configurations.

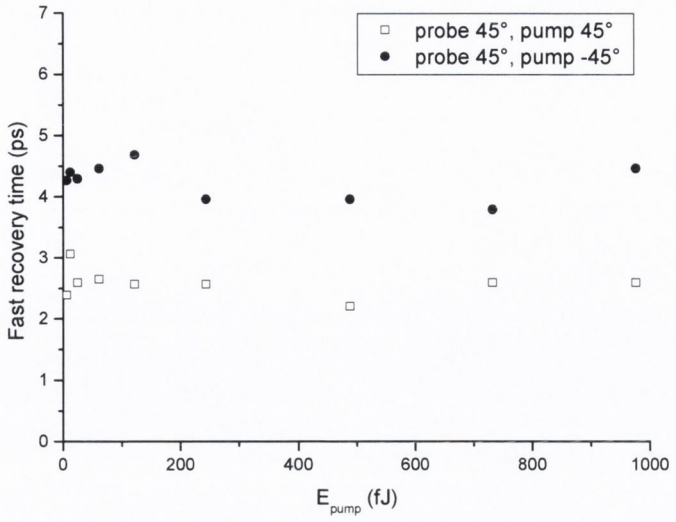

Figure 26. Fast recovery time as a function of input pump energy, probe linearly polarized at 45°, pump 45° and -45°.

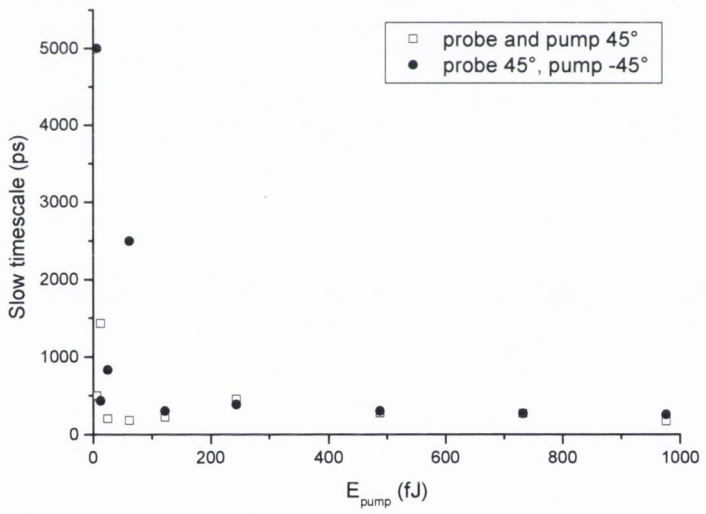

Figure 27. Slow timescale as a function of pump energy for probe linearly polarized at 45° and pump at 45° and -45°.

6. Conclusion

The free space contra-propagation configuration allows us to study the polarization resolved dynamics of the device under test. A series of pump-probe experiments were performed, with co or cross polarised pulses, injecting light polarised along the eigen modes of the device and linearly polarised at 45°. From the transmission of the probe pulse as a function of delay, it was possible to observe the fast and slow recovery components of the gain compression. The gain compression was found to be dependent on the pump and probe state of polarisation and pump pulse energy. When injecting along the eigen modes of the device, the cross-polarised data are dominated by interband effects and show a low cross gain saturation effect between the modes. The maximum gain compression was found to be higher for the TMTM case but with a larger contribution of the slow gain compression than the TETE case. It follows that the prevalence of the fast intraband effects in the TETE case shows the highest potential for ultrafast all-optical gain switching. In order to assess the potential for polarization switching, the device recovery when injecting light at 45° was studied. The gain compression and timescales were found to be dependent on the pump polarization (45° or -45°) due to the presence of rotating fields in these cases. The shorter fast recovery time around 2.5ps and higher gain compression measured in the cross-polarised case, probe 45° pump 45°, make it the most promising configuration for all-optical polarisation switching. Although no direct polarisation measurements are performed in these experiments, some information concerning the birefringence is always present in the gain measurements of the device [12, 41, 42].

REFERENCES

[1] M. Asghari, I. H. White, and R. V. Penty, "Wavelength conversion using semiconductor optical amplifiers," *Journal of Lightwave Technology*, vol. 15, pp. 1181-1190, 1997.

[2] D. Lenstra, Y. Liu, M. T. Hill, G.-D. Khoe, and H. J. S. Dorren, "Nonlinear polarization rotation in semiconductor optical amplifiers: Theory and application to all-optical flip-flop memories," *IEEE Journal of Quantum Electronics*, vol. 39, pp. 141-148, 2003.

[3] Y. Liu, M. T. Hill, E. Tangdiongga, H. De Waardt, N. Calabretta, G. D. Khoe, and H. J. S. Dorren, "Wavelength conversion using nonlinear polarization rotation in a single semiconductor optical amplifier," *IEEE Photonics Technology Letters*, vol. 15, pp. 90-92, 2003.

[4] Y. Liu, E. Tangdiongga, Z. Li, S. Zhang, H. De Waardt, G. D. Khoe, and H. J. S. Dorren, "80 Gbit/s wavelength conversion using semiconductor optical amplifier and optical bandpass filter," *Electronics Letters*, vol. 41, pp. 487-489, 2005.

[5] A. K. Mishra, X. Yang, D. Lenstra, G. D. Khoe, and H. J. S. Dorren, "Wavelength conversion employing 120-fs optical pulses in an SOA-based nonlinear polarization switch," *IEEE Journal on Selected Topics in Quantum Electronics*, vol. 10, pp. 1180-1186, 2004.

[6] H. Soto, C. A. Diaz, J. Topomondzo, D. Erasme, L. Schares, and G. Guekos, "All-optical AND gate implementation using cross-polarization modulation in a semiconductor optical amplifier," *IEEE Photonics Technology Letters*, vol. 14, pp. 498-500, 2002.

[7] H. Soto, D. Erasme, and G. Guekos, "Cross-polarization modulation in semiconductor optical amplifiers," *IEEE Photonics Technology Letters*, vol. 11, pp. 970-972, 1999.

[8] H. Soto, J. D. Topomondzo, D. Erasme, and M. Castro, "All-optical NOR gates with two and three input logic signals based on cross-polarization modulation in a semiconductor optical amplifier," *Optics Communications*, vol. 218, pp. 243-247, 2003.

[9] M. F. C. Stephens, M. Asghari, R. V. Penty, and I. H. White, "Demonstration of ultrafast all-optical wavelength conversion utilizing birefringence in semiconductor optical amplifiers," *IEEE Photonics Technology Letters*, vol. 9, pp. 449-451, 1997.

[10] P. Borri, W. Langbein, J. Mork, and J. M. Hvam, "Heterodyne pump-probe and four-wave mixing in semiconductor optical amplifiers using balanced lock-in detection," *Optics Communications*, vol. 169, pp. 317-324, 1999.

[11] J. Mark and J. Mork, "Subpicosecond Gain Dynamics in Ingaasp Optical Amplifiers - Experiment and Theory," *Applied Physics Letters*, vol. 61, pp. 2281-2283, 1992.

[12] K. L. Hall, J. Mark, E. P. Ippen, and G. Eisenstein, "Femtosecond Gain Dynamics in Ingaasp Optical Amplifiers," *Applied Physics Letters*, vol. 56, pp. 1740-1742, 1990.

[13] K. K. Anderson, M. J. Lagasse, C. A. Wang, J. G. Fujimoto, and H. A. Haus, "Femtosecond Dynamics of the Nonlinear Index near the Band Edge in Algaas Wave-Guides," *Applied Physics Letters*, vol. 56, pp. 1834-1836, 1990.

[14] C. T. Hultgren and E. P. Ippen, "Ultrafast Refractive-Index Dynamics in Algaas Diode-Laser Amplifiers," *Applied Physics Letters*, vol. 59, pp. 635-637, 1991.

[15] H. J. S. Dorren, X. Yang, D. Lenstra, H. De Waardt, G. D. Khoe, T. Simoyama, H. Ishikawa, H. Kawashima, and T. Hasama, "Ultrafast refractive-index dynamics in a multiquantum-well semiconductor optical amplifier," *IEEE Photonics Technology Letters*, vol. 15, pp. 792-794, 2003.

[16] A. Hamie, A. Sharaiha, M. Guegan, and J. Le Bihan, "All-optical inverted and noninverted wavelength conversion using two-cascaded semiconductor optical amplifiers," *IEEE Photonics Technology Letters*, vol. 17, pp. 1229-1231, 2005.

[17] D. Tsiokos, E. Kehayas, K. Vyrsokinos, T. Houbavlis, L. Stampoulidis, G. T. Kanellos, N. Pleros, G. Guekos, and H. Avramopoulos, "10-Gb/s All-Optical Half-Adder with Interferometric SOA Gates," *IEEE Photonics Technology Letters*, vol. 16, pp. 284-286, 2004.

[18] D. M. Patrick, A. D. Ellis, D. A. O. Davies, M. C. Tatham, and G. Sherlock, "Demultiplexing using polarisation rotation in a semiconductor laser amplifier," *Electronics Letters*, vol. 30, pp. 341-342, 1994.

[19] F. Girardin, G. Guekos, and A. Houbavlis, "Gain recovery of bulk semiconductor optical amplifiers," *IEEE Photonics Technology Letters*, vol. 10, pp. 784-786, 1998.

[20] C. S. Wong and H. K. Tsang, "Polarization-independent wavelength conversion at 10 Gb/s using birefringence switching in a semiconductor optical amplifier," *IEEE Photonics Technology Letters*, vol. 15, pp. 87-89, 2003.

[21] C. S. Wong and H. K. Tsang, "High extinction ratio wavelength conversion at 10 Gbit/s using birefringence switching in semiconductor optical amplifier," *Electronics Letters*, vol. 38, pp. 897-898, 2002.

[22] G. Talli and M. J. Adams, "Gain recovery acceleration in semiconductor optical amplifiers employing a holding beam," *Optics Communications*, vol. 245, pp. 363-370, 2005.

[23] L. Cheng Guan, S. Iezekiel, and C. M. Snowden, "Impact of thermal effects on Simulation accuracy of nonlinear dynamics in semiconductor lasers," *Selected Topics in Quantum Electronics, IEEE Journal of*, vol. 11, pp. 1228-1235, 2005.

[24] L. Occhi, Y. Ito, H. Kawaguchi, L. Schares, J. Eckner, and G. Guekos, "Intraband gain dynamics in bulk semiconductor optical amplifiers:

Measurements and simulations," *IEEE Journal of Quantum Electronics*, vol. 38, pp. 54-60, 2002.

[25] P. Borri, S. Scaffetti, J. Mork, W. Langbein, J. M. Hvam, A. Mecozzi, and F. Martelli, "Measurement and calculation of the critical pulsewidth for gain saturation in semiconductor optical amplifiers," *Optics Communications*, vol. 164, pp. 51-55, 1999.

[26] A. Girndt, A. Knorr, M. Hofmann, and S. W. Koch, "Theory of coherent phenomena in pump-probe excitation of semiconductor amplifiers," *Journal of Applied Physics*, vol. 78 (5), pp. 2946-2954, 1995.

[27] S. Philippe, A. L. Bradley, F. Surre, P. Landais, B. Kennedy, and M. Martinez-Rosas, "Polarisation Dependent Dynamics in Bulk Semiconductor Optical Amplifiers," in *ICTON*. Nottingham, 2006.

[28] F. Salleras, M. S. Nomura, J. N. Fehr, M. A. Dupertuis, L. Kappei, D. Marti, B. Deveaud, J. Y. Emery, B. Dagens, and T. Shimura, "Longitudinal spatial hole burning in a gain clamped semiconductor optical amplifier," presented at Pacific Rim Conference on Lasers and Electro-Optics, CLEO - Technical Digest vol.1, 2002.

[29] Y. Takahashi, A. Neogi, and H. Kawaguchi, "Polarization-dependent nonlinear gain in semiconductor lasers," *Quantum Electronics, IEEE Journal of*, vol. 34, pp. 1660-1672, 1998.

[30] H. Ghafouri-Shiraz, *The Principles of Semiconductor Laser Diodes and Amplifiers, Analysis and Transmission Line Laser Modeling*: Imperial College Press, 2004.

[31] J.-N. Fehr, M.-A. Dupertuis, T. P. Hessler, L. Kappei, D. Marti, F. Salleras, M. S. Nomura, B. Deveaud, J.-Y. Emery, and B. Dagens, "Hot phonons and auger related carrier heating in semiconductor optical amplifiers," *IEEE Journal of Quantum Electronics*, vol. 38, pp. 674-681, 2002.

[32] B. N. Gomatam and A. P. DeFonzo, "Theory of hot carrier effects on nonlinear gain in GaAs-GaAlAs lasers and amplifiers," *IEEE Journal of Quantum Electronics*, vol. 26, pp. 1689-1704, 1990.

[33] T. P. Pearsall, *GaInAsP Alloy Semiconductors*: Wiley, 1982.

[34] J. Mork, J. Mark, and C. P. Seltzer, "Carrier heating in InGaAsP laser amplifiers due to two-photon absorption," *Applied Physics Letters*, vol. 64, pp. 2206-2208, 1994.

[35] A. Leitenstorfer and A. Laubereau, "Ultrafast Electron-Phonon Interactions in Semiconductors: Quantum Kinetic Memory Effects," in *Semiconductors and Semimetals: Ultrafast Physical Processes in Semiconductors*, vol. 67, K. T. Tsen, Ed.: Academic Press, 2001.

[36] W. Wang, K. Allaart, and D. Lenstra, "Semiconductor optical amplifier gain anisotropy: Confinement factor against material gain," *Electronics Letters*, vol. 40, pp. 1602-1603, 2004.

[37] T. D. Visser, H. Blok, B. Demeulenaere, and D. Lenstra, "Confinement factors and gain in optical amplifiers," *IEEE Journal of Quantum Electronics*, vol. 33, pp. 1763-1766, 1997.

[38] E. P. O'Reilly and A. R. Adams, "Band-structure engineering in strained semiconductor lasers," *Quantum Electronics, IEEE Journal of*, vol. 30, pp. 366-379, 1994.

[39] R. Gutierrez-Castrejon, L. Schares, L. Occhi, and G. Guekos, "Modeling and measurement of longitudinal gain dynamics in saturated semiconductor optical amplifiers of different length," *IEEE Journal of Quantum Electronics*, vol. 36, pp. 1476-1484, 2000.

[40] W. H. Louisell, *Quantum Statistical Properties of Radiation*: John Wiley & Sons, 1973.

[41] K. L. Hall, G. Lenz, A. M. Darwish, and E. P. Ippen, "Subpicosecond gain and index nonlinearities in InGaAsP diode lasers," *Optics Communications*, vol. 111, pp. 589-612, 1994.

[42] R. Giller, R. J. Manning, and D. Cotter, "Gain and phase recovery of optically excited semiconductor optical amplifiers," *IEEE Photonics Technology Letters*, vol. 18, pp. 1061-1063, 2006.

CHAPTER 6 :
DYNAMICS OF NONLINEAR POLARISATION ROTATION

1. Introduction

A study of the polarisation dependent dynamics was performed in the previous chapter discussing the different behaviours observed when injecting light polarised along the eigen modes of the device or linear with a 45° orientation, both in the co and cross-polarised cases. While the attention was on the underlying physics of the device and gain effects, this chapter focuses on the change in the probe state of polarisation due to the injection of the pump as well as the dynamics of this change. To this end polarisation dependent detection is used, where a polarizer is placed in front of the detector. Firstly the cross-polarised cases of light polarised along the eigen modes of the device are studied as these are most commonly used by other authors [1-3] and rotation of the eigen axes is investigated. We then focus on the 45° injection, where a change in the state of polarisation is expected from the measurements performed with continuous laser beams, and also showed the best potential for polarisation switching in the previous chapter.

2. Experimental set-up

The set-up used for the following experiments has a free space contra-propagation configuration similar to the one used in the previous chapter. The pulsed input is provided by the femtosecond laser providing a 2.5ps pulsewidth and the same device is used, with the temperature set at 20°. In order to avoid the change of polarisation due to the reflection of the output probe beam at the beamsplitter, the location of the detection of the output probe signal is modified. The beamsplitter previously used to separate output probe signals and input pump signals is moved back and used to replace the mirror closest to the SOA output, as shown on Figure 1, and the output probe is monitored after transmission through that beamsplitter.

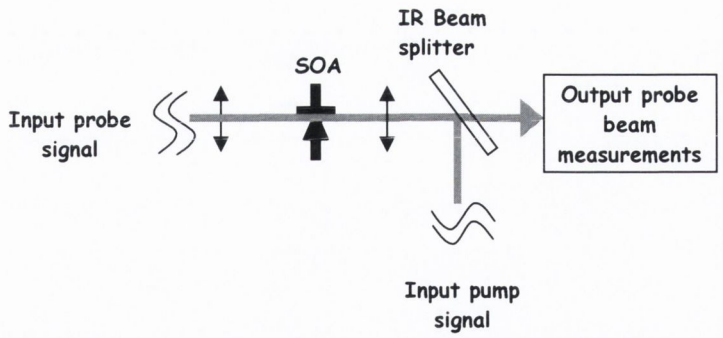

Figure 1. Set-up modified for polarisation dependent detection

The analogue lock-in amplifier is also replaced by a digital one. For very low input signals it was found to give better output stability and also has the capacity for direct phase measurements.

3. Polarization resolved decays

A polarizer is placed in front of the photodiode and the decays are recorded as a function of its orientation for different pump and probe states of polarisation combinations. The polarizer orientation or angle refers to the angle between the polarising axis and the horizontal (or TE) direction. The results are shown on Figure 2 to Figure 13 for the cross-polarised cases TETM and TMTE as well as probe and pump linearly polarised at 45°. The probe has a low energy, 12fJ, below saturation. The measurements are taken for both low pump energy, 12fJ, and high pump energy, 875fJ. As can be seen on Figure 2, the levels measured at more negative delays, when the SOA is not affected by the pump, are strongly dependent on polarizer orientation. As this level is used to express the decays as transmission values and in order not to lose any information, both the direct measured output and the transmission curves are given.

3.1 Eigen modes of the device: cross-polarised cases

Considering first the case of probe and pump cross-polarised along the eigen modes of the device. A number of common features are observed on the polarisation dependent decays. Looking for instance at the low pumping condition Figure 2, probe TM and pump TE. As expected the output signal is largest when polarizer and probe input polarisation are collinear. A faster component, which is absent at low pump energies when the polarizer is aligned with the input probe polarisation, can now be seen when the polarizer is oriented at least 45° away from the probe. Also in some cases, for TMTE with the polarizer set at 0° and 15°, i.e. with the output polarizer and input probe almost crossed, this fast component corresponds to an increase of the output level instead of the gain compression expected. This could be attributed to transfer of energy from one mode to the other. While a more in depth analysis is needed to understand the exact origin of the effect it shows potential for high speed non-inverted switching. This is especially true in the TETM case with a low pump and polarizer oriented at 60°, as can be seen on the transmission curve Figure 7. The large change observed there when rotating the polarizer from 60° to 45° could be explained by a small rotation of the output polarisation. If the output probe polarisation has an orientation just above 45° at negative delay and close to 60° around zero delay then the rotation would be detected as a decrease in transmission when the polarizer is set at 45° and an increase when set at -60°. However such output states of polarisation are not expected when injecting along the eigen modes of the device. It is more likely that both the probe signal and the ASE reach a minimum at 0ps time delay. In the TETM case, no fast component are observed when no polarizer are present at the output because, as discussed in the previous chapter, the carrier heating mainly takes place in the light hole valence band, affecting only a minority of the probe transitions. But it may be possible to observe the carrier heating effect by detecting part of the ASE generated along the TM mode, as it is probably affected by the light hole depletion due to the TM polarised pump. Although in that case a decrease in ASE is expected while the fast components observed in the decays correspond to either an increase or a decrease in the signal depending on the polarizer orientation.

At higher pump energy, Figure 5 and Figure 9, a great diversity of shape is observed in the decays, with the transmission increasing or decreasing as a function of time delay, depending on the polarizer angle. Several minima or maxima can be reached by the same decay, with values going negative in some cases. Although the changes seem quite dramatic when looking at the transmission curves, they actually correspond to low output levels, as can be seen on Figure 4 and Figure 8. At these low levels, where most of the output probe signal is cut-off by the polarizer, the noise due to the amplified spontaneous emission (ASE) could also become significant and contribute to the measured decays. While most of the noise due to ASE is suppressed by the lock-in detection, a small part of it is modulated by the chopped probe signal. The modulated ASE is extremely low since the input probe energy is kept as small as possible, well under the device saturation energy. However it is modulated at the reference frequency used, which makes it impossible to suppress by lock-in detection. As the ASE is largely unpolarised, some will be transmitted through the polarizer no matter what its orientation may be, unlike the output probe signal, which is likely to be linearly polarised and as such can be blocked by the polarizer.

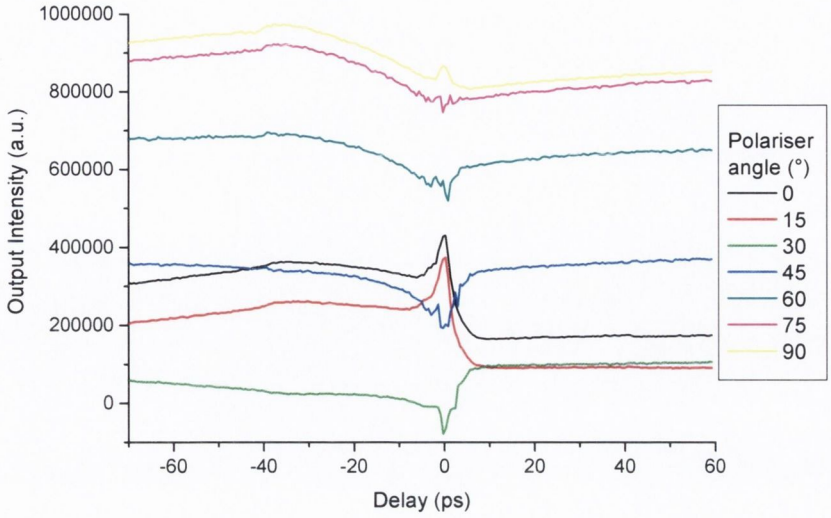

Figure 2. Output probe intensity as a function of pump probe delay, probe TM polarised, 12fJ and pump TE polarised, 12fJ.

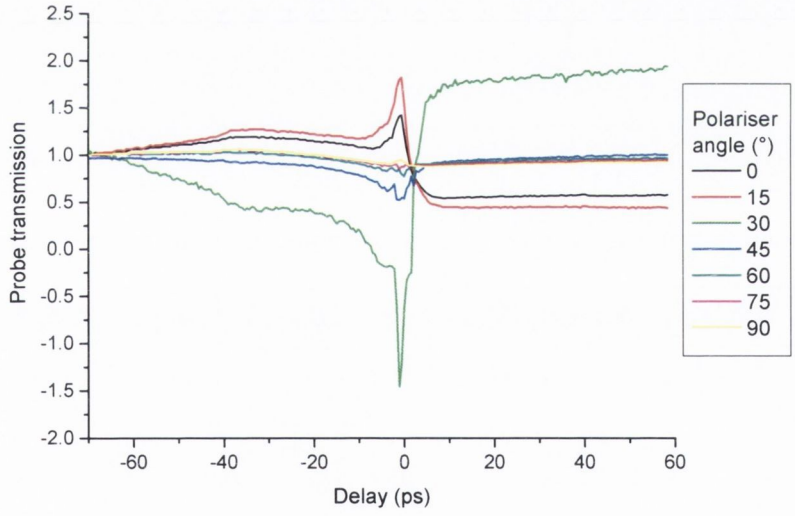

Figure 3. Probe transmission as a function of pump probe delay, probe TM polarised, 12fJ and pump TE polarised, 12fJ.

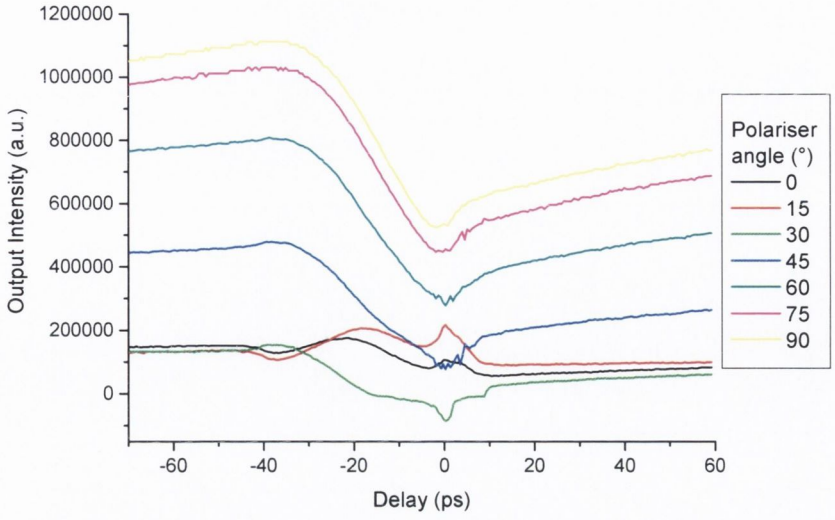

Figure 4 Output probe intensity as a function of pump probe delay, probe TM polarised, 12fJ and pump TE polarised, 875fJ.

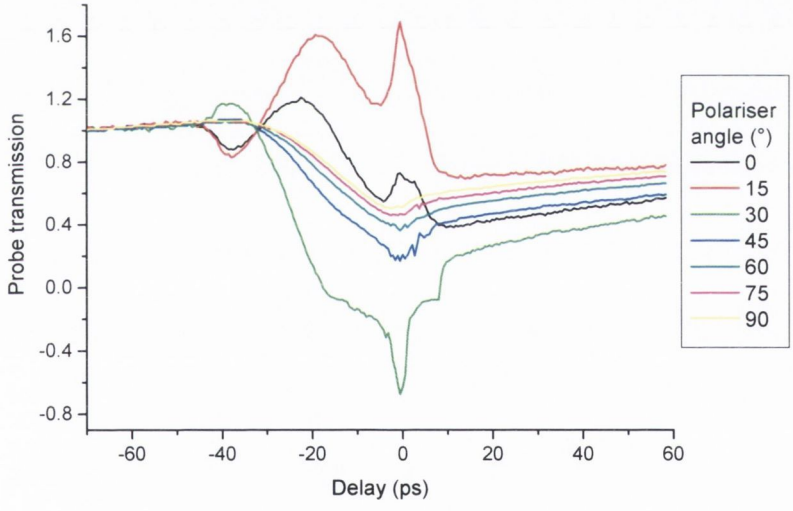

Figure 5. Probe transmission, as a function of pump probe delay, probe TM polarised, 12fJ and pump TE polarised, 875fJ.

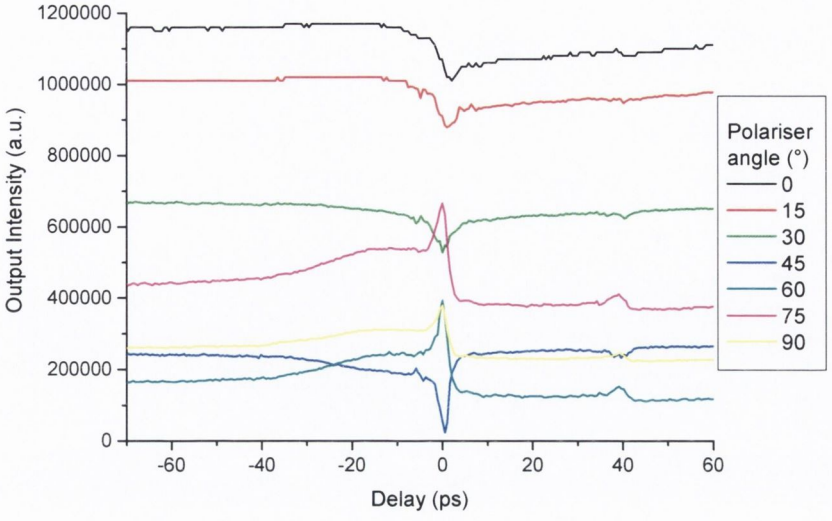

Figure 6. Output probe intensity as a function of pump probe delay, probe TE polarised, 12fJ and pump TM polarised, 12fJ.

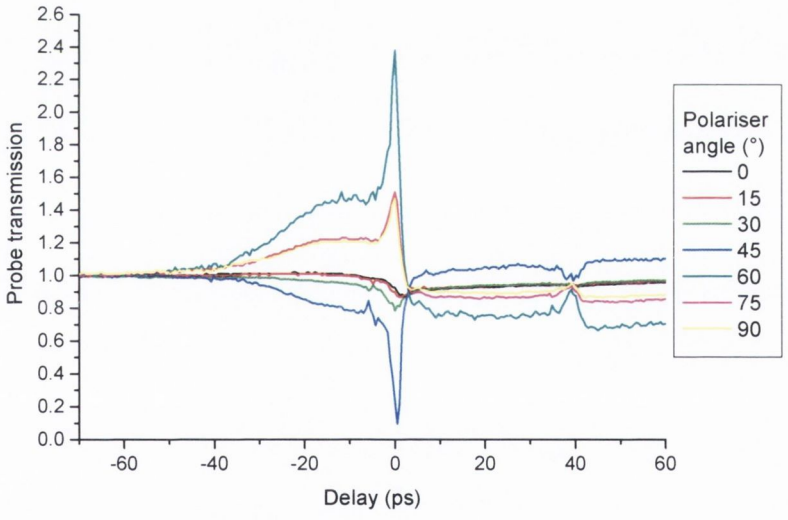

Figure 7. Probe transmission as a function of pump probe delay, probe TE polarised, 12fJ and pump TM polarised, 12fJ.

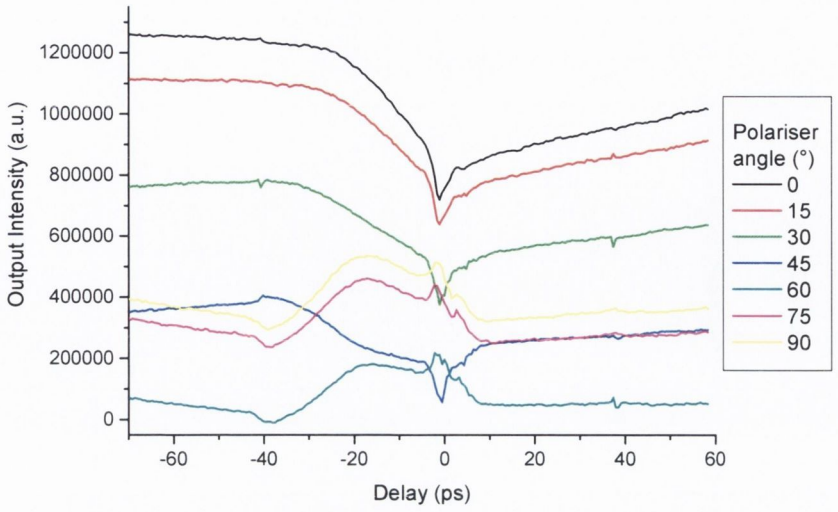

Figure 8. Output probe intensity as a function of pump probe delay, probe TE polarised, 12fJ and pump TM polarised, 875fJ.

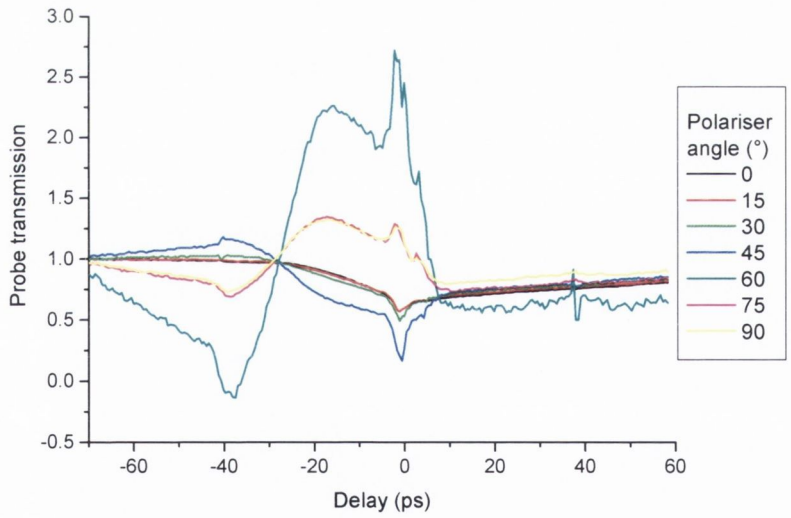

Figure 9. Probe transmission as a function of pump probe delay, probe TE polarised, 12fJ and pump TM polarised, 875fJ.

3.2 Injection at 45°

In contrast with the previous data where light was injected along the eigen modes of the SOA, the decays measured for injection of signal polarised linearly at 45° do not present much variety of behaviour. A significant signal is recorded for each polarizer orientation, without having to adjust the sensitivity of the lock-in detection. As can be seen on Figure 10 to Figure 13, a decrease in transmission is experienced in all cases, followed by gain recovery at positive delays. The minimum transmission however is strongly dependent on the output polarizer angle, especially in the low pumping case (Figure 11) where the transmission varies from 0.5 for polarizer at 0° to 0 for polarizer oriented between 60° and 90°. Considering the maximum gain compression measured without polarizer in chapter 5, about 7dB at low pump energy and 10dB at higher pumping, this variation can be attributed to a change in output probe state of polarisation with time delay. The same can be observed at higher pump energy but to a lesser extent because of the predominance of the gain compression in that case. Also of great interest for ultrafast polarisation switching is the importance of the fast recovering transmission measured at low pump energy, which is strongly dependent on polarizer orientation, going from almost non-existent for polarizer at 0° to dominant for polarizer at 60° to 90°. At low pump energy and polarizer at angles above 45° the slow gain compression, from chapter 5 about 2dB, is compensated for by the change in probe polarisation and no slow recovery is observed. With the polarizer at 75° and 90° the transmission after the fast recovery even reaches a level slightly higher than it was when the pump had no effect. Finally compared to the high pumping case, the perturbation of the probe transmission is more gradual for low pump energy at more negative delays. As can be seen on Figure 11, at more negative delays the output probe signal decreases slowly with time delay (around -40ps) while a large perturbation is recorded in the high pump energy case, Figure 13, with the signal increasing or decreasing depending on polarizer angle, due to the additional polarisation dependent feature present when pump and probe overlap close to the output of the SOA.

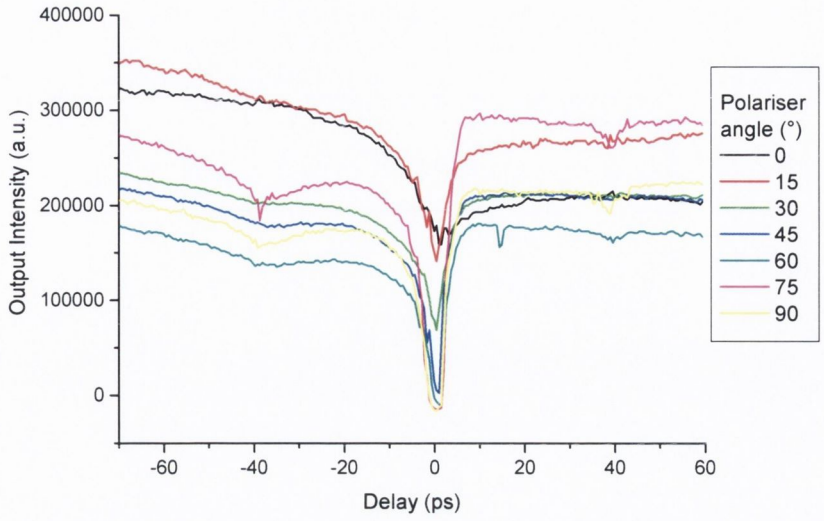

Figure 10. Output probe intensity as a function of pump probe delay, pump and probe linearly polarised at 45°, probe 12fJ and pump 12fJ.

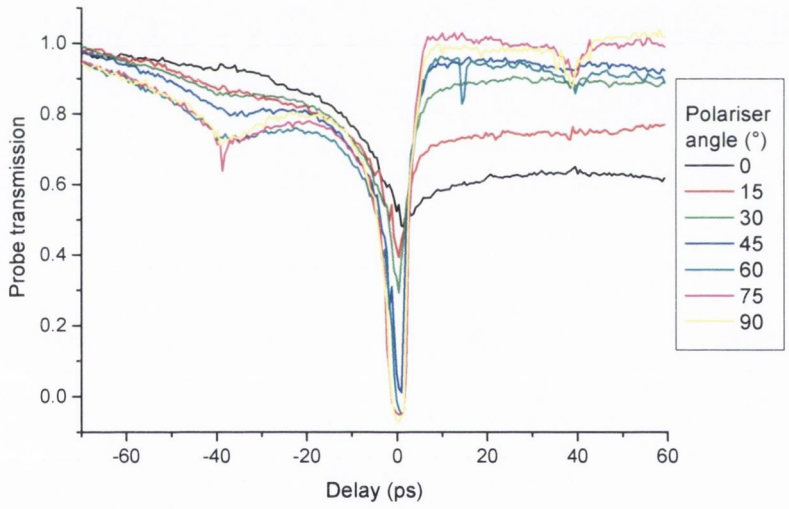

Figure 11. Probe transmission as a function of pump probe delay, pump and probe linearly polarised at 45°, probe 12fJ and pump 12fJ.

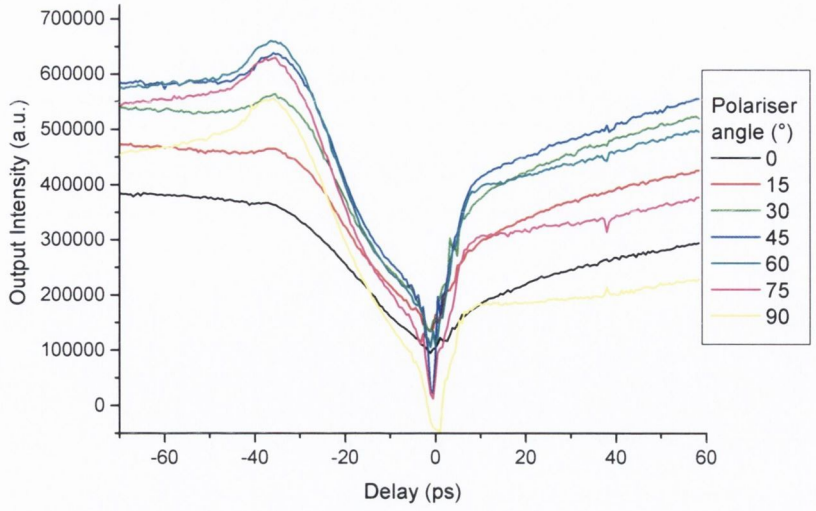

Figure 12. Output probe intensity as a function of pump probe delay, pump and probe linearly polarised at 45°, probe 12fJ and pump 875fJ.

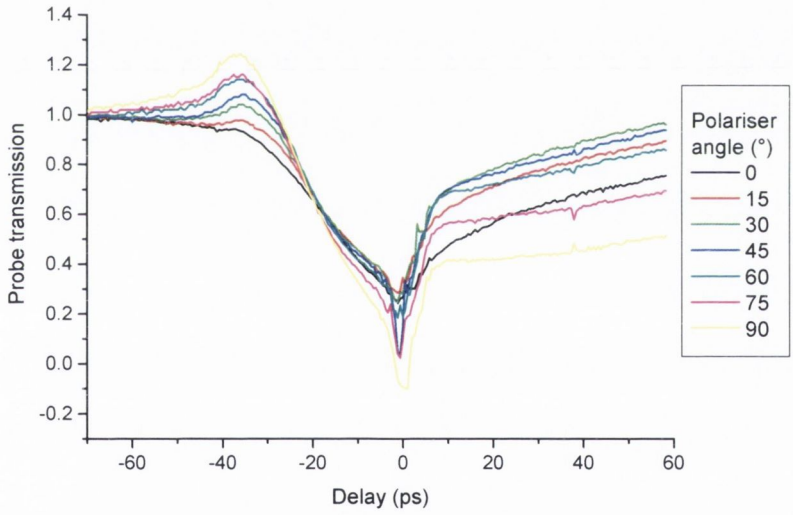

Figure 13. Probe transmission as a function of pump probe delay, pump and probe linearly polarised at 45°, probe 12fJ and pump 875fJ.

At low pump energy the decrease in transmission is then steeper when approaching zero delay. This combined with the dominant fast recovery and high extinction ratio for polarizer orientations above 45° shows a greater potential of the low pump energy case for ultrafast polarisation switching. For comparison, the shortest time taken for the transmission to decrease from 0.5 to zero and increase back to 0.5 is less than 10ps for low pump against about 25ps with high pump.

4. Intensity dependence on polarizer orientation

In order to try to extract the state of polarisation of the output probe from the decays, the output level at different pump probe delays is plotted as a function of the polarizer orientation for each case, as shown on Figure 14. Four different delays are considered, -75ps where the pump has no effect on the probe, -40ps where pump and probe overlap at the input of the SOA, 0ps at maximum effect of the pump, and finally during the slow recovery at -25ps.

Considering first the 45° injection condition, Figure 14 (e) and (f), the maximum variation of the intensity with polarizer angle is about 50% showing that the output probe signal has a high ellipticity. This is observed at all pump probe delays except 0ps, where the intensity reaches zero. Two different conditions can cause a zero transmission: a linear state of polarisation oriented at 90° with the polarizer angle or large carrier depletion due to the pump. Considering that the decays measured without polarizer in chapter 5 did not reach zero transmission and that, as can be seen on Figure 14, the transmission stays constant for different values of polarizer angle, both gain compression and change in polarisation play a part in the high extinction ratio. At low pump energy the variation in intensity with polarizer angle seems noisy. The order of the data taken at different time delays does not change much with polarizer orientation: values measured at -75ps are the highest, with -40ps and 25ps data close to one another and 0ps data much lower. This is similar to what was measured without polarizer in chapter 5, due to the gain compression only. The probe state of polarisation and how it changes as a function of pump probe delay is unclear in this case.

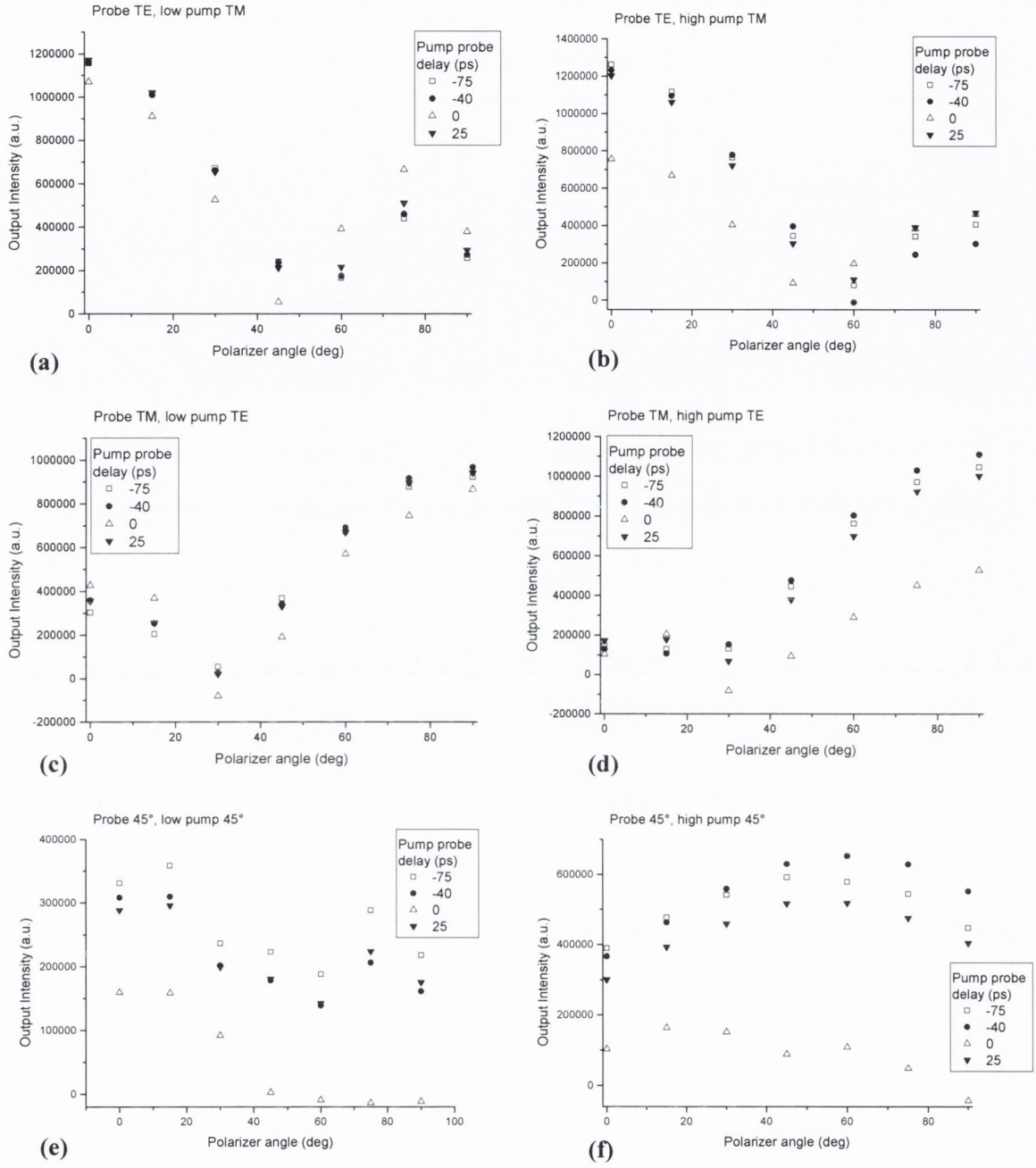

Figure 14. Output intensity as a function of the output polarizer orientation for different values of pump probe delay.

At high pump energy the curves look much smoother. The 0ps data are much lower than the others and the 25ps are always lower than the -75ps due to the slow recovery of the transmission. The -40ps are higher than the 25ps ones, close to the -75ps data for polarizer angles 0° to 30° but reaching higher values for polarizer angles from 45° to 90°. This variation corresponds to the polarisation dependent feature observed when pump and probe pulses overlap close to the output of the SOA. While no dramatic change in probe polarisation is observed, more data points are needed for a better assessment of the states of polarisation, showing at least a maximum and a minimum transmission through the polarizer, as will be shown later.

As far as injection along the eigen modes of the device is concerned, as shown on Figure 14 (a) to (d), when the polarizer and probe input polarisation have close orientations the values at -75ps, -40ps and 25ps tend to be close while the 0ps data are lower due to gain compression. When the difference in orientation is between 60° and 90°, the 0ps data have a higher intensity than other delays in the low pumping cases and become similar to other delays in the high pumping cases. As expected, in all cases the intensity is highest when polarizer and probe input polarisation have same orientation. However a minimum is then reached 45° to 60° away from input probe orientation and the intensity increases again as the polarizer is rotated towards an orientation 90° away from the input probe, where all light is expected to be blocked.

For light polarized along the eigen modes of the device, the output probe is expected to be linearly polarised and Malus's law applies [4]. In that case the output intensity after the polarizer can easily be predicted. If the polarising axis makes an angle ϕ with the linear polarisation orientation, the input signal, can be resolved into two components of same absolute phase φ_0, one parallel to the polarising axis, $E_{//}$, and the other perpendicular, $E_{\perp}$:

$$E_{//} = E\cos\phi.\sin(wt - kz + \varphi_0)i$$
$$E_{\perp} = E\sin\phi.\sin(wt - kz + \varphi_0)j$$

Where E is the amplitude of the electric field, w is the optical frequency, k the wave number, i the unit vector along the polarising axis and y the unit vector perpendicular to it. Only the parallel component, with amplitude E cos ϕ, is transmitted through the

polarizer. Since the intensity of an electromagnetic wave is proportional to the square of its amplitude, the intensity of the signal transmitted through the polarizer, I, is:

$$I = I_{max} \cos^2 \phi$$

Where I_{max} is the maximum intensity of transmitted light (at ϕ=0).
Therefore as the polarizer is rotated the intensity varies with a period of 180°. This is clearly not the case on Figure 14 (a) to (d), where the angle between the maximum and minimum transmissions is close to 45° instead of the 90° expected. This relationship only holds for linearly polarized light and a different behaviour for elliptically polarised light or in the presence of unpolarised light can be expected. However for elliptically polarised light the period of the transmitted intensity versus polarizer angle remains the same, as discussed below. It follows that more experimental data points are needed for a better characterization of the output polarisation, at least over a polarizer rotation of 180°, as will be discussed later.

5. Influence of modulated amplified spontaneous emission

The unexpected behaviour observed in the previous decays, with signal transmission increasing when gain compression occurs and negative values recorded , comes from the noise due to the amplified spontaneous emission (ASE). As discussed previously the average power of the output probe signal is very low compared to the ASE and an interference filter as well as a lock-in detection technique are used to retrieve the signal. However a small part of the ASE is modulated by the chopped probe and therefore has same frequency. As such it cannot be differentiated by the lock-in amplifier. The problem arising when probe signal is low is mostly due to the phase sensitive detector of the lock-in amplifier. In fact as the probe signal is blocked by the polarizer, the modulated ASE signal can become dominant.

5.1 Phase sensitive detector

In a phase sensitive detector, a switching amplifier is used as a synchronous detector and a 2-state switch is controlled electronically from the reference voltage [5]. When the signal is in phase with the reference, rectification is achieved and a dc voltage

proportional to the signal amplitude can be measured after the low-pass filter, as shown on Figure 15.

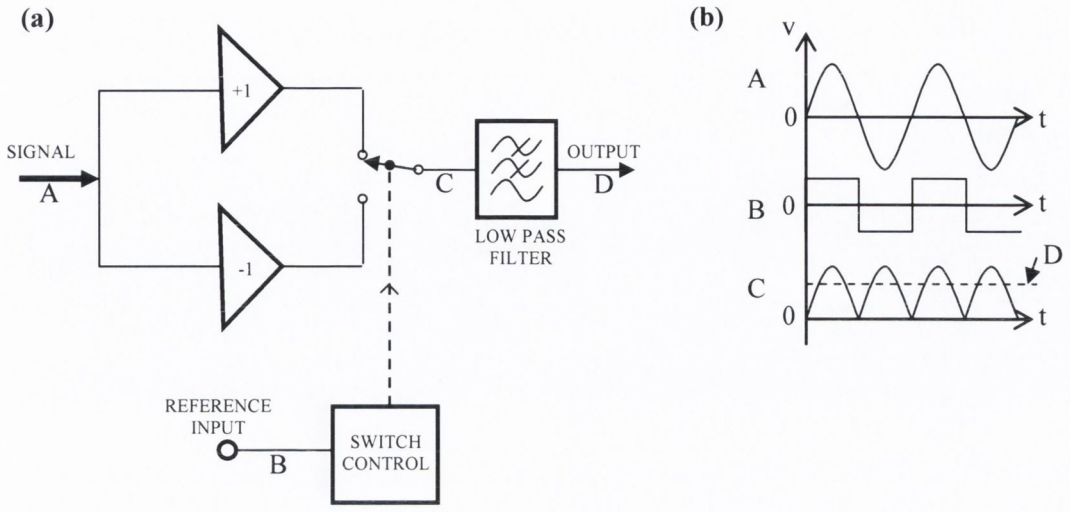

Figure 15. Phase sensitive detector: (a) diagram (b) signal rectification.

The phase of the reference signal is adjusted with a phase shifter so as to maximise the output signal. When the chopper lets light through (B>0) the output probe signal increases while the ASE signal decreases due to carrier depletion. Effectively in this experiment, instead of the sinusoidal signal showed on Figure 15 (b) the input A has two components out of phase with each other. One corresponds to the probe output. It has much higher intensity before the polarizer but can be blocked by it if it is linearly polarised. The other corresponds to the modulated ASE. While its intensity is very low, it is largely unpolarised and thus cannot be totally blocked by the polarizer. Therefore when the probe signal is linearly polarised or close to it, as is the case when injected along the eigen modes of the device, and almost completely blocked by the polarizer, a signal corresponding to the modulated ASE is detected. If, as was the case when measuring the previous decays, this signal is used to set the phase and maximise the lock-in output, the reference is set out of phase with the signal of interest (the output probe signal) since the ASE is higher when the chopper blocks the light. In that case an increase of the ASE or a decrease of the probe signal both results in an increase in the lock-in output. However if the signals have similar amplitudes then the phase could be set to any value and the meaning of the lock-in output becomes quite unclear. This could explain the rise observed in 3.1 when injecting along the eigen modes and blocking most of the output probe with the polarizer. Therefore the phase should always

be maximized using the signal of interest, in this case the probe output, when it is the dominant signal. Another consequence is that when setting the reference in phase with the probe signal, the output voltage will become negative when the modulated ASE becomes higher than the probe signal.

5.2 Phase measurements

The digital lock-in amplifier used here can give a direct measurement of the phase difference between the input and reference signals. It is important to stress here that the phase set when optimizing the output signal is always kept constant, as is the phase oh the chopped input probe signal. What actually varies is the phase of the combined modulated ASE signal and the ouput probe signal. Figure 16 (a) shows both the amplitude and phase measured when injecting light along the TE mode and rotating the output polarizer. The phase is maximised once, when the probe signal is maximum, and the measurements are taken when the pump has no effect on the probe.

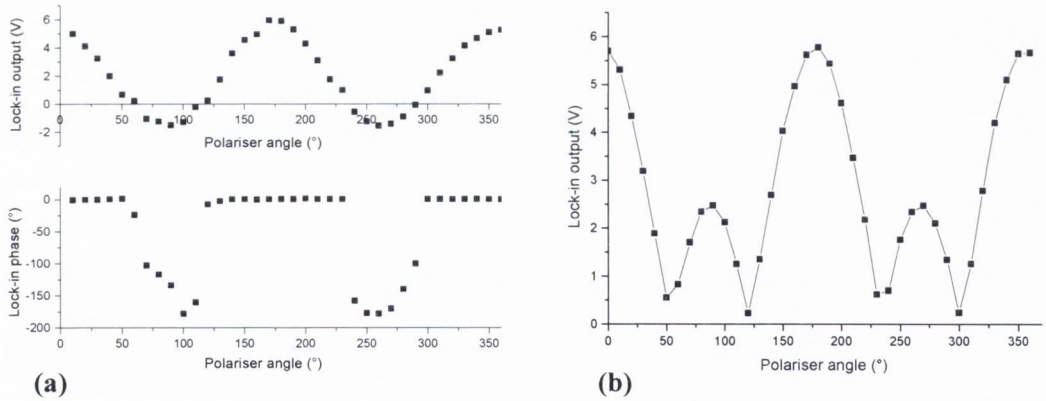

Figure 16. Probe signal as a function of polarizer angle. (a) Lock-in amplifier output phase and voltage, phase adjusted once at maximum transmitted probe as used for following polar plots measurements , (b) lock-in amplifier output voltage, phase adjusted to maximise signal for each data points as used for previous decay measurements.

As the polarizer is rotated from 0° to 50° the phase stays constant and close to zero i.e. the reference and input signals are in phase. Between polarizer orientations of 60° to 120°, the output of the lock-in is negative and the phase changes from 0° to -180° and

back. This shows a competition of the output probe and modulated ASE signals and the negative output reflects the fact that now when the chopper lets the light through, a decrease of the total input signal is registered by the amplifier. The presence of the modulated ASE results in a negative offset in the lock-in output. This is not the case when the phase is adjusted in order to maximise the signal for each data points as Figure 16 (b) shows. This is the procedure that was used when measuring the decays, here the output voltage stays positive but does not always correspond to the output probe signal anymore. When the negative offset is subtracted from the measured data points and values are normalised in order to compare the behaviour with Malus's law, a good agreement is achieved, as can be seen on Figure 17 (a). Here for TE polarised probe a small rotation of 2° is present. However as information is contained in both in minimum and maximum intensity values, only the direct measurements are given in the following results.

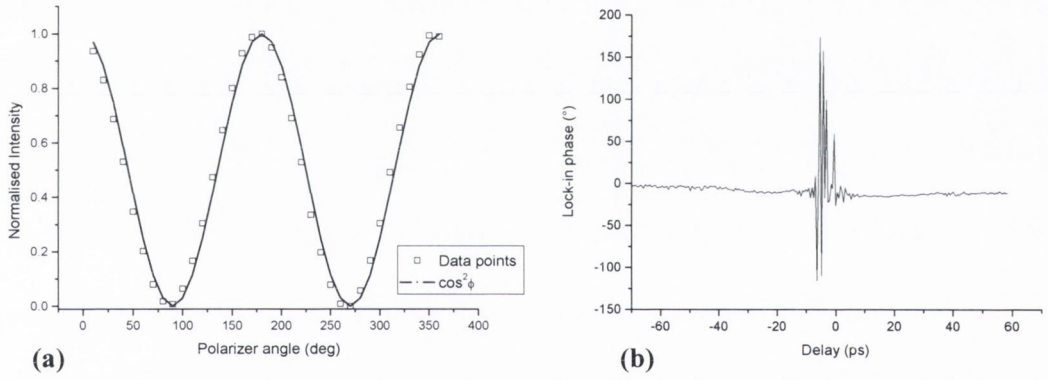

Figure 17. (a) comparison between corrected measured data points and Malus's law, (b) Lock-in phase measurement as a function of pump probe delay.

In order to check the effect of the general gain compression on the phase measured by the lock-in amplifier, a scan is taken for the TETE case with high pump energy. Figure 16 (b) shows the phase measured by the lock-in amplifier as a function of the pump probe delay. Clearly the phase stays constant at 0° except near to zero delay, where the probe signal is the lowest, the modulated ASE signal becomes significant and both interference patterns and coherent artefacts were observed. Clearly the phase should be optimised at delays away from this high gain compression region as well as at high probe transmission through the output polarizer.

6. Change of polarization

6.1 Polar plots

For a better assessment of the states of polarisation of the output probe, its intensity is again recorded as a function of the orientation of the polarizer placed in front of the detector. This time however the pump probe delay is fixed and the polarizer rotated over 360° in steps of 10°. Sets of data are measured at six different values of delay, as shown on Figure 18: **A** before the pump has an effect on the probe, **B** when pump and probe overlap at the output of the SOA, **C** as pump and probe pulses overlap inside the device but before the perturbations due to the modulated ASE signal and the oscillations, **D** during the fast recovery, **E** just after the fast recovery and **F** during the slow recovery. No measurements can be taken at minimum transmission because of oscillations due to the modulated ASE signal and to the coherent artefact.

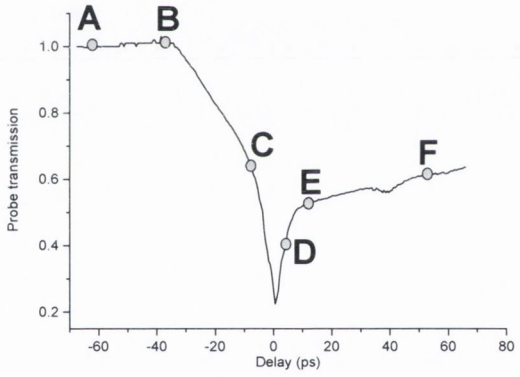

Figure 18. Positions of data points.

In the general case the output of the polarizer can be predicted [4] for any input polarisation multiplying the Stokes vector of the input and the Mueller matrix of a polarizer. Figure 19 shows examples of calculated output intensity for different input polarisation, both as a regular graph and as polar plots. The Stoke vectors used were normalised (S_0=1). The XY graph is more easily used to measure rotations while the polar plots give a more graphic representation of the state of polarisation. While calculating the output Stoke vector is straightforward, finding the exact input polarisation is not as easy because the variation of the intensity are also influenced by

the change in total intensity and the offset due to the ASE. Nevertheless the polar plots give valuable information on the probe output polarisation and how it is changing with pump probe delay.

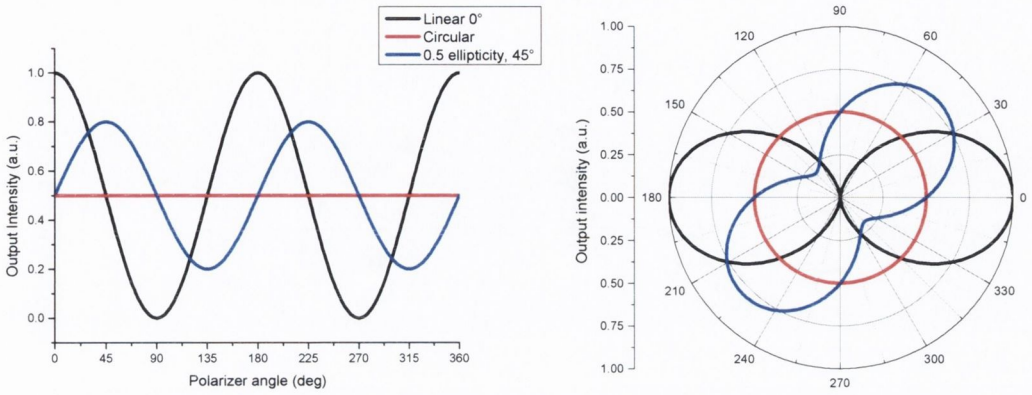

Figure 19. Calculated polarizer output intensity as a function of polarizer orientation for different input polarisations.

6.2 Rotation of eigen axes

Firstly the rotation of the eigen modes of the device is investigated. The probe is TE polarised with a pulse energy of 12fJ and the polar plots are measured for pump TM with 12fJ and 875fJ pulse energy, and pump TE with 875fJ pulse energy, as shown on Figure 20 to Figure 22. A small rotation can be seen, always less than 10°, far too low to be used for polarisation switching. The polarisation of the probe remains almost unchanged, linear and close to 0° orientation, for all pumping conditions and pump probe delays. The decrease in intensity can be attributed to the gain compression and it is greater at high pump energies. In both co-polarised and cross polarised cases the state of polarisation remains largely unchanged as the time delay and pump energy are varied, with a rotation lower than 10°.

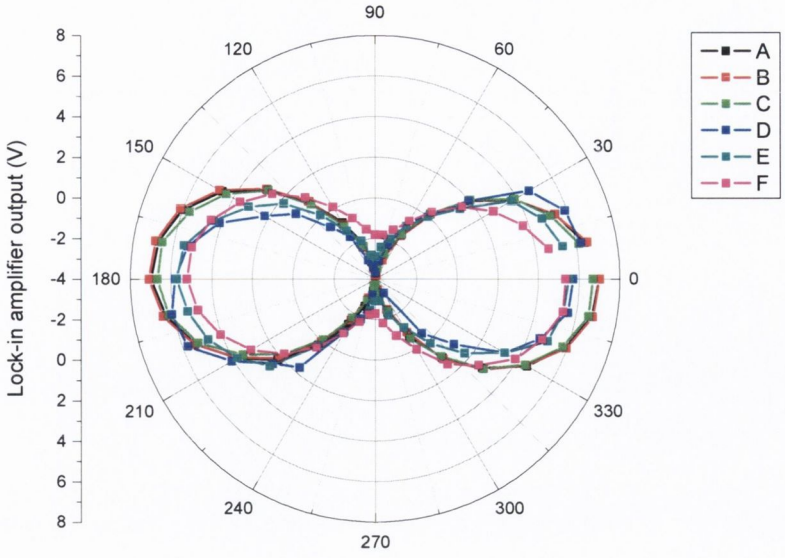

Figure 20. Output intensity as a function of polarizer angle, probe TE, 12fJ and pump TM, 12fJ.

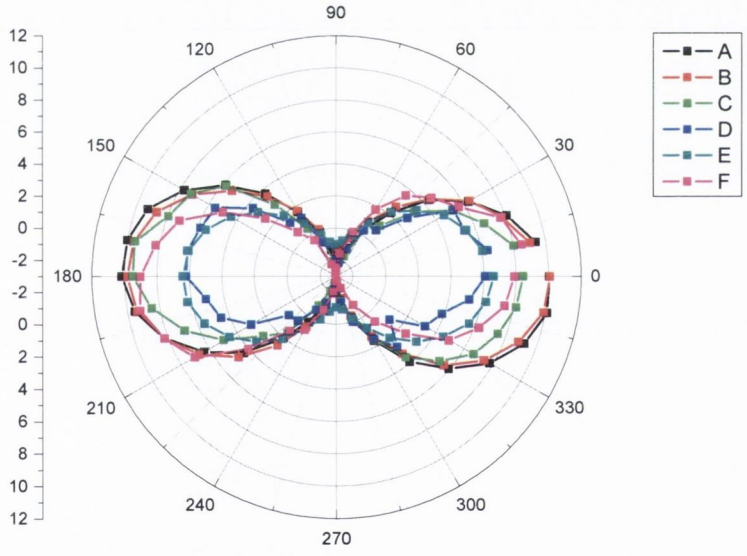

Figure 21. Output intensity as a function of polarizer angle, probe TE, 12fJ and pump TM, 875fJ.

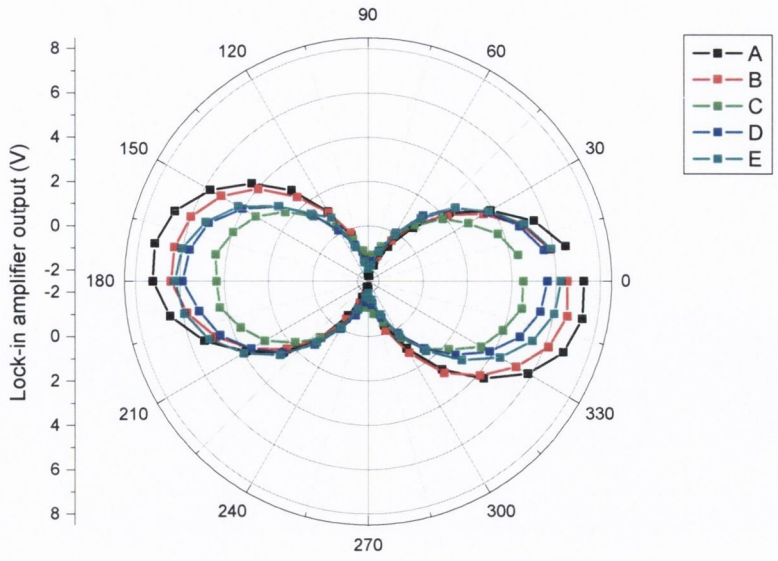

Figure 22. Output intensity as a function of polarizer angle, probe TE, 12fJ and pump TE, 875fJ.

6.3 Polarisation switching

For polarisation switching the combined effects of the polarisation dependent gain compression and the change of the probe state of polarisation have to be taken into account. In the pump probe configuration used here, the probe polarisation should not be set along the eigen modes of the device if polarisation switching is to be achieved as the polarisation remains largely unchanged in this case, as discussed above. In order to assess the potential of our set-up for polarisation switching the pump and probe polarisation are set at 45° with a low probe pulse energy of 12fJ and two different values of pump energy, 12fJ and 875fJ. This corresponds to the cross-polarised case, which was found to be the most promising in the previous chapter. The output probe intensity is then measured as a function of the output polarizer orientation at different positions of the delay line. This allows us to monitor the change in output probe polarisation as a function of pump-probe delay.

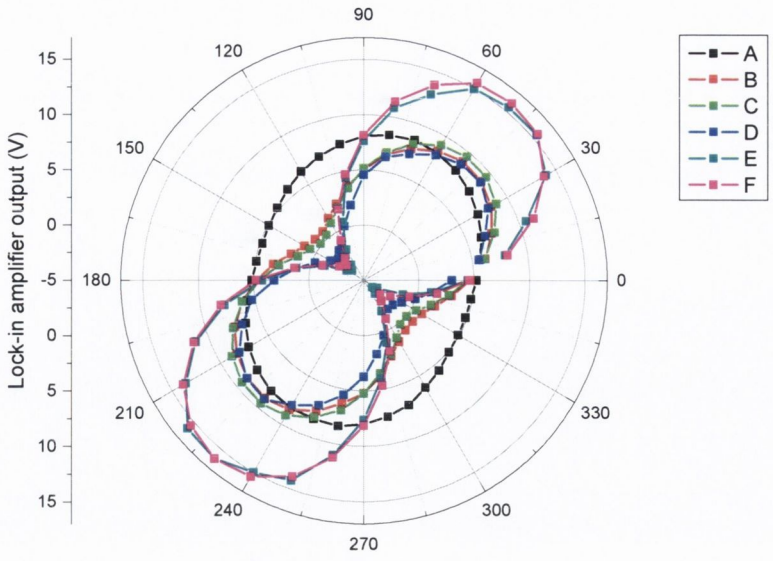

Figure 23. Output intensity as a function of polarizer angle, probe linear 45°, 12fJ and pump linear 45°, 12fJ.

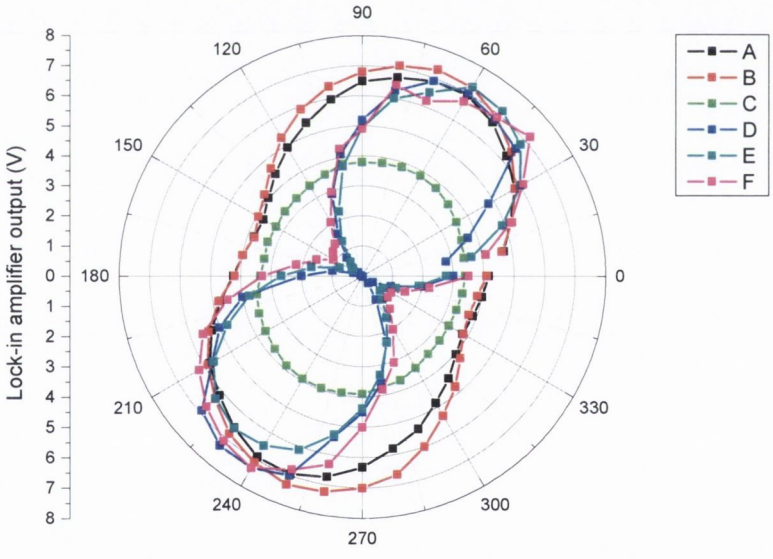

Figure 24. Output intensity as a function of polarizer angle, probe linear 45°, 12fJ and pump linear 45°, 875fJ.

As can be seen in Figure 23, at low pump power the polarisation of the probe output becomes less elliptical as the gain compression increases and is then linear as the device recovers, while the orientation stays almost constant. Similarly at high pump energy, Figure 24, the probe polarisation varies from elliptical to almost circular and is also linear during device recovery. The fact that the polarisation stays quasi linear as the device recovers shows that the recovery of the polarisation state is dominated by the slower interband effects. This is consistent with the results obtained with injected continuous wave laser beams, where interband effects dominate and the injection of a pump beam causes the output probe state of polarisation to become linear at this bias current, as discussed in chapter 4.

However very different performances can be achieved as a function of the polarizer orientation. For example at 0° the change in probe transmission with pump-probe delay is quite small, while the extinction ratio at 320° would be very high (determined by the extinction ratio of the polarizer), since the probe output is linear with a 50° orientation at D, but the recovery slow (longer than 50ps). However at 50° the extinction ratio seems smaller but the output probe level recovers extremely quickly, in about 5ps. The extinction ratio here cannot be precisely predicted as no measurements are taken at minimum probe transmission but from the previous measured decays a high extinction ratio can be expected (about 10dB). At low pump energy, the intensity measured for 50° polarizer angle stays constant except after the fast recovery where it is increased. This is consistent with the decay measured in that case, where the transmission showed a very sharp decrease around zero delay, which is not measured in these polar plots, followed by a fast recovery to a slightly higher level. Figure 23 shows that the gain compression is compensated by the polarisation becoming more linear. As such a greater proportion of the intensity is transmitted through the polarizer. Then as the gain compression recovers but the polarisation stays linear, the intensity measured is higher than when the pump did not affect the probe.

The main result from this experiment is that even though the recovery of the polarisation is dominated by the slower interband effects a fast recovery of the probe transmission level can still be achieved by carefully selecting the output polarizer orientation. It is also interesting to note that although polarisation switching is often referred to in the literature as 'non-linear polarisation rotation' [6-9], in this case it is mainly a change in the ellipticity of the signal that occurs and can be used for switching, while the rotation observed is small, around 10°.

7. Conclusion

Polarisation dependent decays were measured for light polarised along the eigen modes of the device with pump and probe cross-polarised, displaying a large diversity of behaviour which could not be explained without further investigation. The decays measured with light polarised at 45° showed a particularly sharp decrease in transmitted signal and recovery at low input pump energy for a polarizer angle between 45° and 90° which could be of great interest for ultrafast polarisation switching. The ASE modulated by the chopped probe beam was found to have a significant influence on the lock-in detection via the phase optimisation under given experimental condition. While some of the information on the timescales of the events are lost when measuring polar plots at different values of pump probe delay, this technique gives valuable information on both the state of polarisation of the signal and how it changes. The rotation of the eigen mode was found to be small, less than 10°, with the TE polarised probe travelling through the SOA with its polarisation mostly unchanged, when pumping along the TE or TM mode. A modification of the output probe polarisation with delay is clearly observed when injecting light linearly polarised at 45°, under our experimental conditions this was mainly due to a change in ellipticity. Although in that case the polarisation modification was found to be dominated by the interband effects, a fast recovery can still be achieved by the right choice of polarizer orientation. In addition to pure gain switching, a higher extinction ratio, determined by the extinction ratio of the polarizer, can be achieved using polarization switching, as can be seen on Figure 11, and lower pump powers are needed. The change in polarization can also be used to compensate for the slow gain compression, with the output intensity staying at a higher level at more negative delays and recovering to its initial value directly after the fast recovery in about 5ps.

REFERENCES

[1] K. L. Hall, J. Mark, E. P. Ippen, and G. Eisenstein, "Femtosecond Gain Dynamics in Ingaasp Optical Amplifiers," *Applied Physics Letters*, vol. 56, pp. 1740-1742, 1990.

[2] C. T. Hultgren and E. P. Ippen, "Ultrafast Refractive-Index Dynamics in Algaas Diode-Laser Amplifiers," *Applied Physics Letters*, vol. 59, pp. 635-637, 1991.

[3] J. Mark and J. Mork, "Subpicosecond Gain Dynamics in Ingaasp Optical Amplifiers - Experiment and Theory," *Applied Physics Letters*, vol. 61, pp. 2281-2283, 1992.

[4] D. S. Kigler, J. W. Lewis, and C. Einterz Randall, *Polarized light in optics and spectroscopy*: Boston Academic Press, c1990.

[5] Meade, "Lock-in amplifier principles and applications."

[6] D. Lenstra, Y. Liu, M. T. Hill, G.-D. Khoe, and H. J. S. Dorren, "Nonlinear polarization rotation in semiconductor optical amplifiers: Theory and application to all-optical flip-flop memories," *IEEE Journal of Quantum Electronics*, vol. 39, pp. 141-148, 2003.

[7] Y. Liu, M. T. Hill, E. Tangdiongga, H. De Waardt, N. Calabretta, G. D. Khoe, and H. J. S. Dorren, "Wavelength conversion using nonlinear polarization rotation in a single semiconductor optical amplifier," *IEEE Photonics Technology Letters*, vol. 15, pp. 90-92, 2003.

[8] R. J. Manning, A. Antonopoulos, R. Le Roux, and A. E. Kelly, "Experimental measurement of nonlinear polarisation rotation in semiconductor optical amplifiers," *Electronics Letters*, vol. 37, pp. 229-231, 2001.

[9] X. Yang, D. Lenstra, G. D. Khoe, and H. J. S. Dorren, "Nonlinear polarization rotation induced by ultrashort optical pulses in a semiconductor optical amplifier," *Optics Communications*, vol. 223, pp. 169-179, 2003.

CHAPTER 7 :
CONCLUSIONS AND FUTURE WORK

Optical switches based on SOAs are critical elements for the implementation of the all-optical gating necessary in order to overcome the 40Gbit/s limit of electronic elements still in use in optical communication systems [1]. Wavelength conversion at 100Gbit/s has been demonstrated using a number of SOA based methods : cross gain modulation (XGM) [2], cross-phase modulation (XPM) [3] and four wave mixing (4WM) [4]. All these techniques are limited by their sensitivity to the polarisation of the optical input signals. The polarisation sensitivity of SOAs, due to different gain and refractive indices in the TE and TM modes, is well known. Although considerable efforts have been made to reduce it, gain anisotropy of about 2dB usually remains, as does the birefringence. Both effects are dependent on device and optical injection parameters. Therefore the change of polarisation and the gain experienced by a laser beam as it travels through the SOA are both altered when a second laser beam is injected into the device. High speed all-optical switching applications based on this non-linear polarisation rotation (NPR) have been demonstrated [5-8]. A better understanding of polarisation effects is necessary in order to optimize the different wavelength conversion schemes, XGM, XPM, FWM and NPR. In this thesis an experimental investigation of polarisation sensitivity in SOAs was presented, first without optical injection, then both in the continuous wave (CW) and dynamic regimes.

1. Conclusions

The polarisation sensitivity was first measured in the CW regime. The origin of the non-linear polarisation rotation in semiconductor optical amplifiers was studied using two different techniques. Two phenomena were considered as sources of the NRP: the asymmetric gain between the TE and TM modes and the birefringence. In the first experiment, without injected signal, the underlying properties of the waveguide are probed. Polarisation resolved ASE spectra were recorded and the gain and refractive index for the two eigen modes of the SOA waveguide were calculated. As quoted by the manufacturer, the single-pass gains of the TE and TM modes are almost equal without

optical injection (within 1.5dB of each other at the gain peak of 1580nm). It was found using this method, that a difference in the refractive indices of the two modes could be observed, with the refractive index along the TE axis slightly greater than that along the TM axis. Without optical injection the gain anisotropy in this device is low and a small birefringence can be observed.

In the second experiment, a new approach has been developed in order to investigate the gain and refractive index differences of the two eigen modes in the CW regime. A CW signal is injected into the SOA and the change in the state of polarisation at the output of the device is measured using a polarimeter. The input polarisation is linear and rotated over 90°, for a range of input powers. From the fit of the experimental results, with a basic electric field propagation model, we are able to measure the TE and TM gain ratio and the birefringence as a function of injected power. It is found that even though the TE and TM gains are close under low optical injection, consistent with the gain extracted from the analysis of the ASE spectra, the difference in gain between the two modes increases with increasing injected power, the TE gain becoming increasingly larger than the TM gain. The phase difference between TE and TM modes was found to get closer to zero as the injected power is increased, causing the maximum ellipticity to decrease and the orientation curves to become more linear. Finally by measuring the change of polarisation of the input beam over a larger range of input orientation (-90° to 90°), a small rotation of the principal axes, to a maximum of 5°, was observed. Under optical injection the gain anisotropy increases with input power and the TM mode was found to be more susceptible to gain saturation.

Pump-probe measurements were undertaken in the CW regime in order to assess the potential of non-linear polarisation rotation for all-optical switching. In CW the change in probe state of polarisation can be measured directly with a polarimeter and the device and injection parameters affecting it determined. The output probe state of polarisation was found to be strongly dependent on input pump power and bias current while the variation observed with pump polarisation was smaller. The ellipticity decreases with pump power while both the ellipticity and orientation are modified as the bias current is changed. This change in polarisation is always present unless light is injected with a linear polarisation oriented along the eigen modes of the device. As such it should be taken into account for any switching application. Using polarisation switching by

placing a polarizer at the output of the device can lead to an improvement of the extinction ratio (ER), compared to gain switching only, by 2dB or decrease it by 1.5dB depending on the polarizer orientation. This however is not a limitation of the set-up but rather reflects the change in polarisation experienced by the probe when the pump is switched on. The ER could easily be improved by adding extra polarisation controlling components in order to block out the output probe signal when the pump is on.
As the injected power of either the probe or pump signal is increased, the change in probe polarisation becomes more linear, with a more constant rotation and a smaller output ellipticity. A breakdown of the model developed for the single CW beam experiment is observed when fitting the experimental polarisation data under pumping condition, showing that the gain and birefringence effects are now dependent on the input probe state of polarisation. The ellipticity data are more sensitive to the presence of the pump. In all the experiments conducted in the CW regime, the ellipticity was found to be a critical parameter of the polarisation sensitivity in SOAs, while the polarisation rotation is mostly observed at low injected powers and is larger at low bias current.

The polarisation sensitivity was then studied in the picosecond regime. A free space contra-propagation configuration was implemented, allowing the polarization resolved dynamics of the device under test to be studied. A series of pump-probe experiments were performed, with co or cross polarised pulses, injecting light polarised along the eigen modes of the device and linearly polarised at 45°. From the transmission of the probe pulse as a function of delay, it was possible to observe the fast and slow recovery components of the gain compression. The gain compression was found to be dependent on the pump and probe state of polarisation and pump pulse energy. In all cases the gain compression parameters increase with pump energy. When injecting along the eigen modes of the device, the cross-polarised data are dominated by interband effects and show a low coupling between the modes. The maximum gain compression was found to be higher for the TMTM case but with a larger contribution of the slow gain compression than the TETE case. It follows that the prevalence of the fast intraband effects in the TETE case shows the highest potential for ultrafast all-optical gain switching. The fast recovery times measured for the co-polarised cases are close, with the TETE slightly longer, and increase with pump energy. Fast recovery times from 4.5ps to 7ps were recorded, showing potential for ultrafast gating. Furthermore the

rotation of the eigen modes was found to be small, less than 10°, therefore the influence of polarisation rotation is expected to be small as long as light is injected along these eigen modes. In order to take advantage of the larger contribution of the fast recovering gain compression in the co-polarised cases, contra-propagation configurations can be used although in this case the switching speed is limited by the transit time into the device. Another solution would be to use a co-propagation set-up, set the pump and probe signals at different wavelengths and separate them at the output with an optical filter. In order to implement the latter solution, the efficiency of the conversion should first be studied as a function of detuning between the input signals.

In order to assess the potential for polarization switching, the device recovery when injecting light at 45° was studied. The gain compression and timescales were found to be dependent on the pump polarization (45° or -45°) due to the presence of rotating fields in these cases. The shorter fast recovery time, around 2.5ps, and higher gain compression measured in the cross-polarised case, probe 45° pump 45°, make it the most promising configuration for all-optical polarization switching. Therefore this configuration was used for the following investigation of the dynamics of the non-linear polarisation rotation. Under given experimental conditions, the change in polarisation is mainly a change in the ellipticity, the output probe polarisation becoming more linear under the influence of the pump signal. Although in that case the dynamics of the polarisation modification was found to be dominated by the interband effects, a fast recovery can still be achieved by the right choice of polarizer orientation. Compared to pure gain switching, where a maximum extinction ratio of 10dB to 13dB was obtained for the co-polarised cases, with polarisation switching the probe signal could be extinguished to a level below the detection sensitivity, i.e. the extinction ratio was determined by the that of the polarizer. Moreover the slow recovery of the output probe intensity due to the slow recovering gain compression can be compensated for by the increased transmitted intensity through the polarizer due to the change in polarisation. While the complete recovery of the intensity could be observed in less than 5ps, the slower gain recovery is much longer. Therefore the output probe level when a pulse is injected, after intensity recovery but before total gain recovery, should be investigated. And a study at higher repetition rates is necessary in order to determine to what extent the slow gain recovery affects the switching efficiency.

2. SOAs in optical communications

The free space contra-propagation set-up implemented for the present work has proven to be very efficient for the study of polarisation effects in SOAs. However with the use of fibre optics in optical communication, polarisation sensitivity will remain an issue for each component used in all-optical systems.

As linear amplifiers in integrated optics systems the polarisation sensitivity of SOAs remains a drawback. For high speed applications, where pulsed sources are used, more work needs be performed on device technology. Improvements in facets anti-reflection coatings and waveguide design led to low polarisation sensitivity in the CW regime, which as was discussed in this thesis does not extend to the dynamic behaviour of the SOA. As ultra-fast optical communications develop it is their low polarisation in the picosecond regime that becomes critical.

As switching elements the fast recovery observed and large fast recovering gain compression measured in the TETE mode is most promising. However the state of polarisation of the input signals needs be carefully controlled. For switching applications where pure XGM, XPM or FWM is used, polarisation effects may also be reduced by suppressing the TM mode of the device, for example through application of strain in the structure. However the coupling efficiency would still be dependent on the state of polarisation of the input signal, and the effect of strain on dynamics needs to be investigated in more details.

Polarisation switching was found to be most efficient when used in conjunction with XGM, providing a much larger extinction ratio and a faster total recovery of the output probe intensity. Compared to pure XGM, the only additional element is a polarizer placed before detection. The polarisation sensitivity in that case is taken advantage of, so that the presently commercially available components can be used. The dynamic gain anisotropy is actually necessary for polarisation switching. Once again the input state of polarisation needs to be carefully controlled. The implementation of XGM and polarisation switching is much simpler than XPM and FWM schemes, however for any integrated optical gate, the properties of the waveguides placed before and after the SOA have to be carefully chosen. Waveguide polarizers and single polarization waveguides structures have been proposed [9-11] and the efficiency of SOA-based all-optical gating will depend on the development of polarisation controlling waveguides.

The polarisation sensitivity of SOAs can potentially be tailored to suit the application of interest. Low-polarisation sensitivity is needed for linear amplification, while suppression of the one of the eigen modes could improve the performance of all-optical switching based on XGM, XPM and FWM. Finally the gain anisotropy in the dynamic regime can be taken advantage of by using polarisation switching in addition to XGM.

3. Future work

The further development of the model succinctly presented in chapter 2 is under way in Dublin City University. It is now able to deal with two contra-propagating inputs and includes ultrafast effects. Simulations and fitting of the experimental data presented in this work are currently being performed.

Using the same set-up and experimental conditions, investigation of the wavelength dependence of the dynamic behaviour can give further insight into the relative importance of spectral hole burning and carrier heating [12]. As discussed below, the wavelength dependence of the modulation efficiency will be of critical importance for the implementation of co-propagation switching schemes. While this is relevant for optical switching applications, and in particular polarisation switching, investigation of the SOA dynamics in the femtosecond regime would allow events occurring with different timescales to be more easily resolved and their polarisation dependence determined.

As mentioned before, pump-probe studies are usually performed in a co-propagation configuration, with the pump and probe cross-polarised along the eigen modes of the device. However it was clearly demonstrated in chapter 5 that this corresponds to the slower dynamic configuration. Therefore co-propagation pump-probe studies should be undertaken with different combination of input signal polarisation. The interpretation of the pump probe data and the extraction of the different timescales are more straightforward when using a co-propagation set-up. Those timescales could therefore more easily be compared to values found in the literature since a lot of work has been performed in a co-propagation configuration. While the fastest recovery was measured for the TETE case in contra-propagation, the fall time in that case corresponds to twice the propagation time in the SOA. Therefore a much shorter fall time is expected in co-

propagation where it is related to a correlation of the pump and probe pulses. In order to implement co-polarised gain switching or polarisation switching in co-propagation the pump and probe signals have to be set at different wavelengths, which may decrease the efficiency of the modulation.

The work presented in this thesis was performed on a single bulk ridge waveguide. However as was discussed in chapter 2 a number of different structures are available, using bulk and quantum well materials. In this context it would be interesting to determine how polarisation sensitivity affects those SOAs and how much of the experimental configuration optimisation is device specific. The most recent work on quantum dot and quantum dash based SOAs has been focused on gain dynamics, showing behaviour that differs from bulk and quantum well devices [13, 14], while study of polarisation effects is yet to be performed.

REFERENCES

[1] H. G. Weber, R. Ludwig, U. Feiste, C. Schmidt, C. Schubert, J. Berger, E. Hilliger, M. Kroh, and T. Yamamoto, "High-speed all-optical signal processing in optical communication systems," *Pacific Rim Conference on Lasers and Electro-Optics, CLEO - Technical Digest*, pp. 610, 2002.

[2] A. D. Ellis, A. E. Kelly, D. Nesset, D. Pitcher, D. G. Moodie, and R. Kashyap, "Error free 100Gbit/s wavelength conversion using grating assisted cross-gain modulation in 2mm long semiconductor amplifier," *Electronics Letters*, vol. 34, pp. 1958-1959, 1998.

[3] R. P. Schreieck, M. H. Kwakernaak, H. Jackel, and H. Melchior, "All-optical switching at multi-100-Gb/s data rates with Mach-Zehnder interferometer switches," *Quantum Electronics, IEEE Journal of*, vol. 38, pp. 1053-1061, 2002.

[4] A. E. Kelly, A. D. Ellis, D. Nesset, R. Kashyap, and D. G. Moodie, "100Gbit/s wavelength conversion using FWM in an MQW semiconductor optical amplifier," *Electronics Letters*, vol. 34, pp. 1955-1956, 1998.

[5] D. Lenstra, Y. Liu, M. T. Hill, G.-D. Khoe, and H. J. S. Dorren, "Nonlinear polarization rotation in semiconductor optical amplifiers: Theory and application to all-optical flip-flop memories," *IEEE Journal of Quantum Electronics*, vol. 39, pp. 141-148, 2003.

[6] H. Soto, J. C. Dominguez, Erasme D., and G. Guekos, "Demonstration of an all-optical switch using cross-polarization modulation in semiconductor optical amplifiers," *Microwave and Optics Technology Letters*, vol. 29, (3), pp. 205-209, 2001.

[7] H. Soto, J. D. Topomondzo, D. Erasme, and M. Castro, "All-optical NOR gates with two and three input logic signals based on cross-polarization modulation in a semiconductor optical amplifier," *Optics Communications*, vol. 218, pp. 243-247, 2003.

[8] M. F. C. Stephens, M. Asghari, R. V. Penty, and I. H. White, "Demonstration of ultrafast all-optical wavelength conversion utilizing birefringence in semiconductor optical amplifiers," *IEEE Photonics Technology Letters*, vol. 9, pp. 449-451, 1997.

[9] J. Fujita, M. Levy, R. Scarmozzino, R. M. Osgood, Jr., L. Eldada, and J. T. Yardley, "Integrated multistack waveguide polarizer," *IEEE Photonics Technology Letters*, vol. 10, pp. 93-95, 1998.

[10] B. M. A. Rahman, S. S. A. Obayya, W. Boonthitlanont, and J. M. Heaton, "Novel Polarization-Maintaining Semiconductor Waveguide," *IEEE Photonics Technology Letters*, vol. 16, pp. 807-809, 2004.

[11] G. N. de Brabander, J. T. Boyd, and H. E. Jackson, "Single polarization optical waveguide on silicon," *IEEE Journal of Quantum Electronics*, vol. 27, pp. 575-579, 1991.

[12] J. Mark and J. Mork, "Subpicosecond Gain Dynamics in Ingaasp Optical Amplifiers - Experiment and Theory," *Applied Physics Letters*, vol. 61, pp. 2281-2283, 1992.

[13] J. Mork, M. L. Nielsen, and T. W. Berg, "The Dynamics of Semiconductor Optical Amplifiers, Modeling and Applications," in *Optics & Photonics News*, July 2003.

[14] M. Van Der Poel, J. Mork, A. Somers, A. Forchel, J. P. Reithmaier, and G. Eisenstein, "Ultrafast gain and index dynamics of quantum dash structures emitting at 1.55mm," *Applied Physics Letters*, vol. 89, pp. 081102, 2006.